CHALMERS
UNIVERSITY OF TECHNOLOGY

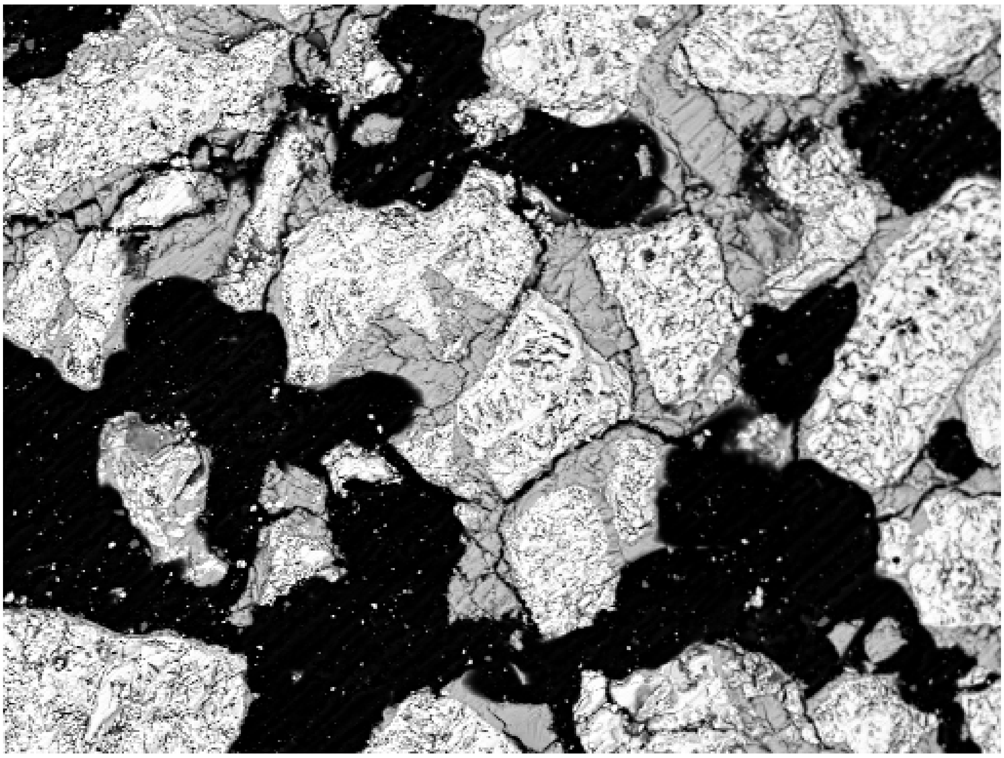

Ash interactions with oxygen carriers Glödskal and LD-slag in biomass-CLC

Master's thesis in Innovative and Sustainable Chemical Engineering

FELICIA ELIASON

Division of Energy and Materials
CHALMERS UNIVERSITY OF TECHNOLOGY
Gothenburg, Sweden 2018

Master's thesis 2018

Ash interactions with oxygen carriers Glödskal and LD-slag in biomass-CLC

FELICIA ELIASON

Division of Energy and Materials
Department of Chemistry and Chemical Engineering
Chalmers University of Technology
Gothenburg, Sweden 2018

Ash interactions with oxygen carriers Glödskal and LD-slag in biomass-CLC
FELICIA ELIASON

Supervisor: Maria Zevenhoven, Laboratory of Inorganic Chemistry, Åbo Akademi
Examiner: Henrik Leion, Department of Chemistry and Biotechnology, Chalmers University of Technology

Master's Thesis 2018
Department of Chemistry and Chemical Engineering
Division of Energy and Materials
Chalmers University of Technology
SE-412 96 Gothenburg
Telephone +46 31 772 1000

Cover: Sweeping Electron Microscopy (SEM) image of particles of Glödskal that have been oxidized in air and reduced in the presence of monopotassium phosphate and steam. The image shows the cross-section of sintered particles.

Gothenburg, Sweden 2018

Ash interactions with oxygen carriers Glödskal and LD-slag in biomass-CLC
FELICIA ELIASON
Department of Chemistry and Chemical Engineering
Chalmers University of Technology

Abstract

Chemical-looping combustion (CLC) is a novel combustion technology where fuel is converted in the absence of air. The process is carried out in two fluidized bed reactors, one in which a metal oxide (oxygen carrier) is oxidized by air and one in which fuel is converted to combustion products through reaction with the oxidized oxygen carrier. The combustion products are thus inherently separated from air and CO_2 can be separated for carbon capture and storage without large energy penalties. Much of the current work with implementing conventional scale CLC aims at evaluating the performance and economic viability of different oxygen carriers. CLC of biomass is of interest for sustainability reasons and evaluating if oxygen carriers are suitable for biomass-CLC includes ensuring that the material can perform well also in the presence of biomass ashes. Glödskal and LD-slag are two low cost steel industry by-products that have shown desirable fuel conversion properties in CLC, and their interactions with some common potassium ash components (KCl, K_2CO_3, K_2SO_4 and KH_2PO_4) in reducing atmosphere have been investigated in this study. Glödskal consists mainly of Fe and Fe oxides and traces of other metals and oil residues from the process. The main components of LD-slag is Ca-oxides and oxides of Fe, Si, Mg and Mn. LD-slag also contains lower concentrations of Al, Ti and V. Utilizing low cost waste materials is beneficial both for economic and sustainable reasons. The materials have been mixed with potassium salt to obtain a mixture with 4wt% potassium content. The mixtures have been reduced in a glass quartz reactor for 8 hours in 850°C. The reduced samples have been analyzed in SEM with EDS. The mixtures have also been tested in Thermogravimetric analysis. It was seen that all the salts except for KH_2PO_4 had positive effect on the porosity of Glödskal. K_2CO_3 increased the reduciton rate of Glödskal. KH_2PO_4 caused agglomeration of Glödskal which had a negative impact on the reactivity. The agglomeration is due to formation of a K-P-Fe component. Some accumulation of K was seen in both Glödskal and LD-slag after reduction in the presence of K_2SO_4. With K_2CO_3 and K_2SO_4 K accumulated in LD-slag together with vanadium. K_2CO_3 deactivated LD-slag. KH_2PO_4 reacted with Ca in LD-slag and formed a K-P-Ca component which caused some agglomeration but didn't affect the reduction rate.

Keywords: Chemical-looping combustion, oxygen carriers, Glödskal, LD-slag, ash interactions, potassium salts, biomass ash

Acknowledgements

First of all, I would like to thank my examiner and co-supervisor Dr. Henrik Leion for recommending me and trusting me to be part of this project.

I would like to thank my supervisor Dr. Maria Zevenhoven at Åbo Akademi for her guidance and the discussions we've had throughout this work. She has been very helpful and has encouraged me to be creative.

For consultation and help in the practical work I would like to thank Jaana Paananen, Linus Silvander, Tor Laurén and Peter Backman. I'm very grateful for their time and the work they have put into helping me obtain good results for this thesis. I would also like to thank the rest of the group at Inorganic Chemistry at Åbo Akademi for being supportive and making me feel welcome from the start.

Last but not least I would like to thank my family for their support and encouragement throughout my studies and in the work on this thesis.

Felicia Eliason, Gothenburg, August 2018

Contents

1. Introduction

The year 2016 was the warmest year on record [1]. Measurements show that the average global temperature during the period 2013-2017 is likely to have been the highest five-year average ever recorded and is close to 1°C above the average global temperature measured between 1880 and 1900. It's generally agreed upon by scientists that a large contributor to the temperature increase is anthropogenic greenhouse gas emission.

The most commonly reported effects of climate change are warming and shifts in precipitation patterns[2, 3]. This in turn has an impact on natural and human systems through damage caused by heat waves, droughts, floods, cyclones, and wildfires to mention some. The effects of climate change can be seen on different levels ranging from economic loss caused by damage to assets and food production, mortality in human populations due to health issues and alterations in ecosystems when species are forced to shift their geographical range to adapt.

Fossil fuels were covering approximately 80% of the global energy use in 2005 [4]. It is estimated by the United Nations Framework Convention on Climate Change that fossil fuels will continue to be the main energy source until at least the middle of the 21st century, since they are cheap, abundant and can be utilized on demand. This means that CO_2 will continue to be produced and if emitted to the atmosphere continue to contribute to climate change. Without additional climate change mitigation measures, it's estimated that the global mean surface temperature will have increased by between 3,7 and 4,8°C by the year 2100, compared to pre-industrial temperature levels [5].

The effects on climate change will vary greatly across regions and populations, making it not only a matter of monetary or technological challenges but also a question of equality and human value. The poorest and most vulnerable people in rural areas in developing countries have been and will be affected the most but might also have the least capability to make a difference. The responsibility for climate change mitigation thus must be shared by all actors. Adapting to and mitigating climate change can't be done by any one single approach; place- and context-specific measures must be taken on different levels in society and the process will be expensive [2]. The adaptation and mitigation choices that are being done in the close future will be a factor in the climate change situation throughout the whole 21st century [4, 2, 5].

One of the technologies that is expected to play an important role in climate change mitigation is Carbon Capture and Storage (CCS). The idea of the concept is to collect and concentrate the CO_2 and transport it to a location for long term storage. The concept ultimately means combustion of fossil fuels with zero emissions. In the case of biomass combustion with CCS, (bio-CCS) carbon bound in organic matter is combusted and stored, leading to what is referred to as negative emissions. According to a report done by the International Panel on Climate Change (IPCC), CCS together with other measures could significantly reduce the impact of climate change [4]. CCS and some proposed technological solutions for implementation are presented and discussed later in this report. One of the main barriers to CCS implementation is that power plants with CCS are still not economically competitive with conventional power plants, the largest cost associated with CCS being the cost for CO_2-separation [4, 6, 7].

The CO_2-separation concept that will be in focus in this report is an emerging technology called Chemical-Looping Combustion (CLC). The idea behind the concept is to provide the oxygen for fuel conversion from air indirectly, by having it oxidize a material that carries the oxygen to a fuel reactor. The combustion products (CO_2 and steam) is thus inherently separated from the nitrogen and the excess oxygen in the air, and a stream of pure CO_2 can be obtained without additional expensive separation processes. The technology will be described in detail in Chapter 3.2. The oxygen transporting material is called Oxygen Carrier (OC) and circulates between the air and the fuel reactor. CLC is a young technology and there are still some considerable barriers to overcome before the technology can be implemented to full scale systems. Finding suitable OCs is one of them and there are some criteria that they should meet. Being economic, reactive, stable, and environmentally friendly are some of them. The most common suggestions are OCs based on oxides of copper, nickel, iron, manganese, and cobalt. [7]. This study focuses on biomass combustion and specifically interactions between OCs and biomass ash. Ash interactions are studied to determine the OC's suitability for biomass CLC.

2. Aim and restrictions of study

The overall aim of this work is to investigate the possibility to use two different iron-based steel industry by-products as oxygen carriers in Chemical-Looping Combustion of biomass-based fuels. Biomass contains a range of different ash components that have been seen to interact with oxygen carriers and alter their composition and properties in CLC. The aim of this study specifically is to investigate how the materials Iron mill scale (Glödskal) and LD-slag interact with some potassium salts that are commonly occurring in biomass (KCl, K_2CO_3, K_2SO_4 and KH_2PO_4). Mechanisms like deactivation, erosion or agglomeration of the material could mean that they must be rejected as oxygen carrier candidates. The goal is that this study will be part of the extensive screening work that is being done to find suitable oxygen carriers that are both efficient in combustion and can be acquired in a sustainable way. The work will aim at taking one step further towards emission free combustion, more sustainable energy production and climate change mitigation.

The focus in the project is to only investigate the interactions between the oxygen carrier and the ash components. Tests regarding fuel conversion, fluidization properties of the oxygen carrier etc. are out of the scope of this project. Previously published works on fuel conversion and fluidization properties of similar materials is revised and included in the discussion. No tests are done with combinations of the different ash components and the potassium concentrations are the same in all the tests.

3. Theory

3.1 Carbon Capture and Storage

The idea with Carbon Capture and Storage (CCS) is to collect the CO_2 produced in the system, compress it and transport it to a location for long-term storage, enabling ideally zero-emission combustion [1]. CO_2-separation has been done by chemical scrubbing since the 60's with the initial purpose being to produce CO_2 to be used for carbonating drinks and brine and for enhanced oil recovery. CO_2 separation in the context of climate change mitigation was first discussed in late 1980's. The cost of CO_2 capture is the largest cost associated with CCS technologies; in a case study done by Rao and Rubin, 79% of the additional cost for implementing an amine absorption CCS system to a coal-fired power plant is associated with capturing the CO_2 [2, 3]. Carbon capturing can be divided into three types of methods; decarbonization prior to combustion, oxy-fuel combustion, and post-combustion CO_2 separation [3, 4]

Post-combustion CO_2 separation is mainly done today by absorption in solvents, adsorption to solid materials or by gas separation in porous membranes [1, 3]. The operational cost and energy penalty for these techniques are large since a lot of energy is consumed to regenerate the sorption material. Heat demand values in an amine absorption process are typically between 2,7 and 3,3 GJ per ton of captured CO_2 [1]. Additional energy required for compression and transportation.

In decarbonization prior to combustion, the primary fuel is reacted with steam or oxygen to produce a mixture of hydrogen and carbon monoxide [1]. The general chemical reactions using steam (steam reforming) and oxygen (partial oxidation) can be seen in Reaction 3.1 and 3.2 respectively. The formed mixture is treated with steam in what is called the water gas shift reaction to produce CO_2 and hydrogen gas. The water gas shift reaction can be seen in Reaction 3.3.

$$C_xH_y + H_2O \leftrightarrow xCO + (x + \frac{y}{2})H_2 \tag{3.1}$$

$$C_xH_y + \frac{x}{2}O_2 \leftrightarrow xCO + \frac{y}{2}H_2 \tag{3.2}$$

$$CO + H_2O \leftrightarrow CO_2 + H_2 \tag{3.3}$$

The CO_2 is separated from the hydrogen and can be compressed and stored. The hydrogen is burned for inherently CO_2-free combustion. The most commonly used way of producing hydrogen is steam reforming, using methane as fuel.[8].

The idea behind the last type of method; oxy-fuel combustion, is that the fuel reacts with oxygen in absence of the other air components, producing a stream consisting ideally of only CO_2 and steam. Providing oxygen for the combustion can be done by separating gaseous oxygen from air in an external air separation unit, which requires energy. Advantages seen with oxy-fuel combustion are flexibility and increased combustion efficiency compared to conventional combustion [5]. An alternative to using gaseous oxygen is to provide the oxygen from an oxidized material, which is the idea used in Chemical-Looping Combustion (CLC). Using CLC avoids the gas separation steps needed in the previously discussed options, which leads to a higher energy efficiency. CLC is the technology that will be the main topic later in this work and is thus only mentioned here.

After capture and compression of the CO_2, it is transported and either utilized or stored. The most popular use of CO_2 is in enhanced oil recovery, where CO_2 is injected into uneconomical oil reserves to extract more oil and natural gas. This technique has been used for some 40 years, so both the transport and the injection technology is mature and well-known [6]. CO_2 can also be utilized to some extent in food production, chemical industries etc. The production, however, by far exceeds the total utilization possibilities, so to mitigate emission other means of CO_2 sequestration are required as well [1, 3].

Some alternatives for carbon storage include mineral carbonation (where rock from magnesium and silica oxides react with CO_2 to form a stable solid material) or dissolving CO_2 into deep saline aquifers. Injecting the CO_2 deep enough into the ocean for the CO_2 to be liquid, sink and create CO_2-lakes on the ocean floor has also been suggested, but is nowadays considered unrealistic from an ecological aspect [3, 6]. Yet an alternative is storage in depleted gas reserves; since they have been long-term storage locations for natural gas, they should also be good storage locations for CO_2. Some of the risks that must be assessed carefully before storing CO_2 is leakage from geological formations which can harm plants and animals, induced seismic activity, and altered aquifer chemistry that can affect drinking water. There is also the risk for economic loss in enhanced oil recovery if the injection misses its target area and the CO_2 mixes with the oil and gas. The overall health and safety risks are however comparable with health and safety risks related to other energy production technologies [6].

The separate components of the CCS concept (separation, transportation and storage) are in use today in the fossil fuel production industry, but the concept has not yet been implemented to any large-scale power plants [7, 5]. Some of the most crucial barriers to implementing commercial-scale CCS are, except the already discussed economic aspects, that there is a need for well-defined regulations on short- and long-term responsibilities for storage [4, 9]. Risk associated with provision of biomass is an additional barrier to investment in bio-CCS power plants.

3.2 Chemical-Looping Combustion

CLC is a combustion concept where a material is oxidized in one reactor and transferred to a separate reactor where it provides the oxygen needed to combust a fuel [4, 10, 9]. A few different suggested technological concepts exist, and the most commonly discussed technology will be presented in section 3.2.2 Combustion system. The term Oxygen Carrier (OC) is used to describe the material that is being oxidized and reduced in the different parts of the system. A range of different OCs have been suggested in previous research and some of them will also be discussed later, in section 3.5 Oxygen Carriers. The OC typically consists of a metal oxide or a combination of metal oxides and a support material.

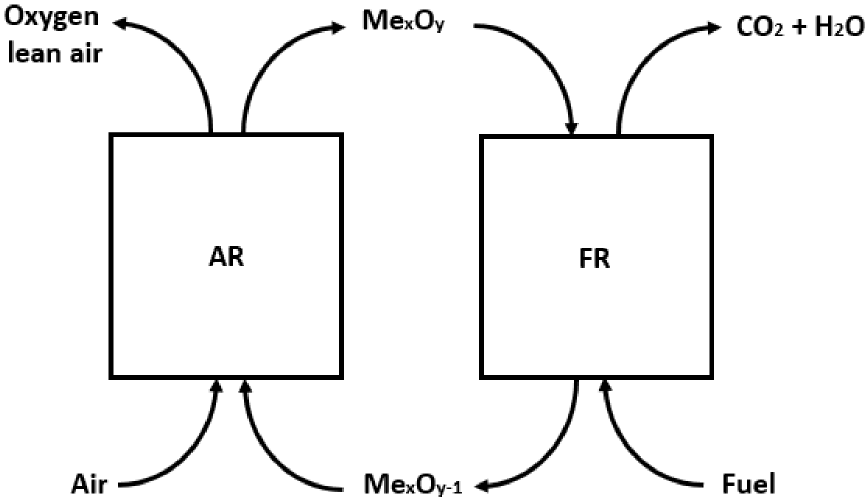

Figure 3.1: Schematic image of the CLC concept

A schematic image of the CLC concept can be seen in Figure 3.1 The terms Air Reactor (AR) and Fuel Reactor (FR) are used to describe the parts of the system where the OC is oxidized and reduced, respectively. What makes CLC an option in CCS is that there are two separate flue gas streams from the system. The OC is typically oxidized by air in the AR, and the outlet gas consists mainly of nitrogen and some excess oxygen. The flue gas from the FR is ideally a pure stream of combustion products, namely CO_2 and steam. The steam is easily condensed to obtain a stream of pure CO_2.

The cost for using CLC for carbon capturing is lower than the other previously mentioned technologies. In an estimation presented by Adánez et. al [4], the capture cost per ton of CO_2 avoided was 6-13 € using CLC, 18-37 € using the pre-combustion technology Integrated Gasification Combined Cycle, (IGCC) and 13-30 € for an oxy-fuel technology with air separation. Carbon capture with CLC has been estimated to increase the price of electricity production by only 12-22%, making it a promising candidate for CCS. [4]

The first idea behind CLC was proposed and patented by Lewis and Gilliand already in 1954. [4, 11] . Their idea was to oxidize carbonaceous materials by solid copper oxides and thus produce CO_2 free from inert gases. The focus was on developing a method for energy efficient production of CO_2 to be used in industrial processes. The concept was later again considered in the early 80's by Richter and Knoche, who suggested using copper-, nickel-, and cadmium-based OC in CLC with the aim to decrease the combustion entropy and increase the thermal efficiency in fossil fuel-fired power plants [4]. The concept has been growing and gaining more interest the last 10-20 years. CLC was still a paper concept in 2000; no continuous tests had been done and only a few OCs had been tested [4], so the technology is in need of more research.

3.2.1 Combustion mechanisms

The CLC systems are commonly classified according to what type pf fuel is combusted; gaseous, liquid or solid fuel. Most of the work in CLC has so far focused on utilizing gaseous fuels and mainly natural gas and methane [10]. The interest in researching solid fuels are growing and especially in the context of biofuels and also coal, which is expected to continue being a main energy source also in the future [4]. Only very limited studies have been done on CLC of liquid fuels. The biggest interest for combustion of liquid fuels is in the fossil fuel industry, with the combustion of heavy residual oils [9]. It is the combustion of solid fuels that will be in focus in this work.

When combusting solid fuels in CLC, the reaction mechanisms differ from conventional combustion of solid fuel with gaseous oxygen. The coal is instead first gasified, and the mechanisms of coal gasification can be seen in Reactions 3.4-3.6. Coal is volatilized (Reaction 3.4) and the remaining char reacts with H_2O and CO_2 according to Reaction 3.5 and Reaction 3.6. The reaction with H_2O is the same type of reaction seen in Reaction 3.1.

$$Coal \rightarrow Volatiles + Char \tag{3.4}$$

$$Char + H_2O \rightarrow H_2 + CO \tag{3.5}$$

$$Char + CO_2 \rightarrow 2CO \tag{3.6}$$

The formed gases react with the OC in the FR according to Reactions 3.7 and 3.8 where Me_xO_y and Me_xO_{y-1} denotes the OC; a metal oxide in two different oxidation states. The notation "Me_xO_{y-1}/Me_xO_y" is commonly used in context of oxygen carriers and is called the metal oxide system.

$$H_2 + CO + Volatiles + Me_xO_y \rightarrow CO_2 + H_2O + Me_xO_{y-1} \tag{3.7}$$

$$H_2O + CO \rightarrow H_2 + CO_2 \tag{3.8}$$

As a final step, the OC is oxidized in the AR according to Reaction 3.9 and is subsequently recirculated to the FR.

$$Me_xO_{y-1} + \frac{1}{2}O_2 \rightarrow Me_xO_y \tag{3.9}$$

The oxidation of the OC is exothermic (Reaction 3.9), increasing the temperature in the AR. The overall reaction in the FR can be either exothermic or endothermic, depending on the OC. Endothermic reaction between the gaseous components and OC leads to a temperature drop in the FR, and the solid circulation must be high enough to not only transfer oxygen but also heat to the FR. [12]. If the overall heat of reaciton is positive in the FR, the circulation rate can therefore be lower.

The intermediate gasification steps (Reaction 3.4-3.6) can be carried out in two different ways; syngas-CLC and in-situ, integrated gasification-CLC (iG-CLC) [13]. In syngas-CLC, the fuel is first gasified in an external gasification unit, and the gas is injected into the FR. In iG-CLC, on the other hand, the solid fuel is inserted directly into the FR and is mixed with either steam, CO_2, or a mixture of the two gases. If the fuel is reactive enough, CO_2 is sufficient for a good solid fuel conversion [4]. The gasification of the solid fuel is the rate-limiting step in the process, and the reaction is inhibited by the hydrogen formed in Reaction 3.5.

It's been concluded through experimental work that the rate of gasification of solid fuels is higher when OCs are used compared to in conventional systems. [14]. It is suggested that the most important reaction is the one between the OC and the gaseous components that are volatilized from the fuel and formed during the gasification of the char (Reaction 3.7) [13, 4, 15]. The reaction rate in Reaction 3.7 is high; hydrogen is efficiently removed from the system by the OC and its inhibiting effect on the gasification reaction is reduced [13, 16, 14]. It is thus important that the OC is highly reactive with the gas components and that the residence time in the reactor is high enough to enable high conversion in the gasification reactions [10]. The solid-solid reaction between the OC and the char does not seem to play a big role in the combustion process. It has also not been seen that the OC has any catalytic effect on the gasification process [4]. Based on that, an alternative to gasification of the char inside the FR would be to externally gasify the solid fuel and inject the gasification products into the FR. This is the idea of the earlier mentioned technology syngas-CLC. Only the Reactions 3.7-3.9 is then taking place inside the CLC system. The beneficial hydrogen-consumption by the OC in the gasification step is thus not a feature in the syngas-CLC technology. This is an advantage that iG-CLC has over syngas-CLC. The syngas production process is endothermic, so either pure oxygen must be used as the gasifying agent, or heat needs to be supplied to the process [9, 4]. Heat can be supplied from the CLC-system. Air can't be used in the gasification reactor, since then the nitrogen would have to be separated either from the gaseous fuel or from the flue gas.

An advantage with syngas-CLC is that the injection locations in the FR can be designed to make sure the fuel residence time is sufficient for complete combustion, which is a challenge in iG-CLC. In iG-CLC, the solid fuel particles are well mixed in the FR, and gasification happens in the bed wherever the char particles are located. Thus, parts of the gasification will take place close to the exhaust gas exit and some uncombusted gas will escape the FR, leading to loss of fuel and dilution of the CO_2-stream. The loss can be reduced by installing multiple FR's in series, separate and recirculate gaseous fuel components, or inject pure, gaseous oxygen after the cyclone [4]. Another challenge with iG-CLC is that a too low solid fuel particle residence time in the FR can cause unconverted char particles to be transferred with the OC to the AR. Char in the AR leads to loss of fuel and char combustion in air, subsequently leading to CO_2-emissions from the AR. Carbon deposition on OC particles causes similar problems, and can be avoided by choosing a deposition-resistant OC.

3.2.1.1 Chemical Looping with Oxygen Uncoupling

Increasing the overall solid fuel conversion rate can be done by the novel combustion technology Chemical-Looping with Oxygen Uncoupling (CLOU) [12]. CLOU is similar to CLC, but utilizes the ability of some oxidized OCs to decompose and release gas-phase oxygen. OCs have CLOU properties if they oxidize in the AR atmosphere and decompose according to Reaction 3.10 at the FR oxygen partial pressure and temperature. The available gas phase oxygen reacts with the solid fuel in the FR directly, according to Reaction 3.11.

$$Me_xO_y \leftrightarrow Me_xO_{y-2} + O_2 \tag{3.10}$$

$$C_xH_y + \frac{x}{2}O_2 \leftrightarrow xCO_2 + \frac{y}{2}H_2O \tag{3.11}$$

Since the gasification is the rate-limiting step in CLC, avoiding it by direct reaction between fuel and gaseous oxygen has been seen to drastically increase the fuel conversion rate. Metal oxide systems that have shown CLOU-properties are CuO/Cu_2O, Mn_2O3/Mn_3O_4 and Co_3O_4/CoO [12].

If the overall reaction in the FR is exothermic, this brings with it even more advantages specifically in CLOU. A higher temperature in the FR shifts the Reaction 3.10 towards more gaseous oxygen, and thus a higher oxygen partial pressure. A higher oxygen partial pressure increases the rate of Reaction 3.11. Having an overall exothermic reaction in the FR also means that the solid recirculation rate can be lower, since heat does not need to be transported to the FR. Decreasing the solid recirculation rate leads to lower temperature in the AR and Reaction 3.10 is shifted towards more solid-bound oxygen and thus a higher actual oxygen transport capacity of the OC.

3.2.2 Combustion system

The most commonly discussed CLC technology is based on Fluidized Bed Combustion (FBC). FBC has been used for decades for combustion of solid fuels like coal, biomass, waste etc. so the technology is mature and well-known [4, 10]. The system consists of two interconnected fluidized bed reactors that make up the AR and the FR. OC is used as bed material and is fluidized by a high-velocity air stream in the AR. The gas leaves the AR through the top of the reactor with a velocity high enough to entrain the fluidized particles and circulate the OC to the FR [9]. The OC particles are separated from the air in a cyclone before entering the FR. The gas outlet from the AR consists mainly of nitrogen and the excess oxygen that is not consumed in Reaction 3.9. The bed particles reach the FR, which is fluidized with a lower gas velocity. The FR is typically placed higher than the AR, and the particles are recirculated to the AR from the bottom of the FR by gravity. It has been seen that using interconnected fluidized bed reactors provides a high circulation of solids and a high flexibility when it comes to fuel types [3].

There are some criteria that the reactor system must fulfill for efficient combustion; there should be good particle circulation between the reactors, the contact time between OC and air and between OC and fuel must be long enough, and the leakage between the reactors should be minimized to mention some. Loop seals are installed between the reactors to avoid gas leakage. Gas leakage from the FR to the AR gives decreased CO_2-capture efficiency; CO_2 can leak directly from the FR to the AR, and fuel gas or particles leaking from the FR gets combusted in the AR which creates CO_2 emissions there. Gas leaking from the AR to the FR dilutes the flue gas (the CO_2-stream) from the FR and gas separation is needed to achieve pure CO_2-production. If the contact time between the OC and air is insufficient, the oxygen transport suffers. If the contact time between the fuel and the OC is too low, fuel conversion is reduced, and energy is lost.

As mentioned earlier, if an iG-CLC system is used, the FR is fluidized by either CO_2, steam, or a mixture of both. If steam is used it is typically produced externally and injected into the reactor, bringing with it an extra energy cost. If the fuel is gaseous, as in syngas-CLC, the fuel itself is the fluidizing gas. Some flue gas from the FR is recirculated to increase the conversion rate.

3.3 Chemical-Looping Reforming

Steam reforming of methane (Reaciton 3.1 was previously mentioned as a way to separate the carbon already before combustion. Steam reforming is typically realized in a catalyst-packed tube reactor. The reaction between steam and methane is endothermic and heat must be supplied for the reaction to continue. Partial oxidation of methane (Reaction 3.2), on the other hand, is mildly exothermic and could be done without addition of heat. [8]. The process is also much faster and could be carried out in smaller reactors, but requires instead expensive catalysts and air separation to obtain pure oxygen for the process. A suggestion is therefore to combine the concepts of partial oxidation and CLC into what is called Chemical-Looping Reforming (CLR) [17, 4]. CLR is similar to CLC, but with partial oxidation instead of combustion of the fuel in the FR. The product is thus not heat, but syngas. CLR enables partial oxidation through Reaction 3.2 without the need for air separation and without the risks associated with having methane in direct contact with gaseous oxygen.

Like in CLC, a considerable challenge in implementing CLR is finding suitable OCs. The OC in CLR must be able to both give a high conversion of methane and a high selectivity towards H_2 and CO. Using Ni-based OC has shown good conversion, but too high selectivity towards complete oxidation (CO_2 and H_2O). Fe-based oxygen carriers at low oxidation numbers show good selectivity but too low conversion of methane [17]. Combinaitons of OCs or metal oxides with catalytic effects might have to be considered.

3.4 Oxygen Carrier Aided Combustion

Using OCs has also been suggested as a method to increase the performance in conventional FBC. Large FBC boilers suffer from oxygen-lean areas and thus incomplete combustion of the fuel. A non-uniform oxygen distribution leads to non-uniform combustion and hot spots in the boiler [18, 19]. Hot spots can in turn lead to the formation of thermal NO_x and heat loss. One way to deal with incomplete combustion is to increase the air-to-fuel ratio, but there are some reasons why a large excess of air in the boiler should be avoided if possible. Excess air flow volume requires a large boiler size, high fan power consumption and heat loss in the exhaust gas. A high gas flow velocity also leads to wear of the equipment material. An OC could act as a buffer in the bed, since it can oxidize in the oxygen-rich areas and provide oxygen in the oxygen-lean areas of the boiler. This means that the air to fuel ratio could be reduced without compromising the completeness of the combustion. The idea of totally or partially replacing the conventional bed material with an OC in FBC is called Oxygen Carrier Aided Combustion (OCAC) and was first tested at Chalmers in 2012 in a 12 MWth circulating fluidized bed research boiler [20]. The silica sand in the boiler was partly replaced by the natural mineral ilmenite, and up to 80% reduction of CO and 30% reduction of NO emissions could be seen compared to operation with only silica sand. Up to 40 wt-% of the bed material was replaced by ilmenite in the test and it was concluded that the addition of the OC improved the oxygen distribution in the boiler.

Apart from oxygen deficiency, yet another problem is that more chemically stable gas fuel components like methane are not combusted in the bottom of the bed due to the cooler temperatures there [21]. The solid-gas reaction with OC adds another reaction path that does not require the same high temperature as conventional flame-combustion. This has been seen to enhance the combustion of gaseous components in the cooler parts of the bed.

What makes OCAC commercially interesting is that the implementation would require very little modification of already existing commercial boilers. Some naturally occurring materials with oxygen carrying properties can be obtained at a cost comparable to silica sand, so it’s easy to see how OCAC implementation can be economically beneficial. What OCAC practically means for heat and power producers is that a higher fuel combustion rate can be obtained in already existing and running plants. The carbon footprint per produced MW of energy is reduced if the combustion is more complete and if the heat loss is decreased. Lowering emissions of NO_x and CO is also desirable for producers.

3.5 Oxygen Carriers

Finding suitable OCs is an important area of research in the development of the CLC technology. The OC consists of a metal oxide or a combination of an active metal oxides and a support material. There's a list of general criteria that the OC should fulfill to be considered suitable, and most commonly mentioned in literature is that the OC should [4, 3, 10].

- Have good oxygen transport capacity
- Efficiently convert fuel to CO_2 and steam.
- Have high reduction and oxidation reactivity during many redox cycles
- Have good mechanical strength to resist attrition
- Be resistant to carbon deposition (this is only likely to be a problem in high degrees of reduction, such as in CLR)
- Have good fluidization properties
- Be economically viable
- Be environmentally friendly.

Fuel type and process temperature puts further context-specific requirements on the OC, so choosing an OC is an important step in CLC plant design.

More than 700 OC materials have been developed and tested so far to find suitable options [4]. The most commonly suggested materials are based on oxides of iron, copper, or nickel as active component because of their thermodynamic properties in fuel and oxygen interaction, and because they are abundant and can be acquired at a low cost [3]. Cobalt- and manganese-based materials are also commonly discussed as possible candidates. The metal oxides alone have been seen to not show the characteristics required for a good OC; they tend to get deactivated and agglomerate and show other operational problems after a few cycles and need to be replaced [4]. The metal oxide is therefore mounted on a support material, which can give the material increased reactive surface area and increase mechanical strength, among other features. Typical support materials are Al_2O_3, $MgAl_2O_4$, SiO_2, and TiO_2.

Producing synthetic OCs, however, significantly increases the cost compared to using ores and waste products as OCs. Synthetic materials might therefore not be a viable option for biomass combustion, due to the ash interactions that are expected to take place with the OC. For combustion of fuels with high ash-content, it could therefore be more economical to accept lower performance parameters and use a material that is cheap enough to be regenerated at a higher rate [21].

3.5.1 Nickel based oxygen carriers

Ni-based OCs have shown very high reactivity at temperatures around 900-1100°C. Tests have shown almost complete conversion of methane. Ni-materials don't seem to be able to perform well without support material; the material in itself has low porosity and thus low contact area with the gases, and suffer from agglomeration problems [4, 3]. Synthetic OC with Ni mounted on Al_2O_3 has shown good performance, but there is a risk of Ni-Al reactions which leads to deactivation. Ni-materials in themselves are more expensive than other materials and the need of support material brings up the price even more. Their very high reactivity could, however, be worth the investment in some types of applications. Ni is toxic and has a catalytic effect on carbon formation. Carbon formation is undesirable and could leads to fuel loss in CLC, but could be avoided by gasifying the fuel with CO_2 and steam and is not expected to be a significant problem in fluidized beds [4]. Due to thermodynamic limitations, complete conversion to CO_2 is not possible using Ni as OC, and some CO will be present in the flue gas.

3.5.2 Cobalt based oxygen carriers

Cobalt OCs have shown CLOU-properties in CLC applications, but with an overall endothermic reaction in the FR [12]. Co materials have high oxygen transport capacity and suffer low carbon deposition, making them an attractive suggestion for CLC applications [4]. Using Co as OC has shown to be difficult though, since there is need for a support material that doesn't react with and deactivate the material. [9]. Co_3O_4 is unstable at temperatures over 900°C, so only lower oxidation states can be used in CLC, which negatively affects the reactivity with the fuel. Co materials are also expensive and the use lead to some environmental concerns.

3.5.3 Copper based oxygen carriers

High reactivity with both oxygen and fuel has been observed when copper oxides have been tested as OC. The system CuO/Cu_2O can be used in CLOU, and leads to an overall exothermic reaction in the FR. [12]. Their relatively low melting point and thus tendency to agglomerate puts a limit on operation temperature, and a support material is needed with copper OCs [3]. It has also been seen to react with some Al- and Ti-based support materials, which deactivates them. Cu has like Ni a catalytic effect on carbon formation but that's also not assumed to be a problem in fluidized beds as long as process parameters are designed with that in mind [4].

3.5.4 Manganese based oxygen carriers

Due to its many oxidation states, manganese oxides have high oxygen transport capacity; about 7-10 wt-% depending on boiler temperature. Both the systems

Mn_2O_3/Mn_3O_4 and Mn_3O_4/MnO are reactive enough with fuel to convert it in the boiler [21]. Mn_2O_3 has been observed to have CLOU-properties [12]. The use of Mn_3O_4 leads to overall exothermic reactions in the FR.

Tests with natural manganese ores as oxygen carriers in OCAC showed that the air to fuel ratio could be significantly decreased without increasing the formation of CO and also showed good operational properties (low agglomeration and attrition etc.) [21]. As discussed earlier, using low cost, natural ores is beneficial if there is ash accumulation and interaction with the bed since the required regeneration rate is expected to be high. Compared to Cu, Ni and Co the cost of Mn materials is low and in addition, they are considered non-toxic [4].

3.5.5 Iron based oxygen carriers

Iron oxides have been recognized as interesting OC candidates since they are abundant, have low price and have shown good reactivity with both oxygen and fuel [22, 3]. High melting points of the materials enable a wide range of process temperatures [23]. Fe-based materials have been seen to lead to no or little carbon formation, are not expected to suffer from agglomeration in continuous fluidized combustion and are considered non-toxic. Similarly to with Mn-based OCs, naturally occuring iron ores can be utilized as OCs in CLC, meaning that the additional cost for producing synthetic material is avoided.

3.5.6 Ilmenite

An OC that has gained much attention in context of biomass combustion is the natural titanium- and iron-based mineral ilmenite. When used as OC, the metal oxide system is $Fe_2TiO_5+TiO_2/FeTiO_3$ with possible intermediate oxidation states [24]. Ilmenite is abundant and is mined in large quintities, and therefore has a relatively low cost. It has shown good performance properties in both CLC and OCAC; as already mentioned, replacing up to 40% of the bed material in a 12 MW CFB boiler with ilmenite in biomass combustion led to up to 80% decrease of CO and 30% decrease of NO in the flue gas [20]. When examining the used ilmenite after the experiment, it could also be concluded that the material has the ability to capture potassium, which is present as ash in the biomass [19]. The problems associated with potassium in the boiler is discussed in Section 3.6: Biomass Ash. When used as OC in a laboratory scale CLC test with syngas as fuel, ilmenite showed good fuel conversion during many cycles [25]. The material thus seems to be resistant to deactivation.

3.5.7 LD-slag and Glödskal

The materials that are being tested on in this study are iron oxide mill scale (Glödskal) and LD-slag, which are by-products from the steel production industry [26, 27, 28]. Glödskal is produced when sheets of steel are hot rolled. Iron on the surface of the steel is oxidized in the process and flakes off. Glödskal mainly contains iron oxides and iron, and can also contain some other metals and oil residue from the production process [26]. 20-50 kg of Glödskal is produced per ton of hot rolled steel. A part of the Glödskal can be recycled to the steel-making industry, but some of it ends up in landfill due to too high content of impurities. LD-slag is a by-product in the Linz-Donawitz process, where scrap and hot iron is processed into low-carbon steel [29]. The raw material is melted in a large vessel and calcium-based fluxing agents are added. The slag is produced when oxygen is blown through the molten metal mixture, and carbon, silica, and other impurities such as manganese, titanium, vanadium and phosphorous are oxidized and separated from the steel. The slag also contains fluxing agent and magnesium oxide dissolved from the lining material of the vessel. The most common phases in LD-slag are calcium oxide (CaO), dicalcium silicate (Ca_2SiO_4), dicalcium ferrite titanate solid solution ($Ca(Al, Fe)_2O_5$-$Ca(Si, Ti)O_3$) and magnesio wüstit ((Mg, Fe)O) [28]. In a study where several different samples of LD-slag were analyzed, the total iron content of the slag was determined to be between 17-27 wt%, and the main component to be CaO (39-50 wt%) [28]. Producing one ton of crude steel generates approximately 150-180 kg of LD-slag [27] and the global generation is approximately 47 million ton per year.

Iron-based industrial residues can be obtained at low cost, and using waste products reduces the environmental stress of mining and processing virgin materials. A sample of LD-slag (LDst) and three other iron-based industrial waste materials were tested as OCs in a laboratory scale fluidized bed simulating CLC of syngas [16]. The tests showed good conversion of the fuel and it was concluded that all the materials could be possible options in CLC. The Glödskal used in this study is called Glödskal B and its properties as an OC (fluidization properties, reactivity stability and fuel conversion) has been tested in a study by Leion et. al [30] in a laboratory scale fluidized bed simulating CLC conditions. The OC showed no fluidization problems in operation and high fuel conversion both with syngas and methane. The material was tested in 25 reduction/oxidation cycles and never reached stable reactivity, meaning that there is an activation of the material continuing during the whole test. That the stable reactivity is not reached could be a problem since it might mean a continuous increase in porosity and thus a risk for the material to decompose into dust.

In another study, another sample of Glödskal (Glödskal A) and a sample of unprocessed iron ore were tested as OC in FBC of solid fuels (petroleum coke, charcoal, lignite and bitominous coals) and both showed good conversion rate and good fluidizing properties over many oxidation cycles [15]. The sample of Glödskal showed even better gasification rates than the previously discussed material ilmenite, and about twice as high gasification rates compared to when silica sand was used as bed material. Reactivity with syngas was seen to increase after the Glödskal had been used in solid fuel combustion, and the reason was thought to be that the fuel ash had a positive effect on the porosity and thus the surface area of the OC.

The promising results from these tests and the previously discussed advantages of utilizing industrial by-products gives a motivation to continue researching the different aspects of using Glödskal and LD-slag in CLC, OCAC and CLR.

3.6 Biomass ashes

The ash content and composition differ greatly between different types of biomass and must be considered in combustion. On a dry mass basis, the ash content can vary between 0,5 and 20 wt-% [31]. Cereal and agricultural waste have high ash content, while wood usually has lower. Considering the biomass composition has been seen to be especially important when designing combustion systems for industrial waste and energy crops, due to their high mineral content. Compared to coal ashes, that mainly consist of Si, Al, Ca and S, biomass ashes have higher content of alkali metals that are prone to cause problems in combustion [32].

The ash components' fate in the boiler depend on the composition of the ash and the process temperatures. Potassium is the alkali associated with by far the most problems when it comes to biomass combustion [32]. K exists in biomass mainly in the form of water-soluble salts, and are available for evaporation and reactions. Alkali metals react with other components in the ash and are most likely released in the gas phase as hydroxides, sulfates and chlorides [33, 31]. For this reason, four potassium salts that are likely to form in the boiler are used in these tests to simulate the problems that might appear during combustion. The potassium salts are KCl, K_2CO_3, K_2SO_4 and KH_2PO_4. These compounds can subsequently exit with the flue gas or deposit on heat exchanger walls, where it causes blockage of gas flow, corrosion of the material and decreased heat transfer and thermal efficiency. Precipitating gas phase metal oxides also agglomerates together and become fly-ash in the boiler [31]. Material selection, flue gas treatment and handling of ash are design factors in which the ash composition of the fuel must be considered. Handling of contaminated bed material is another aspect in FBC and CLC.

3.6.1 Agglomeration

Agglomeration of bed material is another problem caused by alkali metals in FBC. Agglomeration negatively affects the fluidization properties and shortens the lifetime of the material. Heavy agglomeration causes the fluidized bed to collapse. Agglomeration happens through two mechanisms; either ash components melt and the melt acts as a glue that holds the particles together, or ash components react with the bed material and the reaction product is what causes the particles to agglomerate. [33]. Analysis of agglomerates formed in FBC of biomass with silica sand as bed material showed that potassium was the main contributor to agglomeration [33, 19]. The potassium from the ash was seen to react with silica and form a sticky potassium-silica smelt that coats the bed particles and glues them together. A way to deal with agglomeration in silica sand is to add calcium in the form of calcium-rich fuels or limestone. Ca has been seen to hinder agglomeration mechanisms in two ways [34, 35, 36]; (i) Ca and Si react and form a layer of $CaSiO_3$, which protects the particles from agglomeration, (ii) Ca reacts with the P and K in the biomass ash and forms a Ca-K-P rich component with high melting temperature. K and P are otherwise likely to form sticky components with low melting temperature and contribute to agglomeration.

3.6.2 Interactions with Oxygen Carriers

Both in conventional FBC and CLC, bed material has been seen to undergo changes due to interactions with ash components in the fuel [33, 19, 37]. In iG-CLC, the biomass ash is present in the FR together with the OC at high temperatures, so interactions between the ash and the OC could be significant. The ash might cause deactivation of the OC surface or alter its internal composition through diffusion.

In some cases, interactions with ash components have been reported to have positive effects on the OC. In one fixed bed laboratory scale test, an iron ore was allowed to react with ashes from three different types of biomass [37]. In two of the cases, the reactivity with the gaseous fuels CO and H_2 increased when using the reacted iron ore as an OC. The biomass ashes that increased the reactivity of the OC were high in K_2O and low in SiO_2 and the increased reactivity was thought to be from increased BET surface area. Another explanation for increased reduction rate was that the K in the formed K-Fe-O-component weakens the Fe-O bond and thus enhances the reduction of the OC. In the same study, another ash high in SiO_2 decreased the reactivity with the fuel, with the reason proposed being that the silica-rich ash created molten potassium silicate which caused the bed particles to agglomerate.

Alkali metals have also been seen to react with Fe_2O_3 in OCs and form eutectic mixtures with high melting points, thus alkali metals can be captured by the OC and are then less likely to form those low-temperature melting alkali silicates [33]. This has also been observed in OCAC with ilmenite added to the silica sand bed. The potassium was captured in the ilmenite by the formation of KTi_8O_{16}, and the OC thus helps decreasing the risk of agglomeration in the bed and evaporation of alkali and subsequently deposition and corrosion of equipment [19].

4. Methods

4.1 Chemicals and raw materials

Four analytical grade potassium salts (KCl, K_2SO_4, K_2CO_3, and KH_2PO_4) were used in the tests to simulate ash components in biomass combustion. The molar mass, melting point, purity and origin of the salts used in the mixtures can be seen in Table 4.1.

Component	**Molar mass [g]**	**Melting point**	**Purity**	**Origin**
KCl - Potassium chloride	74,55	776°C	>=99,5	Riedel-de Haën
K_2CO_3 - Potassium carbonate	138,20	891°C	>=99,8	J. T. Baker
K_2SO_4 - Potassium sulphate	174,26	1069°C	>= 99	Riedel-de Haën
KH_2PO_4 - Monopotassium phosphate	136,09	252,6°C	>= 99,5	Merck

Table 4.1: Potassium salts used in the experiments

The OCs that were tested in the study were iron mill scale (Glödskal) and LD-slag. The LD-slag is provided by Merox. It's been crushed, dried by heat and sieved and the 150-400µm fraction of the material was provided to Chalmers. The Glödskal sample (Glödskal B) is provided by SSAB. Glödskal B has previously been tested as OC in laboratory scale fluidized bed simulating CLC, and showed good performance with methane and syngas as fuel [30]. The elemental compositions of the material have been measured with Energy Dispersive X-ray Spectroscopy (see Section 4.5) and the oxygen-free composition in wt-% is presented in Table 4.2.

Material	**Fe [wt%]**	**Si [wt%]**	**Mn [wt%]**	**Mg [wt%]**	**Al [wt%]**	**P [wt%]**	**Ca [wt%]**	**Ti [wt%]**	**V [wt%]**
Glödskal	95,1	4,0	0,9	-	-	-	-	-	-
LD-slag	24,0	10,2	3,6	6,5	1,3	0,5	49,5	1,1	3,3

Table 4.2: Oxygen free elemental composition in wt-% of Glödskal B and LD-slag used in the experiments. The composition is analyzed with SEM-EDS.

4.2 Pretreatment and preparations

To fully oxidize the OC before the reduction tests they were pretreated in an oven at 950°C for 6 hours. The oven used was an electrically heated Carbolite RHF 16/35 high-temperature laboratory furnace with a maximum temperature of 1600°C. The pretreatment was done at ambient pressure and in air to ensure complete oxidation of the material. After the treatment, the samples were left to cool in air overnight. The pretreated OCs were mixed with the salt and the mixture was grinded for 4 minutes using a mortar and pestle. Since previous continuous fluidized bed combustion experiments showed that the potassium content in the bed material may reach approximately 4 wt-% [19], the samples were prepared with a potassium content in the mixture of 4 wt-%.

4.3 Reduction test in a tubular oven

Reduction tests were conducted in a tubular oven on the pure, pretreated OC alone and on mixtures of one OC and one potassium salt. The salts used in the reduction tests were KCl, K_2SO_4, K_2CO_3, and KH_2PO_4.

Since the biomass gasification happens inside the FR in an iG-CLC system, this is where the oxygen carrier is exposed to the ash components. To simulate the reducing atmosphere caused by the gasification products in the FR, the materials were exposed to carbon monoxide and steam carried by a flow of inert nitrogen.

The tests were conducted in a cylindrical quartz glass reactor mounted in a Carbolite tubular oven. A schematic image of the experimental setup is shown in Figure 4.1. A preheater was inserted into one end of the reactor. During the tests, the gases and the water were injected into the preheater to allow for mixing and evaporation before entering the reactor. The preheater and the end of the reactor were both insulated with glass wool. The sample was placed in a ceramic boat and placed on a ceramic sample holder equipped with a thermocouple. Hereafter, the sample holder was

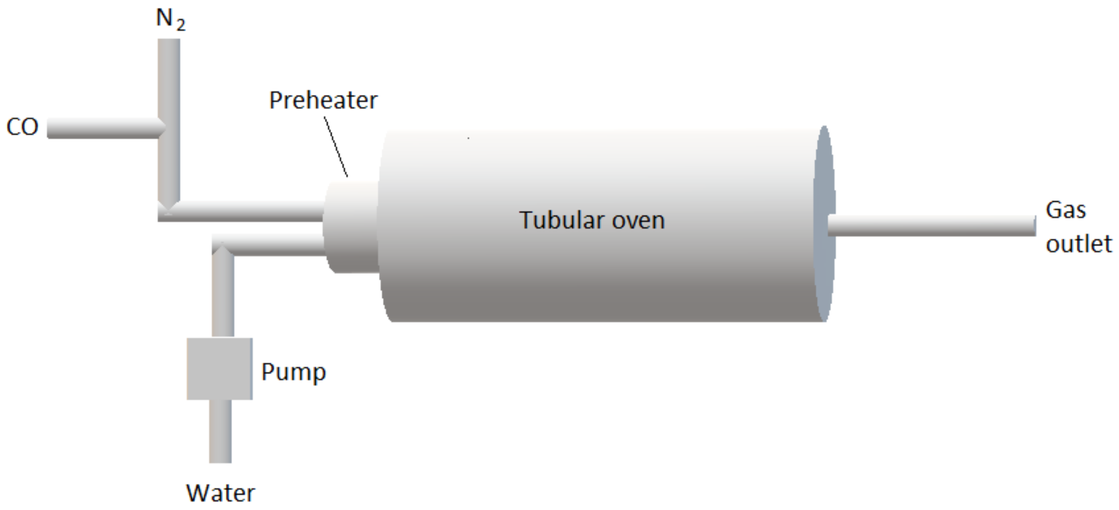

Figure 4.1: Schematic diagram of the reduction test setup

inserted into the reactor at ambient temperature. The reactor was heated at a fixed ramp rate of 15°C/min until the desired temperature of 850°C was registered inside the reactor by the thermocouple. Simultaneously, the preheater was heated at a ramp rate of 10°C/min to the set temperature of 300°C. The registered temperature in the preheater was around 250°C during the tests. The heating was done under an inert gas flow of 0,45 Nl/min N_2. When the desired reactor temperature was reached, the flow of CO and water was started with a flow of 0,050 Nl/min and 0,4ml/min of CO and water respectively. This gave a reducing atmosphere of 45% N_2, 5% CO and 50% steam in the tests. After the heat-up period, the sample was reduced isothermally for 6 hours and then left to cool for approximately 17 hours under a flow of 0,45 Nl/min of N_2. The same setup was used for all 10 reduction tests.

4.4 Thermogravimetric analysis

The same salts except KCl were used in the TGA. The reason for not using KCl in the TGA is the risk of corrosion of the equipment. The thermogravimetric analysis was used to investigate how the OC behaves in repeated reduction and oxidation cycles. The test was meant to simulate that the OC already has been oxidized in the AR, enters the FR and is reduced, is transferred back to the AR to oxidize, and is then finally reduced once more in the FR. The run schedule used in the tests is presented in Table 4.3. The following section includes a general description of the equipment and afterward, the parameters used in the tests are presented.

	Gas flow		**Time [min]**
Heating 15°C/min	1000	Nml/min N_2	45
Stabilizing	1000	Nml/min N_2	15
Reduction	450 5 500	Nml/min N_2 Nml/min CO Nml/min steam	60
Flushing/stabilizing	1000	Nml/min N_2	5
Oxidation	800 200	Nml/min N_2 Nml/min O_2	30
Flushing/stabilizing	1000	Nml/min N_2	30
Reduction	450 5 500	Nml/min N_2 Nml/min CO Nml/min steam	60
Cooling	1000	Nml/min N_2	

Table 4.3: Run schedule used in TGA

The temperature and the gas flows are the parameters that were controlled during the experiments. The sample is places in the sample holder and the sample holder is attached to a platinum hanging in a high-precision scale where the weight is measured. The atmosphere in the reactor is changed to simulate the different environments; inert, oxidizing and reducing. The weight of the sample in the reactor and temperature are being measured continuously and the weight change indicates that the material is getting oxidized and reduced during the experiment. The temperature is measured in a thermocouple located close to the sample holder. The weight change can also be due to other mechanisms, like evaporation of components in the sample. The gases enter at the bottom of the vessel. Water is pumped to a hot, porous sintered metal material where it is evaporated. Hereafter, the steam enters the bottom of the vessel together with the gases. Dry atmosphere in the reactor chamber is acquired by having the steam bypass the reactor. All reactor surfaces are heated to avoid condensation of steam. The gas exits the vessel above the sample and is cooled to allow condensation of the water in the outlet. A stream of dry helium above the sample holder protects the scale from contamination.

100 mg of sample was used for the experiments. A ceramic Al_2O_3 cup-shaped sample holder was used and the sample was inserted into the oven at ambient temperature. To ensure steady-state steam flow during the whole test, the water pump was started at approximately 200°C after a period of manually increasing the temperature. The steam flow was in bypass mode during the heat-up period. The temperature was kept at 200°C until the steam had reached the condenser and water was seen dripping out of the system. When the steady-state steam flow was reached, the temperature was increased by a controller to 850°C at a rate of 15°C/minute. The gas flows and the time intervals used in the tests are presented in Table 4.3. The heating, cooling, and stabilizing/flushing was done in N_2. The reduction was done in 45% N_2, 5% CO and 50% steam to simulate the environment in the FR. The oxidation was done in synthetic air; 80% N_2 and 20% O_2 to simulate the environment in the AR.

The reason for flushing/stabilizing sections in the test is to purge the reaction chamber to ensure that no gas from the FR simulation will disturb the oxidation, etc. There can also be gas left in the pores of the sample, which get time to react or leave the sample during the stabilization time.

The aim of the test is to study possible interaction between the OC and the ash component, if the gasification is inhibited, unchanged or if the ash component itself even catalyzes the reduction of the OC. Resistance to deactivation by ash components is an important feature of the OC, to ensure that the lifetime of the OC is sufficient.

4.5 Sweeping electron microscopy and Energy Dispersive X-ray spectroscopy

Scanning electron microscopy (SEM) is a method for analyzing the surface of a sample to see what the structure looks like and if there are any apparent differences in composition throughout the sample.

In SEM, the sample is placed in a vacuum, and electrons are beamed at the sample. Two different types of electrons are emitted from the sample; backscattered electrons and secondary electrons. Backscattered electrons are primary electrons from the electron beam that are reflected off the sample. Secondary electrons are valence electrons that originates from the atoms of the sample, gets energized by the primary electron, and are released from the atom. By scanning the sample with the electron beam, the secondary electrons and backscattered electrons can be registered and give an image of the sample surface [38].

When the primary electron hits the sample, there is a probability that it causes an inner-shell electron to be excited. The X-ray photon that is being released when the atom is again de-excited has an element-specific energy level. Reading the energy levels of the photons and utilizing the information to create elemental maps of the sample is the technique used in Energy Dispersive X-ray Spectroscopy (EDS). The technique can be used to identify what elements are present in the sample, give an approximate quantitative elemental analysis, and to identify possible patterns in the distribution of the elements in the sample.

By mounting the sample particles in epoxy resin and polishing the surface, a cross-section of the particles can be obtained and analyzed. SEM-EDS analysis of the cross-section of the particles has been concluded to be a useful tool in analyzing bed materials with ash layers [33]. The technique has therefore been used also in this study.

4.6 X-Ray Diffraction

X-Ray Diffraction (XRD) is used to analyze the crystalline structures of a sample [39]. X-rays are electromagnetic waves that are in the same wavelength range as the length between the atoms in the sample. The analysis is based on the effect that the atomic electrical and magnetic potential in a sample depend on the distances between the atoms in the sample. X-rays hitting the sample will be affected by the atom's electric and magnetic potential and can thus be used to analyze the sample. X-rays are beamed at the sample and deflected off, and the deflection angle depends on the electric and magnetic potential in the sample. Reading the deflection angle for a range of different incidence angles gives a diffraction pattern that is compared with a database of known diffraction patterns of different crystal structured material. The analysis method is restricted to identifying crystalline structures and can't be used to identify the composition of non-crystalline phases.

The oxidized material and the reduced samples have been analyzed with XRD. The aim of using the analysis in this study was to identify what oxidation states the pretreated and reduced materials are in and to evaluate if the ash components have been reacting with the material to form new compounds. The SEM-EDS tells where the elements are present in the material after reduction, but not in what compounds. The analyses could thus complement each other to give an idea of the mechanisms taking place in the interaction reactions. This, in turn, could help conclude how the ash compounds would affect the material in the long run.

5. Results

5.1 Reduction tests in tubular oven

The weight change in percent from reducing the samples in the tubular oven with 5% CO and 45% steam can be seen in Table 5.1. The weight reduction seen in the unmixed Glödskal is 3,35%, which corresponds to reduction of hematite (Fe_3O_2) to magnetite (Fe_4O_3). LD-slag has a lower oxygen transport capacity (1,12 wt-%).

Sample	**wt. change [%]**	**Sample**	**wt. change [%]**
Glödskal	-3,35	LD-slag	-1,12
Glödskal + KH_2PO_4	-5,07	LD-slag + KH_2PO_4	-3,00
Glödskal + K_2CO_3	-5,92	LD-slag + K_2CO_3	-3,80
Glödskal + K_2SO_4	-6,85	LD-slag + K_2SO_4	-4,59
Glödskal + KCl	-8,98	LD-slag + KCl	-7,53

Table 5.1: Weight changes registered in the reduction tests

5.1.1 X-Ray diffraction spectroscopy

The XRD diffractograms obtained when analyzing pure, pretreated Glödskal and the reduced Glödskal samples with and without salt added is presented in Figure 5.1. The diffractograms show that the pretreated material consists of hematite (Fe_2O_3). All the reduced samples show magnetite (Fe_3O_4). The diffractogram of the sample of Glödskal reduced with KH_2PO_4 suggests the presence of KPO_3 in the sample. No other crystalline compound can be seen from the diffractograms of Glödskal reduced with KCl, K_2CO_3 or K_2SO_4. This does not prove the absence of formed compounds, since they can be amorphous or in too low concentration to be detected by XRD.

Corresponding XRD diffractograms of the LD-slag is presented in Figure 5.2. Using XRD to analyze the samples of LD-slag was seen to be difficult due to the high number of components present in the sample. Amorphous phases are also likely to be present in the LD-slag. The sample reduced in the presence of KH_2PO_4 was also analyzed with 20 minutes run time, in an attempt to obtain diffractograms with more information. The different run times gave no noticeable difference in results.

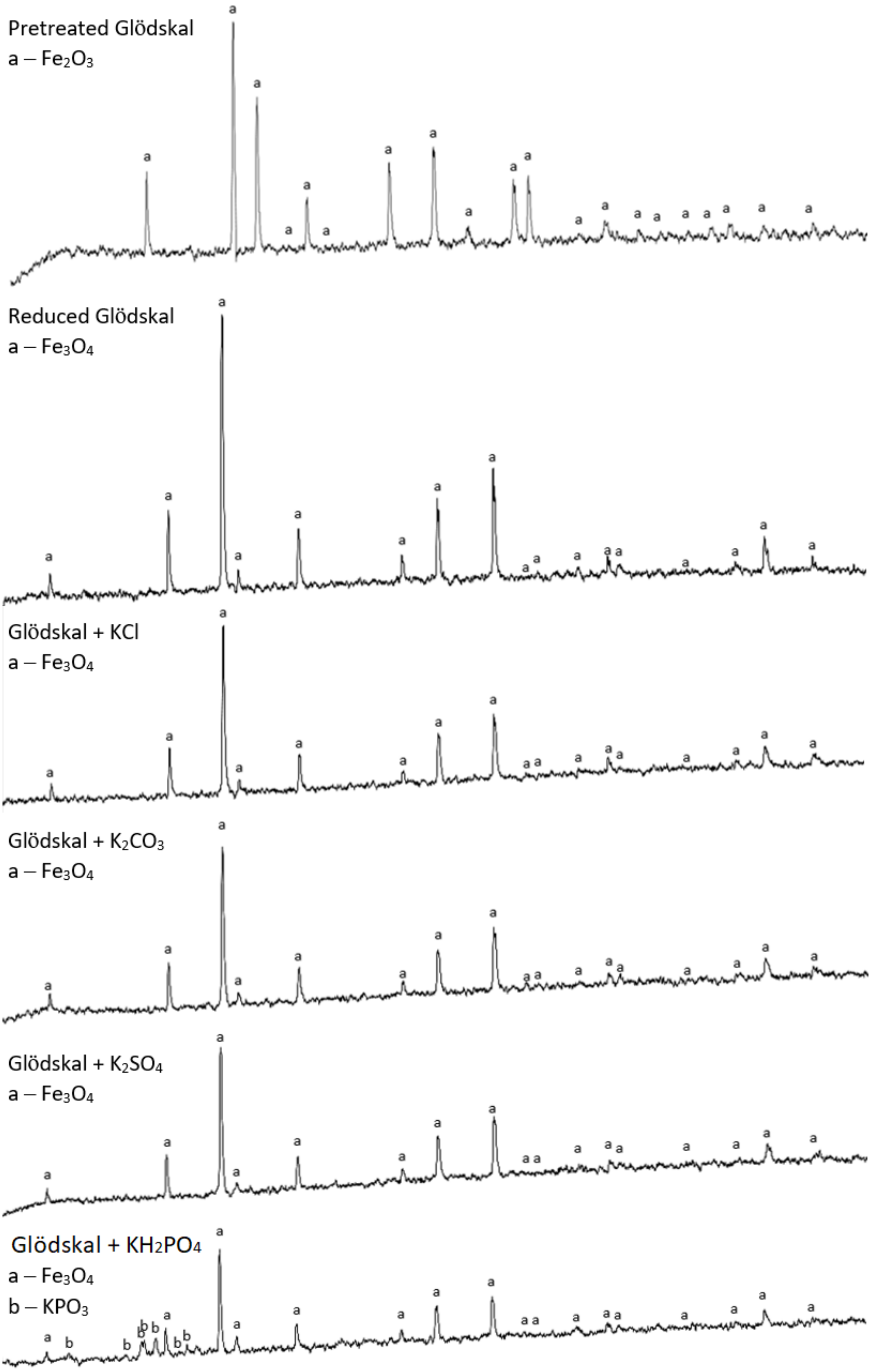

Figure 5.1: XRD diffractograms of the Glödskal samples

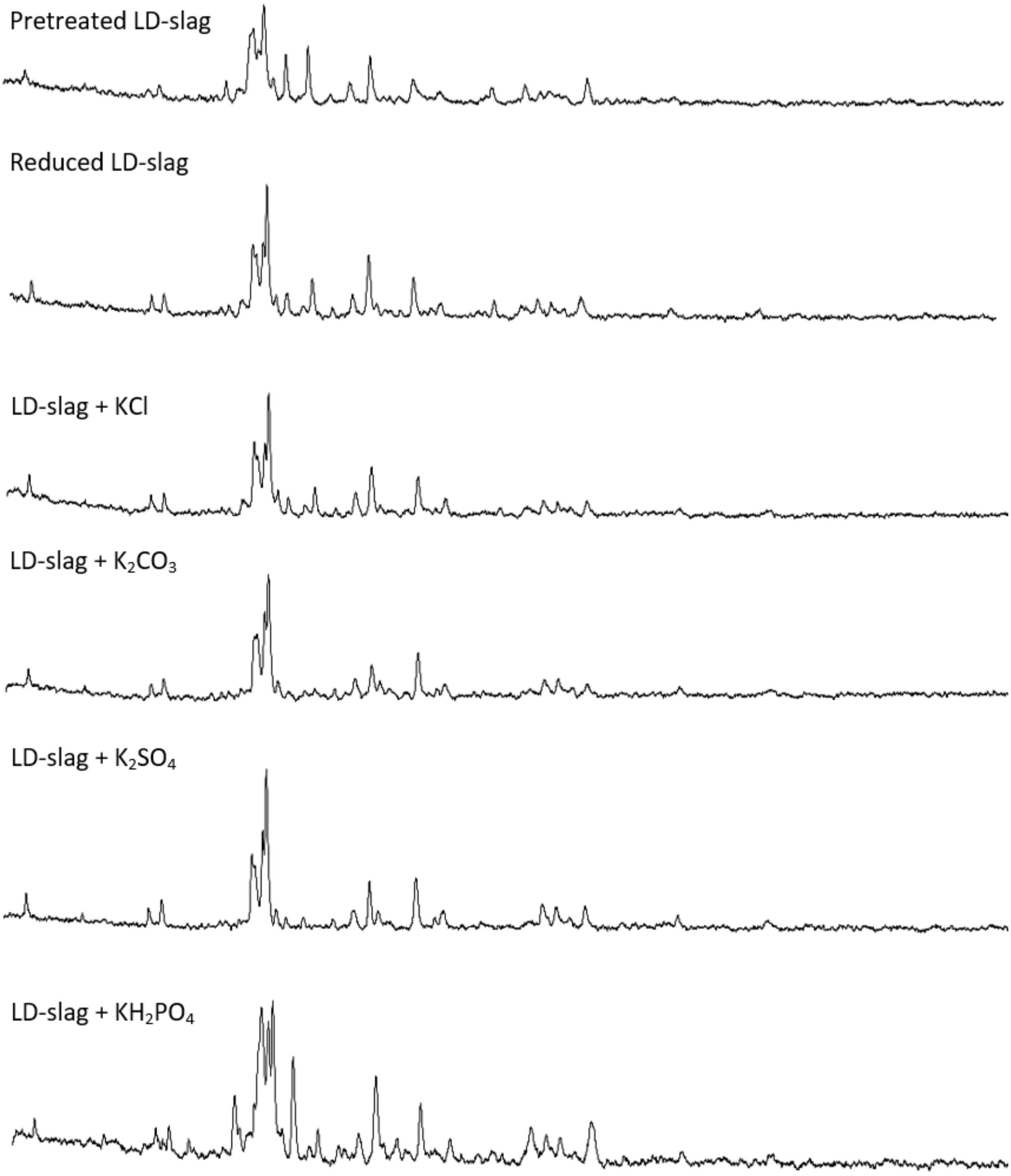

Figure 5.2: XRD diffractograms of the LD-slag samples

5.1.2 Glödskal

SEM-images of the unreduced Glödskal are presented in Figure 5.3A. The pretreated material has been grinded before this analysis, for better comparison with the reduced samples. SEM-images taken of all the reduced Glödskal samples can be seen in Figure 5.3B-F. The larger images and the smaller images are taken at 250 and 5000 times magnification, respectively. The unreduced material is without larger cracks, and shallow, round pores can be seen on the surface (Figure 5.3A). The sample reduced with no salt present has some cracks, and the surface shows a

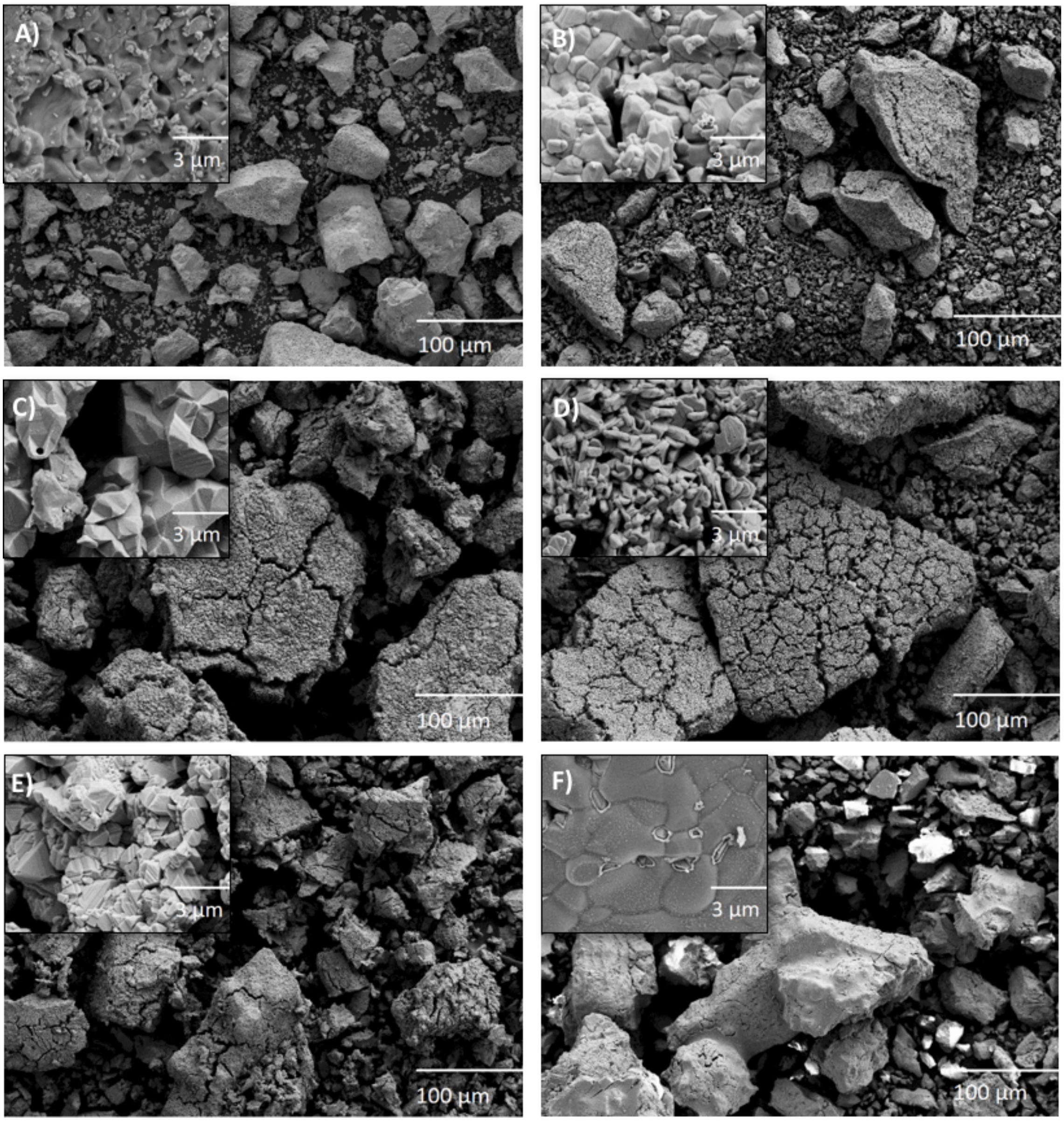

Figure 5.3: Surface images of the samples of Glödskal A) heat treated and grinded B) reduced without salt, C) reduced in the presence of KCl, D) reduced in the presence of K_2CO_3, E) reduced in the presence of K_2SO_4, F) reduced in the presence of KH_2PO_4.

pyramid-like structure (Figure 5.3B). The sample reduced with KCl present shows more and larger cracks (Figure 5.3C) and a similar pyramid-like structure on the surface. The sample reduced in the presence of K_2CO_3 shows the most cracks (Figure 5.3D). Its surface shows a more random and potentially more porous structure than those of the other samples. The image of the sample reduced in the presence of K_2SO_4 (Figure 5.3E) could suggest that smaller particles have agglomerated onto the bigger particles. The surface has a crystal-like structure seemingly made up of thin layers, and thus differs from the more solid pyramid shaped structure that can be seen in the first two reduced samples. The sample reduced in the presence of KH_2PO_4 shows agglomeration (Figure 5.3F). A few cracks and pores can be seen on the surface, but the images show a generally smooth structure covering the particles.

The consistency of the sample beds differed slightly between the five reduced samples. The bed of the samples reduced without salt and in the presence of KCl or K_2CO_3 were completely loose, like dry sand. The sample reduced with K_2SO_4 present resembled that of wet, compact sand but was easily worked to finely flowing particles. The sample with KH_2PO_4 present in reduction was in the form of one solid slab, showing sintering of the particles. It had to be worked with a spatula to become a loosely flowing sand again. The pretreated sample had a similar consistency, suggesting sintering also during pretreatment. Composition bulk analyses and elemental maps in grey scale are included in Appendix A and C.

5.1.2.1 Pretreated Glödskal

SEM-EDS elemental maps of pretreated Glödskal showing Fe, Si and Mn are presented in Figure 5.4. The sample was grinded before the analysis, for better comparison with the reduced samples. The analysis shows large particles consisting of Fe and traces of Mn. Small particles consisting of Si are identified in the analysis. Mn

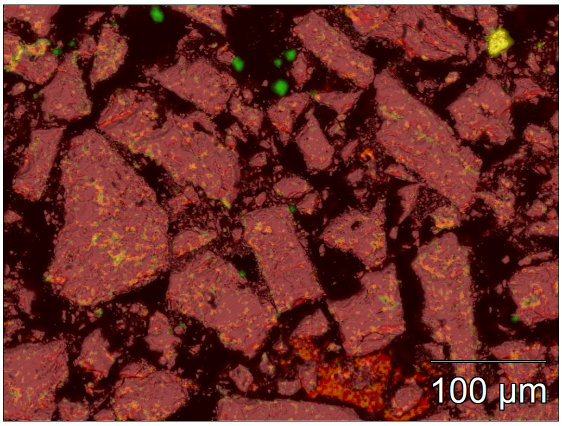

Figure 5.4: SEM-EDS elemental maps of cross-section of pretreated and grinded Glödskal. Fe in red, Si in green and Mn in yellow

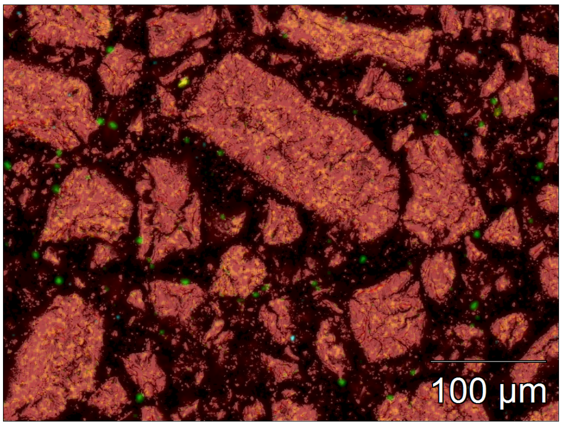

Figure 5.5: SEM-EDS elemental maps of cross-section of Glödskal reduced without salt. Fe in red, Si in green and Mn in yellow

exists as segregated islands in the material. SEM-images of pretreated sample without grinding are included in Figure B.1 in Appendix and confirm sintering. Sintering is expected to happen to hematite at the temperature used in the pretreatment.

5.1.2.2 Glödskal reduced without salt

SEM-EDS elemental maps of the sample of Glödskal reduced with no ash component present are presented in Figure 5.5. Fe, Mn and Si are marked and show a composition similar to that of the pretreated sample. The Si is also here located in small particles separate from the Fe. The distribution of Mn differ slightly, suggesting Mn is more spread out in the reduced sample. The SEM images show an increased porosity compared to the pretreated sample, which could also be seen on the surface.

5.1.2.3 Glödskal reduced in the presence of KCl

The SEM-EDS elemental maps of the sample of Glödskal reduced in the presence of KCl are presented in Figure 5.6. The location of Fe is marked in red in Figure 5.6A. K and Cl are marked in yellow and purple in Figure 5.6B. The maps show a composition similar to that of the unmixed, reduced sample, but with a low concentration of K and Cl mainly located in the epoxy matrix, outside of the material. With complete reduction of hematite to magnetite, the additional weight change in the reduction test corresponds to approximately 70% of the salt weight. KCl is likely evaporating in the reduction test temperatures and some unevaporated particles stay in the sample.

The increased porosity seen in Figure 5.3C compared to 5.3B can also be noticed in this cross-section SEM-analysis. The cross-section image further suggests that the cracks have reached all the way through the material. Adding KCl to hematite prior

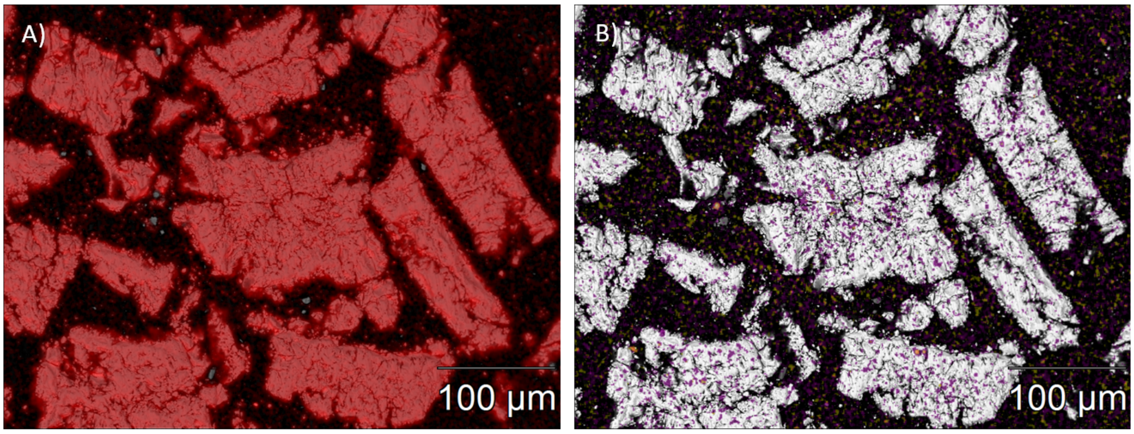

Figure 5.6: SEM-EDS elemental maps of the sample of Glödskal reduced in the presence of KCl. A) Fe in red B) K in yellow and Cl in purple

to reduction has previously been reported to increase the porosity and due to that also the reduction rate of the material [40]. No other interaction between the ash component and the material can be concluded from this test.

5.1.2.4 Glödskal reduced in the presence of K_2CO_3

SEM-EDS elemental maps of the sample of Glödskal reduced in the presence of K_2CO_3 are presented in Figure 5.7, and show a second phase containing K, Si, Al and Fe. Quantitative analysis of the EDS-maps showed a high K-concentration in the K-rich area (approximately 20 wt-%) and no to very low K-concentration in the rest of the OC material. Thus, there is no evidence of diffusion of K into the material.

The porosity of the material is increased compared to that of Glödskal reduced without ash component. As was mentioned in Section 3.6.2 Interactions with Oxygen Carriers, the reaction rate with CO and H_2 was seen to be higher after iron ore OC had been allowed to interact with biomass ash high in K_2O [37]. The increase in porosity was thought to be the reason, and that the K in the formed K-Fe-O species is an electron donor that weakens the Fe-O bond, and thus enhances the reduction rate of the material.

At high temperatures and low partial pressure of CO_2, K_2CO_3 decomposes to K_2O according to reaction 5.1. K_2O is not stable, and is expected to react with steam if present according to Reaction 5.2. KOH has a melting point of 360°C.

$$K_2CO_3 \rightarrow K_2O + CO_2(g) \tag{5.1}$$

$$K_2O + H_2O \rightarrow 2KOH \tag{5.2}$$

With complete reduction of hematite to magnetite in the reduction test, the additional weight change corresponds to approximately 35% of the salt weight. The

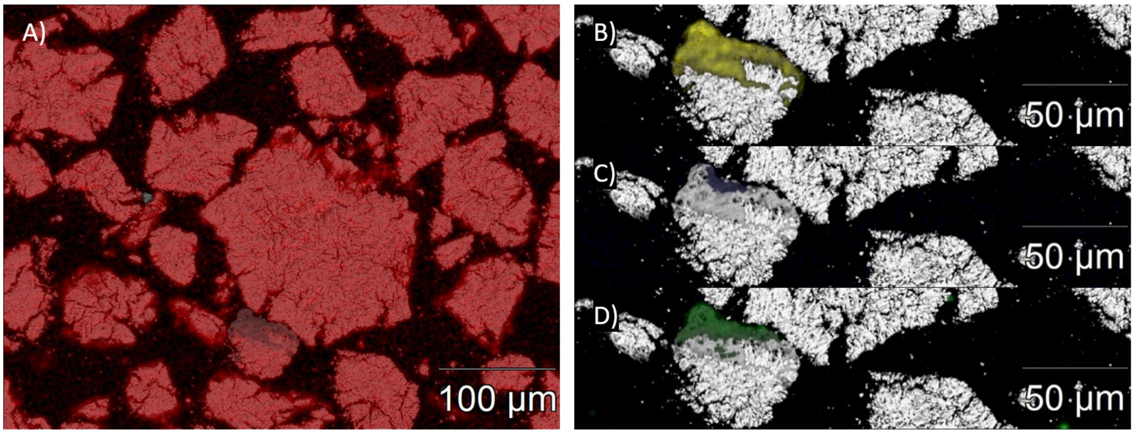

Figure 5.7: SEM-EDS elemental maps of the sample of Glödskal reduced in the presence of K_2CO_3. A) Fe in red, B) K in yellow, C) Al in blue, D) Si in green.

interactions between Glödskal and K_2CO_3 are more thoroughly discussed in context of the TGA results (Section 5.2: Thermogravimetric analysis).

5.1.2.5 Glödskal reduced in the presence of K_2SO_4

SEM-EDS elemental maps of K and S of Glödskal reduced in the presence of K_2SO_4 are presented in Figure 5.8 and shows that K and S is present in and outside of the material. A quantitative analysis of the EDS elemental maps showed that the mass ratio between K and S is higher than the mass ratio in K_2SO_4, suggesting decomposition of the salt and the formation of a gaseous S-component.

With complete reduction of hematite to magentite, the additional weight change corresponds to approximately 35% of the salt weight, so like in the test with K_2CO_3, a significant amount of ash component should still be present in the bed. This high presence of ash component can't be identified in the SEM-EDS analysis.

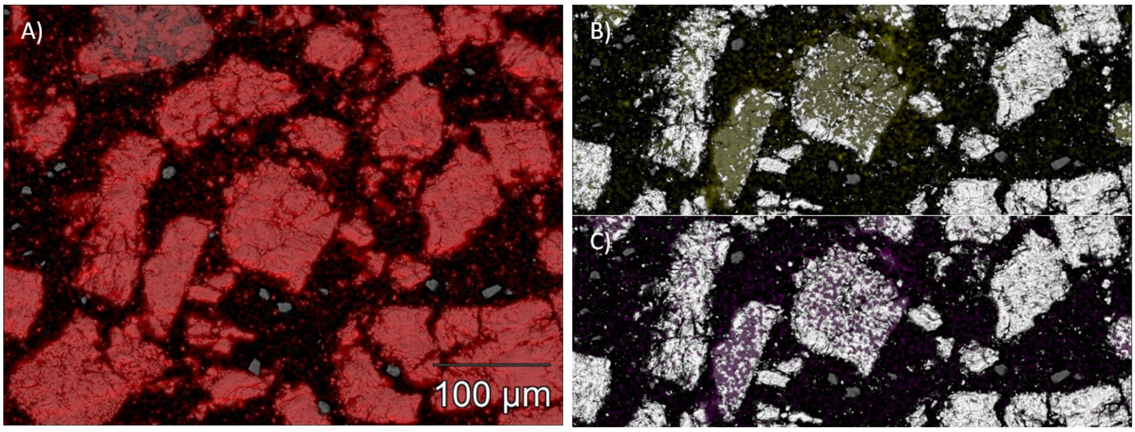

Figure 5.8: SEM-EDS elemental maps of the sample of Glödskal reduced with K_2SO_4. A) Fe in red B) K in yellow and C) S in purple.

5.1.2.6 Glödskal reduced in the presence of KH_2PO_4

When initially examining the sample bed of Glödskal reduced with KH_2PO_4 present, agglomerates could be seen with the bare eye. At temperatures over 209°C, KH_2PO_4 decomposes according to Reaction 5.3.

$$KH_2PO_4 \rightarrow KPO_3 + H_2O \tag{5.3}$$

Assuming complete reduction of hematite to magnetite in the reduction test, the additional weight change corresponds to the weight of steam in Reaction 5.3. KPO_3 has a melting temperature of 810°C, and KPO_3 has been observed in previous studies to create a melt that glues particles together [41]. The elemental maps of the sample is presented in Figure 5.9 and shows the presence of also Fe in the agglomeration bridge. Quantitative point analysis was done and the analysis in point 1 in Table 5.2

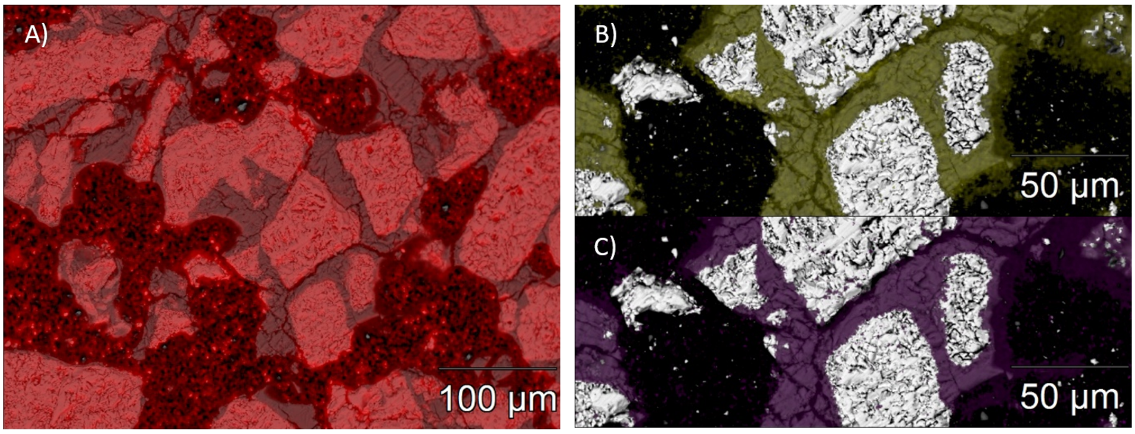

Figure 5.9: SEM-EDS elemental maps of the sample of Glödskal reduced in the presence of KH_2PO_4. A) Fe in red, B) K in yellow, C) P in purple.

show a molar ratio of 1:1:1 of Fe:K:P in the bridge. The high concentration of Fe in the bridge suggests that the agglomeration happens through the second mechanism described in Section 3.6.1 Agglomeration; that a component formed through reaction between the bed material and the ash is what contributes to agglomeration. The results for point 2, which is located in a Glödskal particle, show a low concentration of K and P.

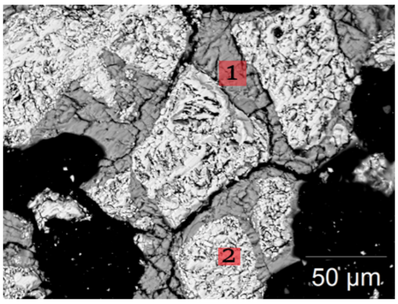

Point 1	Weight %		Point 2	Weight %	
O	33.77	± 0.38	Fe	72.37	± 0.48
Fe	29.33	± 0.32	O	26.80	± 0.17
K	19.46	± 0.16	Mn	0.36	± 0.07
P	16.38	± 0.12	K	0.18	± 0.03
Mn	0.57	± 0.07	P	0.15	± 0.04
Ca	0.37	± 0.05	Si	0.12	± 0.04
Al	0.11	± 0.03	Al	0.01	± 0.01
Si	0.00	± 0.00	...		

Table 5.2: Point analyses of the sample of Glödskal reduced in the presence of KH_2PO_4.

5.1.3 LD-slag

SEM-images of the surface of the pretreated and grinded LD-slag is presented in Figure 5.11A. Images of the reduced samples of LD-slag is presented in Figure 5.11B-F. The samples reduced with no salt present (Figure 5.11B) and reduced in the presence of KCl (Figure 5.11A) show similar structure of that of the pretreated, grinded sample; a material with a grain-like structure on the surface of the particles can be seen. The images of the samples reduced in the presence of K_2CO_3 and K_2SO_4 (Figure 5.11D and 5.11E), show a partly smooth structure which can suggest a melt has been formed during reduction that covers parts of the particles. The image of the sample reduced in the presence of KH_2PO_4 (Figure 5.11F) also suggests that a phase has melted and later solidified on the surface. It also looks like several small particles are attached to the larger particle in the image, and that the salt thus has caused agglomeration in the material. The beds of reduced samples were all similar in consistency; they were all compact like wet sand and the beds fell apart easily upon disturbance. Agglomerated particles could be seen when KH_2PO_4 had been present during reduction.

Due to the presence of many different phases in LD-slag, phase analysis has been done on the SEM-EDS elemental maps for better understanding of the composition and interaction with the ash components. Both phase maps and elemental maps are used in the following sections to present the findings from the reduction tests of LD-slag. Composition bulk analyses of all the samples are included in Appendix A and elemental maps in grey-scale are included in Appendix C.

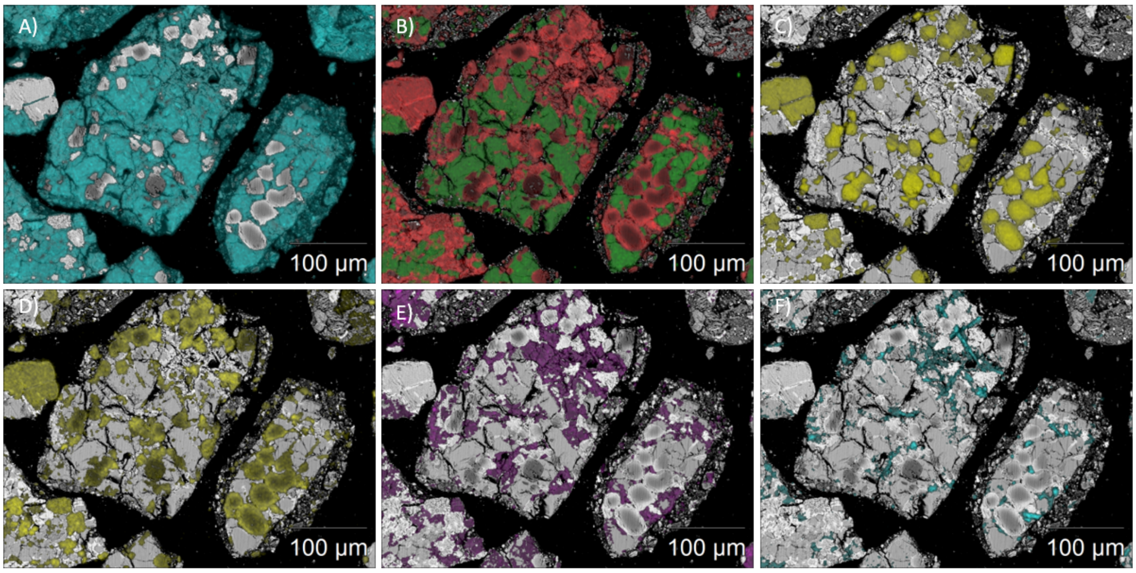

Figure 5.10: SEM-EDS elemental maps of the cross-section of pretreated LD-slag. A) Ca in cyan, B) Fe in red and Si in green, C) Mg in yellow, D) Mn in yellow, E) V in purple and F) Ti in cyan.

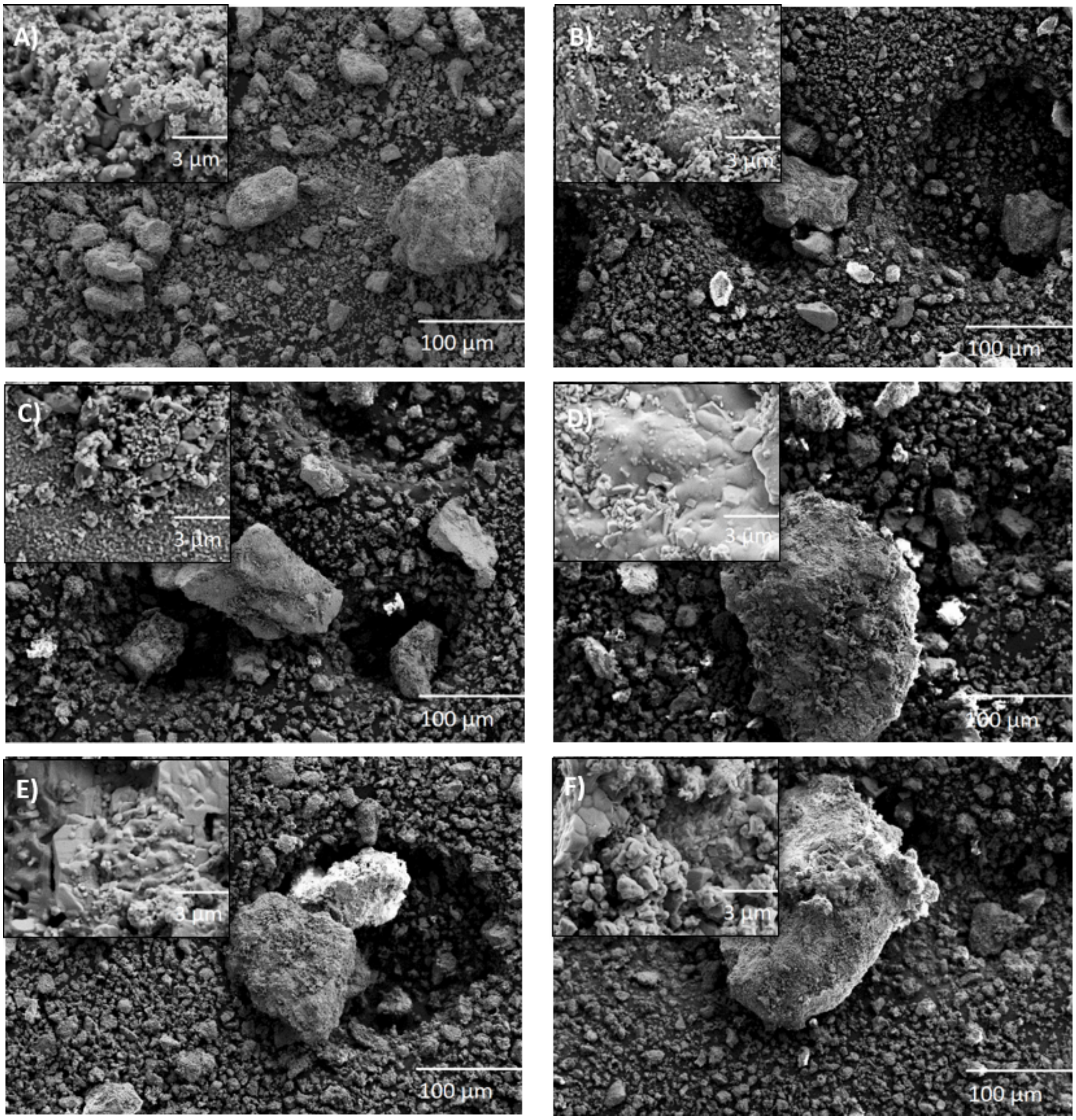

Figure 5.11: Surface images of the samples of LD-slag A) heat treated and grinded B) reduced without salt, C) reduced in the presence of KCl, D) reduced in the presence of K_2CO_3, E) reduced in the presence of K_2SO_4, F) reduced in the presence of KH_2PO_4.

5.1.3.1 Pretreated LD-slag

SEM-EDS elemental maps of pretreated LD-slag can be seen in Figure 5.10. The particles have not been grinded before the analysis presented here. The maps show that LD-slag consists of many different phases.

5.1.3.2 LD-slag reduced without salt

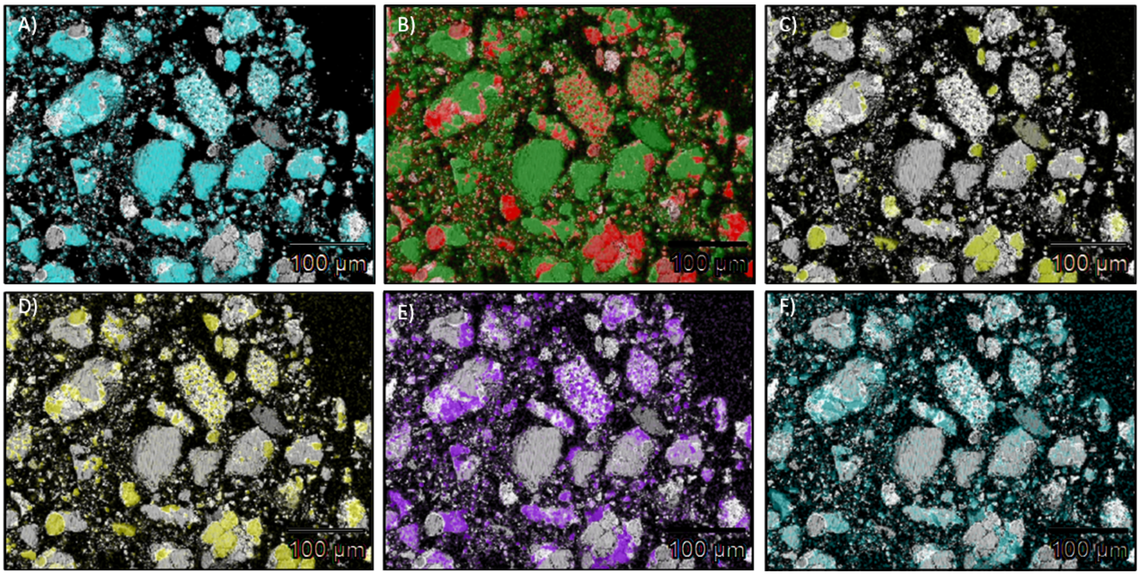

Figure 5.12: SEM-EDS elemental maps of the cross-section of LD-slag reduced without salt. A) Ca in cyan, B) Fe in red and Si in green, C) Mg in yellow, D) Mn in yellow, E) V in purple and F) Ti in cyan.

SEM-EDS elemental maps of the sample of LD-slag reduced with no salt present are presented in Figure 5.12. The location of Ca, Fe, Si, Mg, Mn V and Ti are marked. No clear differences can be seen between LD-slag before and after reduction.

5.1.3.3 LD-slag reduced in the presence of KCl

The two phases with the highest K-concentration can be seen in Figure 5.13, marked in pink and blue. The concentration of K is low (0,21 wt% K and 0,66 wt% in the phases marked in pink and blue, respectively), so no potassium can be said to have diffused into the particles.

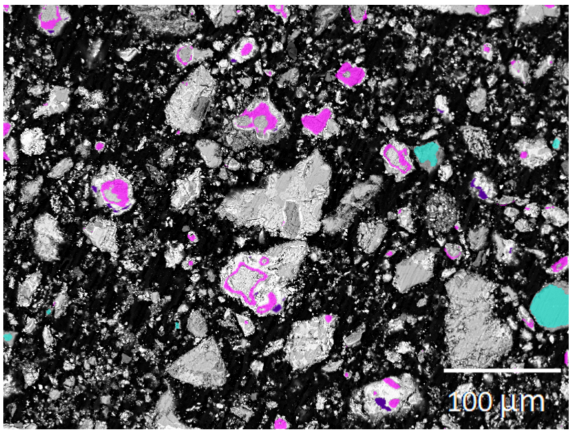

Figure 5.13: Map of the two phases containing the highest amount of K

The large weight reduction and the low K-concentration in the sample results from that KCl evaporates in the reduction and is not captured by the material, which was also the case with Glödskal.

5.1.3.4 LD-slag reduced in the presence of K_2CO_3

SEM-EDS analysis of LD-slag reduced in the presence of K_2CO_3 showed the presence of K, and it seems to be located mainly close to the surface of the particles. The elemental map of K had significant overlapping with the map of P and was almost identical to the map of V, as can be seen in Figure 5.14

The location and composition of the four most K-rich phases are presented in Table 5.3. The green-, blue-, orange-, and purple-marked phases contain 14,55, 7,65, 7,53 and 6,70 wt-% K respectively. The phase maps show that K is located mainly together with Ca (in 19-34wt-%), Fe (in 4-11wt-%) and V (in 5-11wt-%). The presence of Ca and Fe in the phases can be explained by that they are the most abundant components in the LD-slag, but the concentration of V is significantly higher in the K-rich phases compared to the V-concentration seen in the bulk analysis. A comparison of the elemental maps of V and K presented in Figure 5.7 show a significant

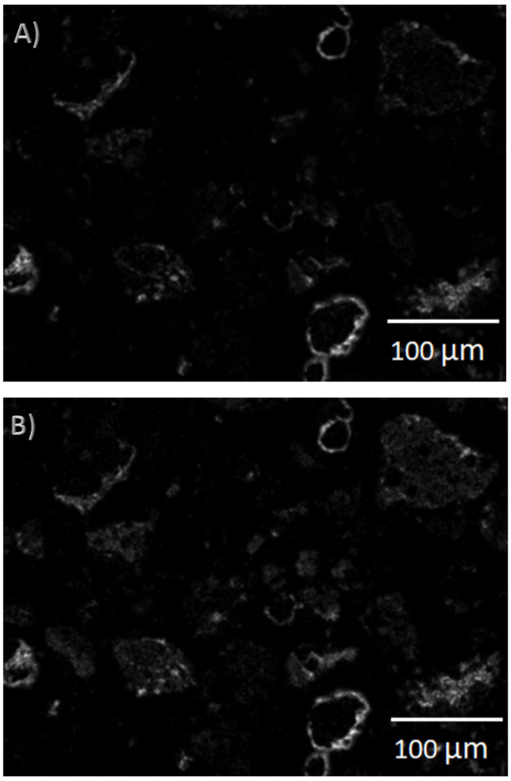

Figure 5.14: SEM-EDS elemental map of the sample of LD-slag reduced in the presence of K_2CO_3 A) map of K B) map of V

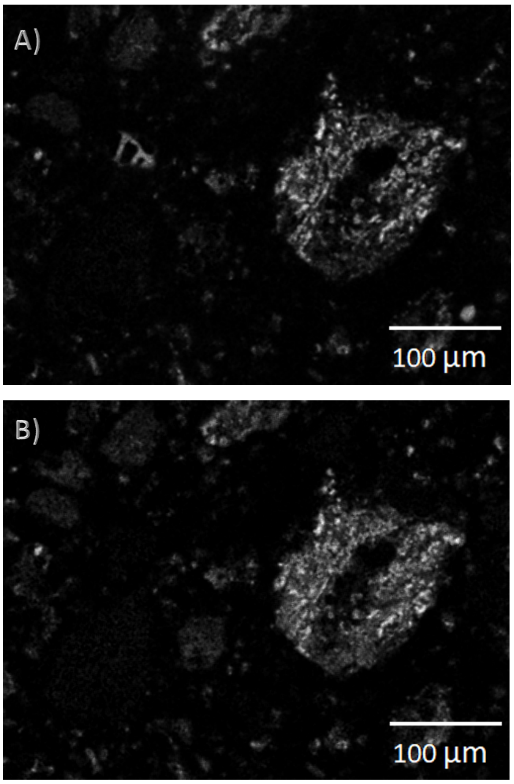

Figure 5.15: SEM-EDS elemental map of the sample of LD-slag reduced in the presence of K_2SO_4 A) map of K B) map of V

overlapping of the two elements. This overlapping can't be observed with any other element in the LD-slag. The mass ratio between K and V is similar for the four phases (between 1,16 and 1,31), suggesting the formation of a specific component with V and K.

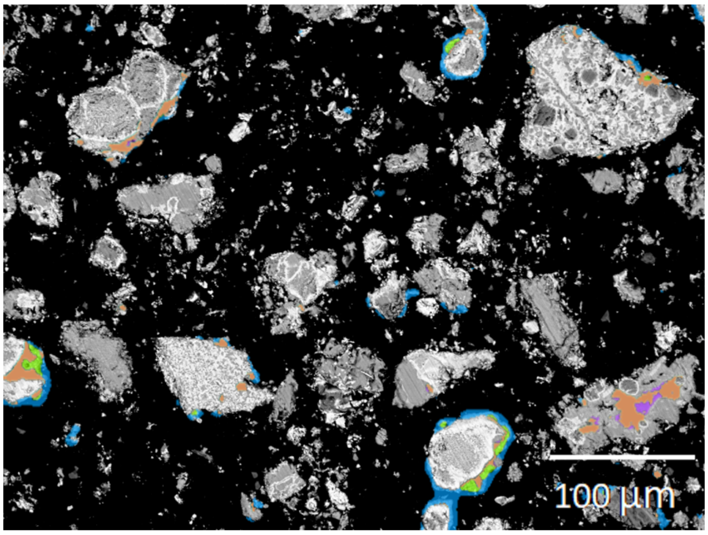

Green	**Weight%**	**Blue**	**Weight%**
O	24.13 ± 0.39	O	19.27 ± 0.36
Ca	19.47 ± 0.17	Ca	14.80 ± 0.07
K	14.55 ± 0.12	K	7.65 ± 0.05
V	11.16 ± 0.14	V	6.60 ± 0.05
Fe	7.58 ± 0.11	Fe	5.72 ± 0.07
Na	1.75 ± 0.09	Si	1.60 ± 0.02
Si	1.75 ± 0.03	Mn	0.56 ± 0.02
...		...	

Orange	**Weight%**	**Purple**	**Weight%**
Ca	26.27 ± 0.10	Ca	34.00 ± 0.28
O	24.21 ± 0.37	O	29.29 ± 0.52
Fe	11.17 ± 0.10	Si	9.21 ± 0.12
K	7.52 ± 0.05	K	6.66 ± 0.14
V	5.72 ± 0.06	V	5.32 ± 0.18
Si	4.91 ± 0.04	Fe	4.48 ± 0.23
Mg	1.67 ± 0.04	Ti	1.07 ± 0.07
Mn	1.43 ± 0.06	...	
...			

Table 5.3: The four most K-rich phases identified in the sample of LD-slag reduced in the presence of K_2CO_3

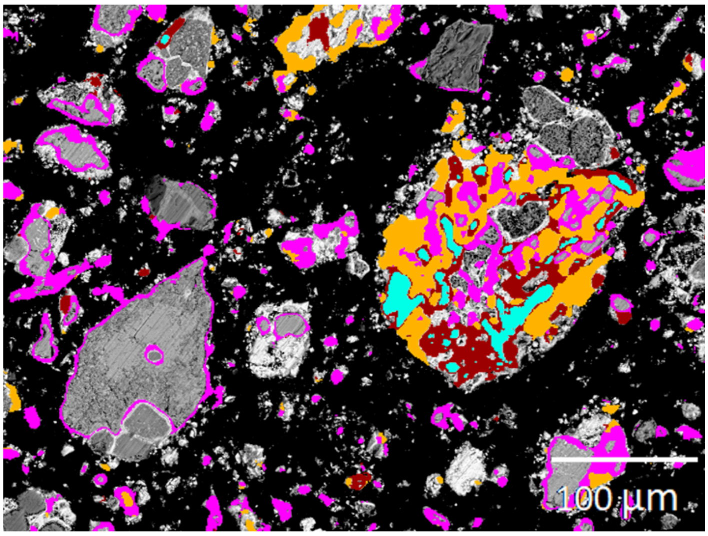

Yellow	**Weight%**	**Red**	**Weight%**
Ca	26.78 ± 0.07	Ca	27.32 ± 0.07
O	23.24 ± 0.24	O	23.60 ± 0.26
Fe	7.91 ± 0.04	Fe	18.11 ± 0.07
K	6.58 ± 0.03	Ti	3.86 ± 0.03
V	6.11 ± 0.03	V	3.58 ± 0.03
Si	5.05 ± 0.02	Al	2.37 ± 0.02
P	0.49 ± 0.01	K	2.25 ± 0.02
...		Si	1.43 ± 0.01
		...	

Cyan	**Weight%**	**Pink**	**Weight%**
O	30.96 ± 0.30	O	29.32 ± 0.24
Ca	26.96 ± 0.09	Ca	26.27 ± 0.06
Fe	16.48 ± 0.11	Si	7.19 ± 0.02
Ti	5.78 ± 0.06	Fe	5.57 ± 0.03
V	4.29 ± 0.06	K	1.63 ± 0.01
Al	2.75 ± 0.03	V	1.57 ± 0.02
K	2.22 ± 0.04	Na	0.35 ± 0.01
...		...	

Table 5.4: The four most K-rich phases identified in the sample of LD-slag reduced in the presence of K_2CO_3

5.1.3.5 LD-slag reduced in the presence of K_2SO_4

The SEM-EDS analysis of the sample of LD-slag reduced in the presence of K_2SO_4 showed a high K-content, and no to very low S content. Similarly to in the LD-slag reduced with K_2CO_3, the elemental maps of K and V are very similar and are presented together in Figure 5.15. The locations and compositions of the four most K-rich phases are presented in Table 5.4 and show that K exists mainly together with Ca, Fe, V, Si, and Ti. The yellow-, red-, cyan-, and pink-colored phases contain 6,58, 2,25, 2,22 and 1,63 wt-% respectively.

5.1.3.6 LD-slag reduced in the presence of KH_2PO_4

When KH_2PO_4 had been present in the reduction of LD-slag agglomerated, black particles could be seen on the surface of the sample. The most K-rich phases obtained from phase analysis on the SEM-EDS maps can be seen in Table 5.5. The phase analysis show that the bridge between the OC particles (marked in Cyan) mainly consists of K, Ca and P, approximately in the molar ratio 1:1:1. Fe is also present in the bridge, but in lower concentration. Other phases with high K-content is has similar composition. It can be concluded that the ash component has interacted with both Ca and Fe in the LD-slag.

The structure of the agglomerates differ from that of the Glödskal reduced with KH_2PO_4. The agglomeration bridge in the LD-slag does not show the same coating properties. The bridge can be seen to create a more web-like, porous structure between the particles. The sample bed also didn't have the same solid consistency as the Glödskal sample bed, which suggests the LD-slag does not suffer from agglomeration by KH_2PO_4 in the same extent as Glödskal does. The interaction between LD-slag is discussed more thoroughly in the context of the TGA results (Section 5.2: Thermogravimetric analysis.)

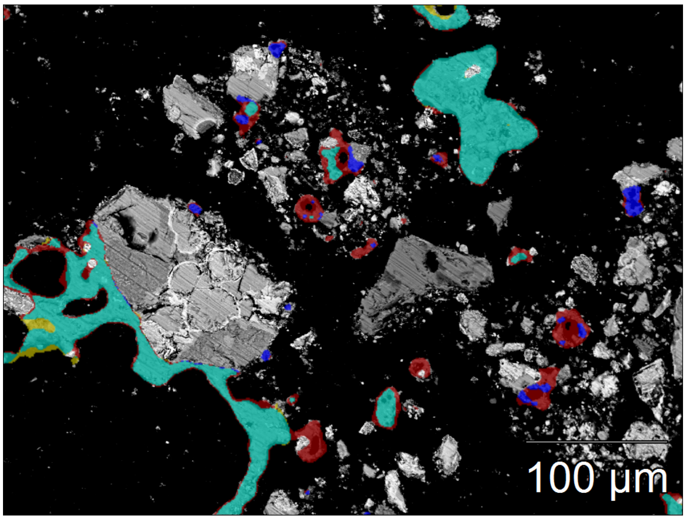

Cyan	**Weight%**		**Yellow**	**Weight%**	
K	30.50	± 0.09	O	24.37	± 0.84
P	22.41	± 0.07	K	23.37	± 0.20
Ca	24.89	± 0.08	Fe	15.59	± 0.32
O	12.37	± 0.42	Ca	10.18	± 0.11
Fe	4.08	± 0.05	P	8.11	± 0.15
Si	1.57	± 0.01	Si	7.54	± 0.13
Mg	1.33	± 0.02	Mg	3.82	± 0.10
Mn	1.01	± 0.04	Mn	2.89	± 0.12
...			Ti	1.99	± 0.12
Red	**Weight%**		**Blue**	**Weight%**	
Ca	36.46	± 0.14	Ca	40.58	± 0.18
P	22.34	± 0.09	O	27.57	± 0.58
K	19.55	± 0.10	P	18.80	± 0.10
Fe	9.69	± 0.11	K	5.55	± 0.08
Si	2.82	± 0.02	Fe	3.42	± 0.08
Mg	2.70	± 0.04	Si	2.07	± 0.03
Mn	2.31	± 0.05	...		

Table 5.5: The four most K-rich phases identified in the sample of LD-slag reduced with KH_2PO_4

5.2 Termogravimetric analysis

5.2.1 Glödskal

The weight and temperature measured in TGA of the Glödskal samples can be seen in Figure 5.16. For the sample containing KH_2PO_4, a weight decrease is measured during the whole heating period and the first stabilization period, with a start at around 250°C. The weight change corresponds to the decomposition into KPO_3 and H_2O (Reaction 5.3). For the sample with K_2CO_3 a small weight change is measured in the beginning, at around 200°C. A larger weight drop is measured at around 670°C, which corresponds to decomposition into K_2O and CO_2 (Reaction 5.1). Both KH_2PO_4 and K_2CO_3 are hygroscopic, so a small part of the weight change is due to water evaporating from the sample. No weight change can be seen during the heating period for the control sample or for the sample mixed with K_2SO_4. There is thus no decomposition of K_2SO_4 in inert atmosphere.

In the first reduction period, the weight of the control sample is stabilized after approximately 20 minutes. The weight change corresponds to complete reduction of hematite to magnetite. The reduction of the sample with K_2CO_3 is faster than

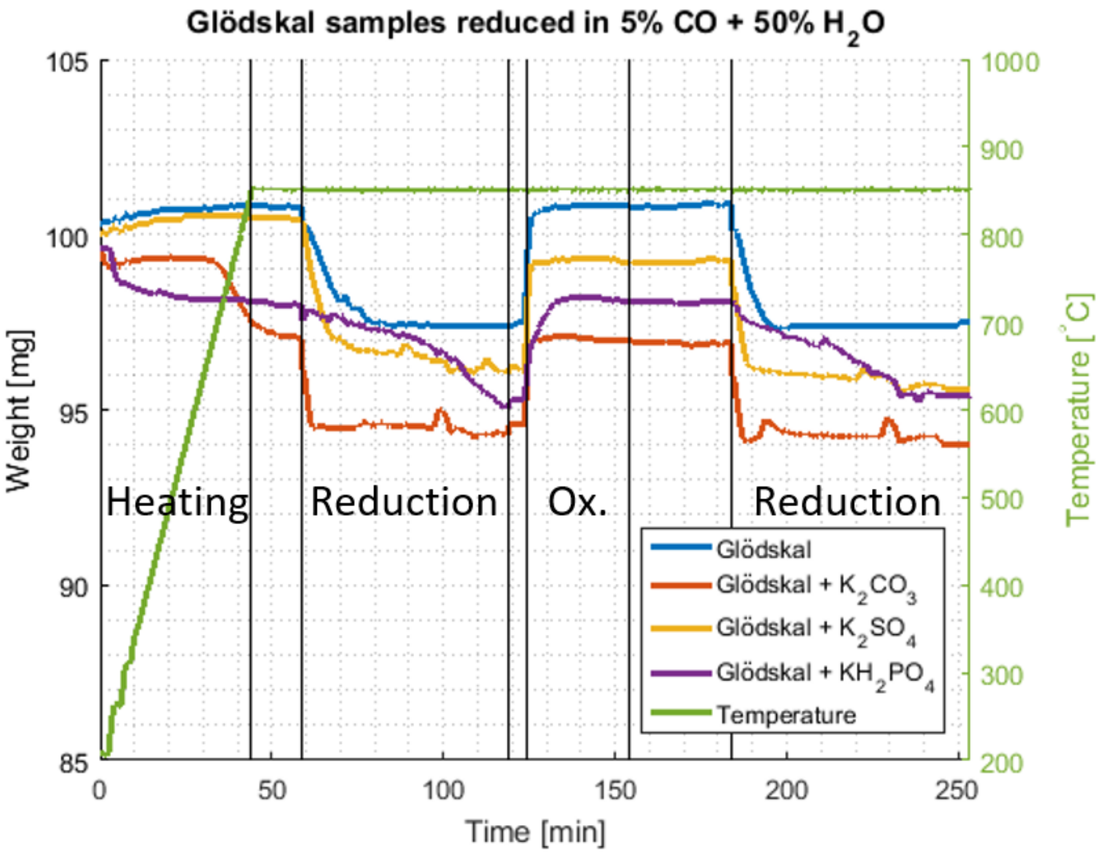

Figure 5.16: The temperature (°C) and weights (mg) measured in the 4 TGA tests using Glödskal as oxygen carrier and 5% CO and 50% steam as reducing atmosphere.

control, and the sample is fully reduced within the first 5 minutes. Both samples are fully oxidized within 5 minutes. The sample with K_2CO_3 reaches the weight seen immediately before reduction, suggesting no further evaporation of ash component is happening in reducing atmosphere. The weight of the sample with K_2SO_4 is decreasing during the whole reduction period and the weight change exceeds that of complete reduction of hematite to magnetite with about 1,2% of the sample weight. K_2SO_4 is thus decomposing in the presence of steam and CO. The reduction rate is similar to that of the control sample. The sample is fully oxidized within 5 minutes. The reduction of the sample with KH_2PO_4 is slow, and the weight is never stabilized. The oxidation of the sample takes approximately 10 minutes.

The reduction rate if faster for control sample, the sample with K_2SO_4 and the sample with KH_2PO_4 in the second reduction period compared to the first. The material is thus activated during the test. The weight of the sample with K_2SO_4 is not stabilizing, which suggests a continuing decomposition of K_2SO_4 also in the second reduction period.

The results from reduction tests and TGA are the basis to some discussion about the interactions between Glödskal and ash components. The elemental maps of the sample reduced with K_2SO_4 suggested some diffusion of K and potentially also S into the Glödskal particles, while the sample with K_2CO_3 showed no sign of diffusion. The surface also looked different between the two samples, as was mentioned earlier. The difference in interactions could be due to the difference in decomposition mechanisms; K_2SO_4 only decomposes in the presence of steam and CO, and thus KOH is likely to form and react with Glödskal. K_2CO_3, on the other hand, is decomposing already in the heating period (Reaction 5.1). K_2O is unstable, and thus likely to either react with Glödskal directly when it's formed or decompose further. A fast reduction rate is seen already in the beginning of the first reduction period which further suggests that interactions between Glödskal and K_2CO_3 are happening already in the dry, inert heating period. Future work could test if the reaction mechanisms differ if steam is present also in the heating or loading of the ash, which might be is a more realistic simulation of a real CLC system. According to the weight change in the tests, Glödskal has the ability to capture K from both K_2SO_4 and K_2CO_3. The form and location of the captured K is not fully understood from the XRD and SEM-EDS analysis. The diffractograms show no significant unidentified peaks that suggest that another component is present except for magnetite.

The SEM-EDS results showed that interaction with KH_2PO_4 leads to agglomeration by a molten phase consisting of K, P and Fe. This phase can be seen in the images to not only bind the particles together but also to create a coating around them, which blocks the contact between oxygen carrier and gas. This also explains the low reduction and oxidation rates in TGA.

5.2.2 LD-slag

The weight and temperature measured in TGA of the LD-slag samples can be seen in Figure 5.17. The LD-slag samples show similar behaviour as the Glödskal samples in the heating period; the control sample and the sample with K_2SO_4 show no weight change, and the weight change with K_2CO_3 and KH_2PO_4 corresponds to decomposition of the ash component.

In the first reduction period, the weight of the control sample is stabilized after approximately 10 minutes. The weight change in percent is the same as seen in the reduction test, and is thus assumed to correspond to complete reduction of the material. The sample with K_2SO_4 show a continuous weight change during the whole reduction period, and the total weight change exceeds that of complete reduction. This behaviour was seen also for the sample of Glödskal and K_2SO_4, and means that the salt decomposes in reducing atmosphere. The sample with KH_2PO_4 is fully reduced after approximately 15 minutes. The sample with K_2CO_3 is the one that differs the most from the control; showing a slow weight reduction in the reducing period. It thus seems like the ash component is inhibiting the reduction of the material. There is also a small weight increase in the beginning of the reduction period. All the samples, except the one with K_2CO_3, show a fast weight increase that

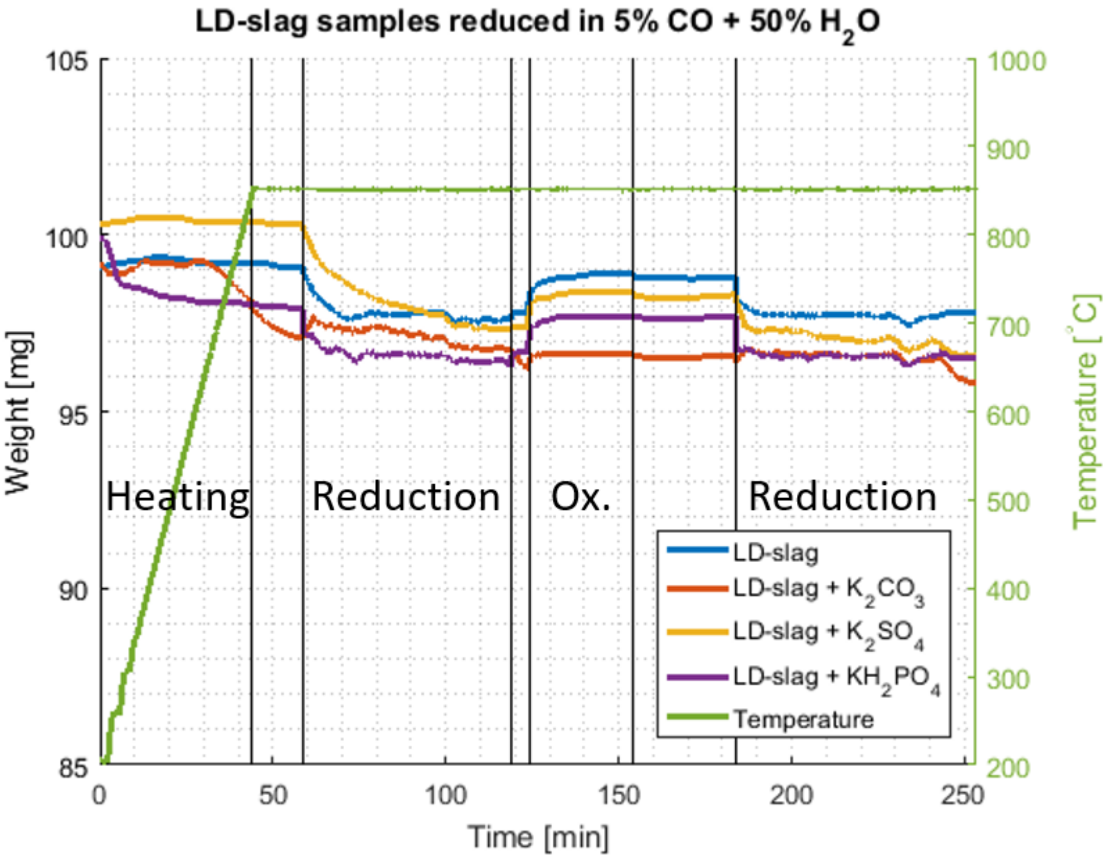

Figure 5.17: The temperature (°C) and weights (mg) measured in the 4 TGA tests using LD-slag as oxygen carrier and 5% CO and 50% steam as reducing atmosphere.

corresponds to complete oxidation in the oxidation period. The control sample and the sample with KH_2PO_4 reaches the same weights they had before the reduction step. The weight of the sample with K_2SO_4 is 2% lower after oxidation compared to before reduction, due to the decomposition of the ash component. The sample with K_2CO_3 shows only a small weight increase in the oxidation period, and much smaller than would be expected for complete oxidation.

For the control sample, the sample with KH_2PO_4 and possibly also the sample with K_2SO_4, the reduction rates are higher in the second reduction step compared to the first, which suggests that the material is activated in the first cycle. The sample with K_2SO_4 shows a weight change also during the whole second reduction period. The total weight change in the TGA of the sample with K_2SO_4 (3,4%) does not reach that seen in the reduction test (4,6%), so the salt decomposition is possibly continuing and slow.

6. Discussion

The presence of KH_2PO_4 causes agglomeration in LD-slag, but the reduction and oxidation rates are not affected. As with Glödskal, the agglomeration is described by the second mechanism in Section 3.6.1 Agglomeration. The weight ratio in the Glödskal sample suggests the formation of $KFePO_4$, but in the LD-slag sample, the agglomeration is caused by reaction with Ca instead of Fe. As was also discussed earlier, adding limestone to fluidized beds is a method used to reduce agglomeration in biomass combustion. When no Ca is present, (as is the case with Glödskal), the formed P- and K-rich components have lower melting temperatures and cause more agglomeration problems. Theses tests suggest that the Ca-content inherent to LD-slag makes it more resistant to agglomeration compared to Glödskal. This positive effect can be seen both in TGA (reactivity is not affected), and in the SEM-images (the particle surface is not covered).

It should be noted that these tests are done in a fixed bed, so the agglomeration effects shown here might not be representative for what happens in an actual fluidized bed. In a fluidized bed, the particles are moving at high speed and don't have the same time to sinter. The agglomeration glue is liquid in combustion temperatures and other problems like deposition on boiler surfaces could be more significant.

KCl seems to evaporate in the reduction tests and have no or little interaction with wither LD-slag or Glödskal. Traces of K and Cl can be seen in the samples, but mainly in the epoxy matrix outside of the particles. The porosity of Glödskal increases when KCl is added in the reduction.

K_2CO_3 seems to interact with both Glödskal and LD-slag. The most significant findings with Glödskal is that the porosity and the reduction rate increases compared to without ash component. Porosity increase is beneficial for the contact between the material and the gases. However, as discussed by Leion et. al [30], a continuous porosity increase without stabilization can lead to the material breaking down to a fine dust and leaving with the flue gases. Previous tests have not determined how many cycles it takes for Glödskal to stabilize. Future work could thus focus on how the material is affected by more reduction and oxidation cycles to evaluate if this is a risk for Glödskal in its expected lifetime in the bed. The same type of porosity increase was not seen for LD-slag. LD-slag suffers instead from deactivation when K_2CO_3 is present in the ash; there is a drastic decrease in reduction rate, and the material doesn't seem to be fully reoxidized in the oxidation period of the TGA. No explanation for the deactivation has been suggested on the basis of these tests.

The effect could possibly be explained with more knowledge about the reduction and oxidation mechanisms of the LD-slag.

When K_2SO_4 is added to the reduction tests, K and traces of S can be seen in both the Glödskal and the LD-slag samples, suggesting that the ash component diffuses into the particles and stays in the material. The weight reduction and the TGA results are similar for both Glödskal and LD-slag, and shows that the ash component decomposes in reducing atmosphere. Having K_2SO_4 present in the TGA has no or little effect on the reduction rate of either Glödskal or LD-slag. The weight difference before reduction and after oxidation when K_2SO_4 is present is larger when LD-slag is used as oxygen carrier (2% difference), compared to when Glödskal is used (1,2%), suggesting that some component in the LD-slag is enhancing the decomposition of K_2SO_4. SiO_2 is likely present in LD-slag and has previously been observed to decrease the decomposition temperature of K_2SO_4 while forming K_2SiO_3 and gaseous S-components [42]. This effect could explain the higher decomposition rate with LD-slag. The SEM-EDS analysis showed that the locations of V and K in LD-slag were practically identical after K_2CO_3 or K_2SO_4 had been present during reduction. No further conclusions have been drawn from these tests on what is causing this or how this might affect the OC, but it could be interesting to investigate more in future studies.

Even if the oxygen transport capacity of the LD-slag seems low (about 1wt-%), the OC can still be efficient in CLC application. In the CLC system, the solid circulation must be high enough to supply heat form the AR, where the reactions are overall exothermic, to the overall endothermic reactions in the FR [30]. 1wt-% oxygen transport capacity could therefor be sufficient, if the material is reactive enough to reach complete reduction of the fuel. The high reduction rate of the material seen in the TGA supports the option of having LD-slag as a OC. The lower oxygen transport capacity might also be beneficial in the context of using LD-slag as an OC for CLR. As discussed earlier, the reaction in the FR of a CLR system should have selectivity towards partial oxidation to produce CO and H_2. Having an OC with low oxygen transport capacity could mean possibility to perform the partial oxidation in a more controlled way. Suitability for CLR would also focus on other properties like catalytic effects on the reaction, and these are not discussed in this study.

Future studies could include investigating the interacitons between the OCs and KOH, to see how it differs from K_2SO_4 and K_2CO_3. It could also be interesting to investigate how having steam in the heating period would affect the salt decompostition and if this effects the OC differently. Further experiments should be done to conclude what causes the deactivation of LD-slag when K_2CO_3 is present, if this effect (a) is significant in real CLC of biomass and (b) can be avoided by addition of some sorbent material or similar. Analysing the LD-slag more carefully to determine the exact reduciton and oxidation mechanisms should also be done to better understand how the ash components are affecting the material.

As a final remark, it should be noted that most of these tests have been conducted only once. Repeating them and doing more extensive SEM-EDS analyses would give more reliable results, but this could not be done due to time restriction. The TGA of LD-slag and K_2CO_3 was repeated due to the unexpected results in the first run. The second test gave similar results.

7. Conclusion

In an atmosphere of 5% CO and 45% steam and at 850°C, Glödskal is reduced after 20 minutes. LD-slag is reduced after 10 minutes in the same environment. The presence of KCl, K_2CO_3 or K_2SO_4 has a positive effect on the porosity increase of Glödskal in reduction. K_2CO_3 has the largest effect on porosity.

The presence of K_2CO_3 increases the reduction rate of Glödskal. This has been seen in previous studies and has been concluded to be due to the increased porosity.

With Glödskal, KH_2PO_4 creates a phase consisting of Fe, K and P that melts, covers the particles, and makes them agglomerate. The presence of KH_2PO_4 greatly reduces the reduction rate of Glödskal for this reason.

With LD-slag, KH_2PO_4 creates a phase consisting mainly of Ca, K and P. The phase exists as bridges holding the particles together but does not create a coating on the outside of the particles. KH_2PO_4 has no or little effect on the reduction rate of the LD-slag.

SEM-EDS analysis of LD-slag reduced in the presence of K_2CO_3 showed K located together with Ca and Fe.

SEM-EDS analysis of LD-slag reduced in the presence of K_2CO_3 or K_2SO_4 showed accumulation of K in the same location as V.

7. Bibliography

[1] B. Metz, O. Davidson, H. C. de Coninck, M. Loos, and L. A. Meyer (eds.) *IPCC Special Report on Carbon Dioxide Capture and Storage.* 2005, p. 442.

[2] Anand B. Rao and Edward S. Rubin. "A Technical, Economic, and Environmental Assessment of Amine-Based CO2 Capture Technology for Power Plant Greenhouse Gas Control". In: *Environmental Science & Technology* 36.20 (2002), pp. 4467–4475.

[3] Mohammad M. Hossain and Hugo I. de Lasa. "Chemical-looping combustion (CLC) for inherent CO2-separations - a review". In: *Chemical Engineering Science* 63.18 (2008), pp. 4433–4451.

[4] Juan Adánez et al. "Progress in chemical-looping combustion and reforming technologies". In: *Progress in Energy and Combustion Science* 38.2 (2012), pp. 215–282.

[5] Matthew E. Boot-Handford et al. "Carbon capture and storage update". In: *Energy Environ. Sci.* 7.1 (2014), pp. 130–189.

[6] Berend Smit et al. *Introduction to carbon capture and sequestration.* 2014, pp. 281–354.

[7] IPCC. *Climate Change 2014: Mitigation of Climate Change.* 2014, p. 1454.

[8] Saleh A. Al-Sayari. "Recent Developments in the Partial Oxidation of Methane to Syngas". In: *The Open Catalysis Journal* 6.1 (2013), pp. 17–28.

[9] Anirban Nandy et al. "Present status and overview of Chemical Looping Combustion technology". In: *Renewable and Sustainable Energy Reviews* 59 (2016), pp. 597–619.

[10] Anders Lyngfelt. "Chemical-looping combustion of solid fuels - Status of development". In: *Applied Energy* 113 (2014), pp. 1869–1873.

[11] Warren K. Lewis and Edwin R. Gilliand. *Production of Pure Carbon Monoxide.* 1954.

[12] Tobias Mattisson, Anders Lyngfelt, and Henrik Leion. "Chemical-looping with oxygen uncoupling for combustion of solid fuels". In: *International Journal of Greenhouse Gas Control* 3.1 (2009), pp. 11–19.

[13] Henrik Leion, Tobias Mattisson, and Anders Lyngfelt. "Solid fuels in chemical-looping combustion". In: *International Journal of Greenhouse Gas Control* 2.2 (2008), pp. 180–193.

[14] Martin Keller, Henrik Leion, and Tobias Mattisson. "Mechanisms of Solid Fuel Conversion by Chemical Looping Combusiton (CLC) using Mangenese Ore: Catalytic Gasification by Potassion Compounds". In: *Energy Technology* 1 (2013), pp. 273–282.

[15] Henrik Leion et al. “Solid fuels in chemical-looping combustion using oxide scale and unprocessed iron ore as oxygen carriers”. In: *Fuel* 88.10 (2009), pp. 1945–1954.

[16] Lei Xu et al. “Performance of Industrial Residues as Low Cost Oxygen Carriers”. In: *Energy Procedia*. 2017.

[17] Mingchen Tang, Long Xu, and Maohong Fan. “Progress in oxygen carrier development of methane-based chemical-looping reforming: A review”. In: *Applied Energy* 151 (2015), pp. 143–156.

[18] Peining Wang, Henrik Leion, and Hairui Yang. “Oxygen-Carrier-Aided Combustion in a Bench-Scale Fluidized Bed”. In: *Energy and Fuels* 31.6 (2017), pp. 6463–6471.

[19] Angelica Corcoran et al. “Ash properties of ilmenite used as bed material for combustion of biomass in a circulating fluidized bed boiler”. In: *Energy and Fuels* 28.12 (2014), pp. 7672–7679.

[20] Henrik Thunman et al. “Using an oxygen-carrier as bed material for combustion of biomass in a 12-MWth circulating fluidized-bed boiler”. In: *Fuel* 113.x (2013), pp. 300–309.

[21] Magnus Rydén et al. “Oxygen Carrier Aided Combustion (OCAC) of Wood Chips in a Semi-Commercial Circulating Fluidized Bed Boiler Using Manganese Ore as Bed Material”. In: *Applied Sciences* 6.11 (2016), p. 347.

[22] Changqing Dong et al. “Research on the reactivity of oxygen carrier Fe2O3 for chemical looping combustion (CLC)”. In: *Asia-Pacific Power and Energy Engineering Conference, APPEEC* Clc (2010), pp. 1–4.

[23] Haiming Gu et al. *Iron ore as oxygen carrier improved with potassium for chemical looping combustion of anthracite coal.* 2012.

[24] P. den Hoed and A. Luckos. “Oxidation and Reduction of Iron-Titanium Oxides in Chemical Looping Combustion: A Phase-Chemical Description”. In: *Oil & Gas Science and Technology – Revue d’IFP Energies nouvelles* 66.2 (2011), pp. 249–263.

[25] Henrik Leion et al. “The use of ilmenite as an oxygen carrier in chemical-looping combustion”. In: *Chemical Engineering Research and Design* 86.9 (2008), pp. 1017–1026.

[26] M I Martín, F A López, and J M Torralba. “Production of sponge iron powder by reduction of rolling mill scale”. In: *Ironmaking & Steelmaking* 39.3 (2012), pp. 155–162.

[27] J. Pal, P. N. Chaudhary, and M. C. Goswami. “Utilisation of LD slag — An overview”. In: *Journal of Metallurgy and Materials Science* 45.2 (2003), pp. 61–72.

[28] Hitoshi Ono et al. “Removal of Phosphorus From LD Converter Slag By Floating of Dicalcium Silicate During Solidification.” In: *Tetsu-To-Hagane/Journal of the Iron and Steel Institute of Japan* 66.9 (1980), pp. 1317–1326.

[29] Heikki Jalkanen and Lauri Holappa. *Converter Steelmaking.* Vol. 3. Elsevier Ltd., 2014, pp. 223–270.

[30] Henrik Leion, Tobias Mattisson, and Anders Lyngfelt. “Use of Ores and Industrial Products As Oxygen Carriers in Chemical-Looping Combustion Use

of Ores and Industrial Products As Oxygen Carriers in Chemical-Looping Combustion”. In: *Energy & Fuels* 23 (2009), pp. 2307–2315.

[31] L. J.R. Nunes, J. C.O. Matias, and J. P.S. Catalão. “Biomass combustion systems: A review on the physical and chemical properties of the ashes”. In: *Renewable and Sustainable Energy Reviews* 53 (2016), pp. 235–242.

[32] Maria Zevenhoven, Patrik Yrjas, and Mikko Hupa. “Ash-Forming Matter and Ash-Related Problems”. In: *Handbook of Combustion.* Vol. 4. 2010. Chap. 14.

[33] A.-L. Elled, L.-E. Åmand, and B.-M. Steenari. “Composition of agglomerates in fluidized bed reactors for thermochemical conversion of biomass and waste fuels Experimental data in comparison with predictions by a thermodynamic equilibrium model”. In: *Fuel* 111.1 (2013), pp. 696–708.

[34] Erica Lindström et al. “Slagging Characteristics during Combustion of Cereal Grains Rich in Phosphorus”. In: *Energy & Fuels* 21.2 (2007), pp. 710–717.

[35] V Barišić, L E Åmand, and E Coda Zabetta. “The role of limestone in preventing agglomeration and slagging during CFB combustion of high phosphorus fuels”. In: *World Bioenergy* July 2015 (2008), pp. 1–6.

[36] Patrycja Piotrowska et al. “Fate of alkali metals and phosphorus of rapeseed cake in circulating fluidized bed boiler part 1: Cocombustion with wood”. In: *Energy and Fuels* 24.1 (2010), pp. 333–345.

[37] Haiming Gu et al. “Interaction between biomass ash and iron ore oxygen carrier during chemical looping combustion”. In: *Chemical Engineering Journal* 277 (2015), pp. 70–78.

[38] R.F. Egerton. *Physical Principles of Electron Microscopy.* 2016, 203 pp.

[39] Oliver H. Seeck and Bridget Murphy. *Overview of X-Ray Scattering and Diffraction Theory and Techniques.* 1st ed. New York: Pan Stanford, 2015. Chap. 1, pp. 1–12.

[40] Hiroshi Nakagawa and Yoichi Ono. “Effects of potassium chloride on the reduction of iron oxides.” In: *Transactions of the Iron and Steel Institute of Japan* 25.10 (1985), pp. 1021–1024.

[41] Hui Li et al. “Influence of ammonium phosphates on gaseous potassium release and ash-forming characteristics during combustion of biomass”. In: *Energy and Fuels* 29.4 (2015), pp. 2555–2563.

[42] Lan Zhang et al. “The Promotion Mechanism of Silicon-Aluminum on the Decomposition of Sulfates in Biomass Ash”. In: *Clean Coal Technology and Sustainable Development - Proceedings of the 8th International Synopsium on Coal Combustion, 2015.* 2016, pp. 603–607.

1. Appendix: Bulk analyses

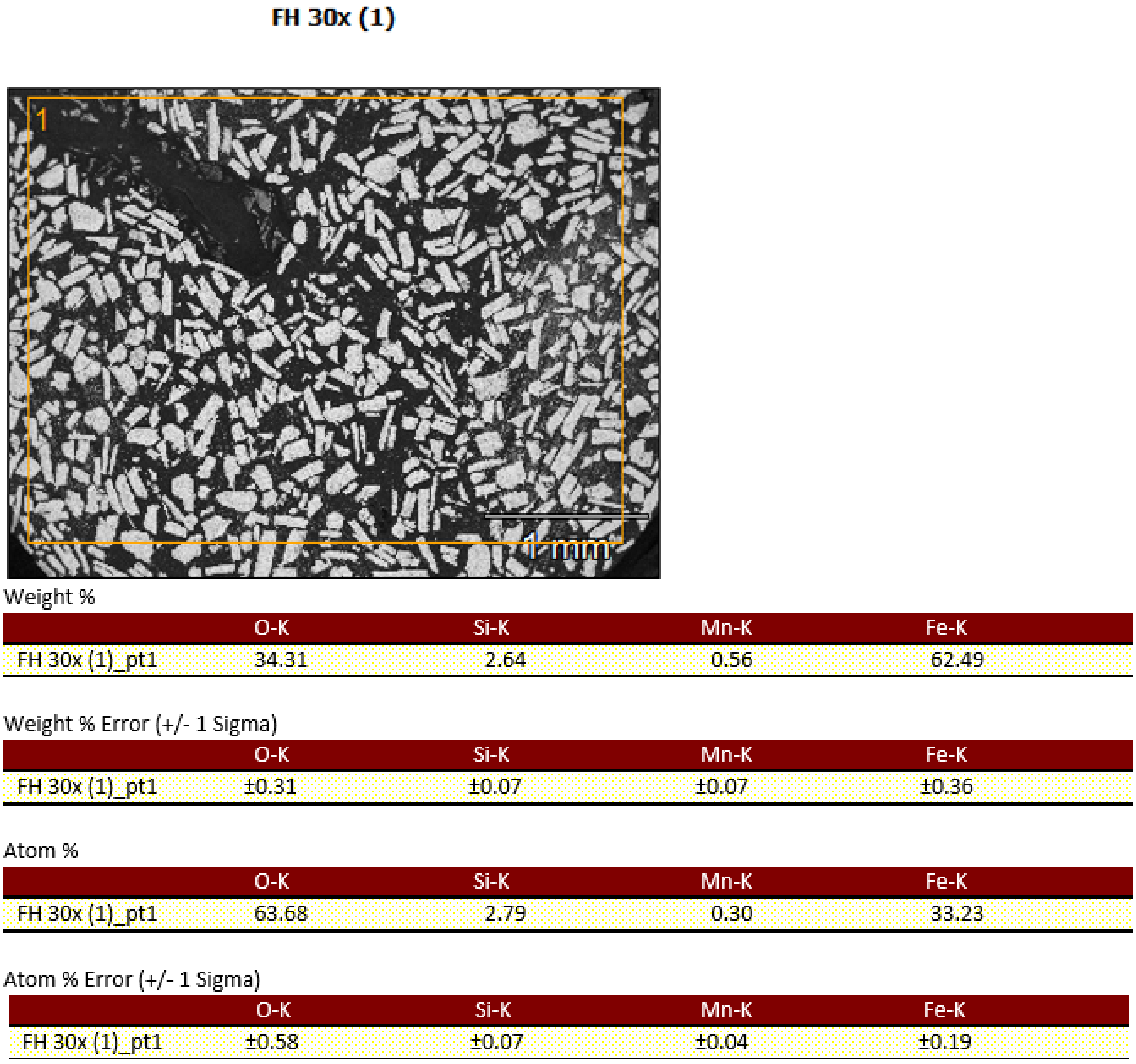

FH 30x (1)

Weight %

	O-K	Si-K	Mn-K	Fe-K
FH 30x (1)_pt1	34.31	2.64	0.56	62.49

Weight % Error (+/- 1 Sigma)

	O-K	Si-K	Mn-K	Fe-K
FH 30x (1)_pt1	±0.31	±0.07	±0.07	±0.36

Atom %

	O-K	Si-K	Mn-K	Fe-K
FH 30x (1)_pt1	63.68	2.79	0.30	33.23

Atom % Error (+/- 1 Sigma)

	O-K	Si-K	Mn-K	Fe-K
FH 30x (1)_pt1	±0.58	±0.07	±0.04	±0.19

Figure A.1: Bulk analysis of pretreated Glödskal, done with SEM-EDS analysis. The oxygen in the epoxy matrix is contributing to the wt% of oxygen in the analysis

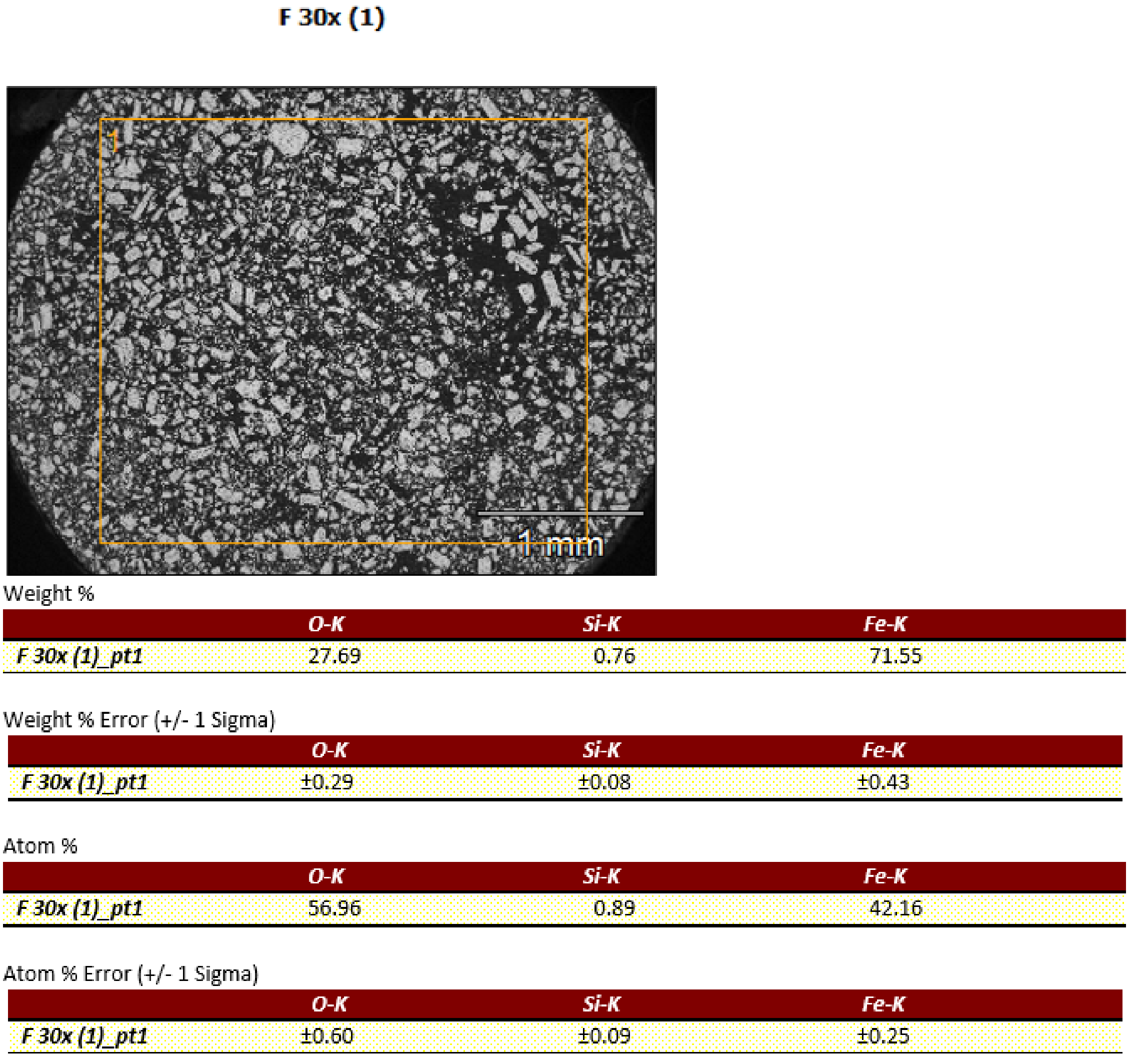

F 30x (1)

Weight %

	O-K	Si-K	Fe-K
F 30x (1)_pt1	27.69	0.76	71.55

Weight % Error (+/- 1 Sigma)

	O-K	Si-K	Fe-K
F 30x (1)_pt1	±0.29	±0.08	±0.43

Atom %

	O-K	Si-K	Fe-K
F 30x (1)_pt1	56.96	0.89	42.16

Atom % Error (+/- 1 Sigma)

	O-K	Si-K	Fe-K
F 30x (1)_pt1	±0.60	±0.09	±0.25

Figure A.2: Bulk analysis of reduced Glödskal, done with SEM-EDS analysis. The oxygen in the epoxy matrix is contributing to the wt% of oxygen in the analysis

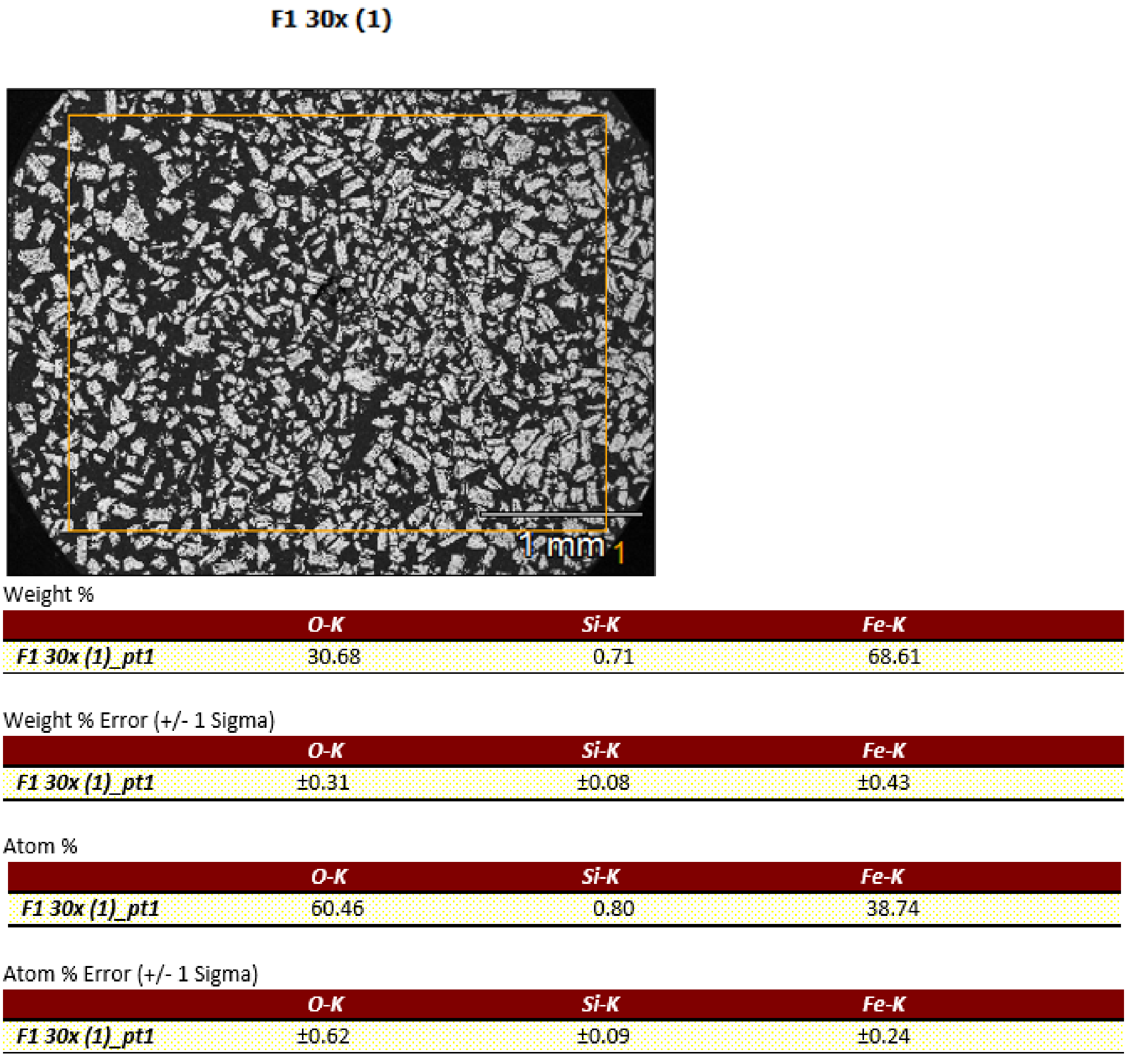

F1 30x (1)

Weight %

	O-K	Si-K	Fe-K
F1 30x (1)_pt1	30.68	0.71	68.61

Weight % Error (+/- 1 Sigma)

	O-K	Si-K	Fe-K
F1 30x (1)_pt1	±0.31	±0.08	±0.43

Atom %

	O-K	Si-K	Fe-K
F1 30x (1)_pt1	60.46	0.80	38.74

Atom % Error (+/- 1 Sigma)

	O-K	Si-K	Fe-K
F1 30x (1)_pt1	±0.62	±0.09	±0.24

Figure A.3: Bulk analysis of Glödskal reduced in the presence of KCl, done with SEM-EDS analysis. The oxygen in the epoxy matrix is contributing to the wt% of oxygen in the analysis

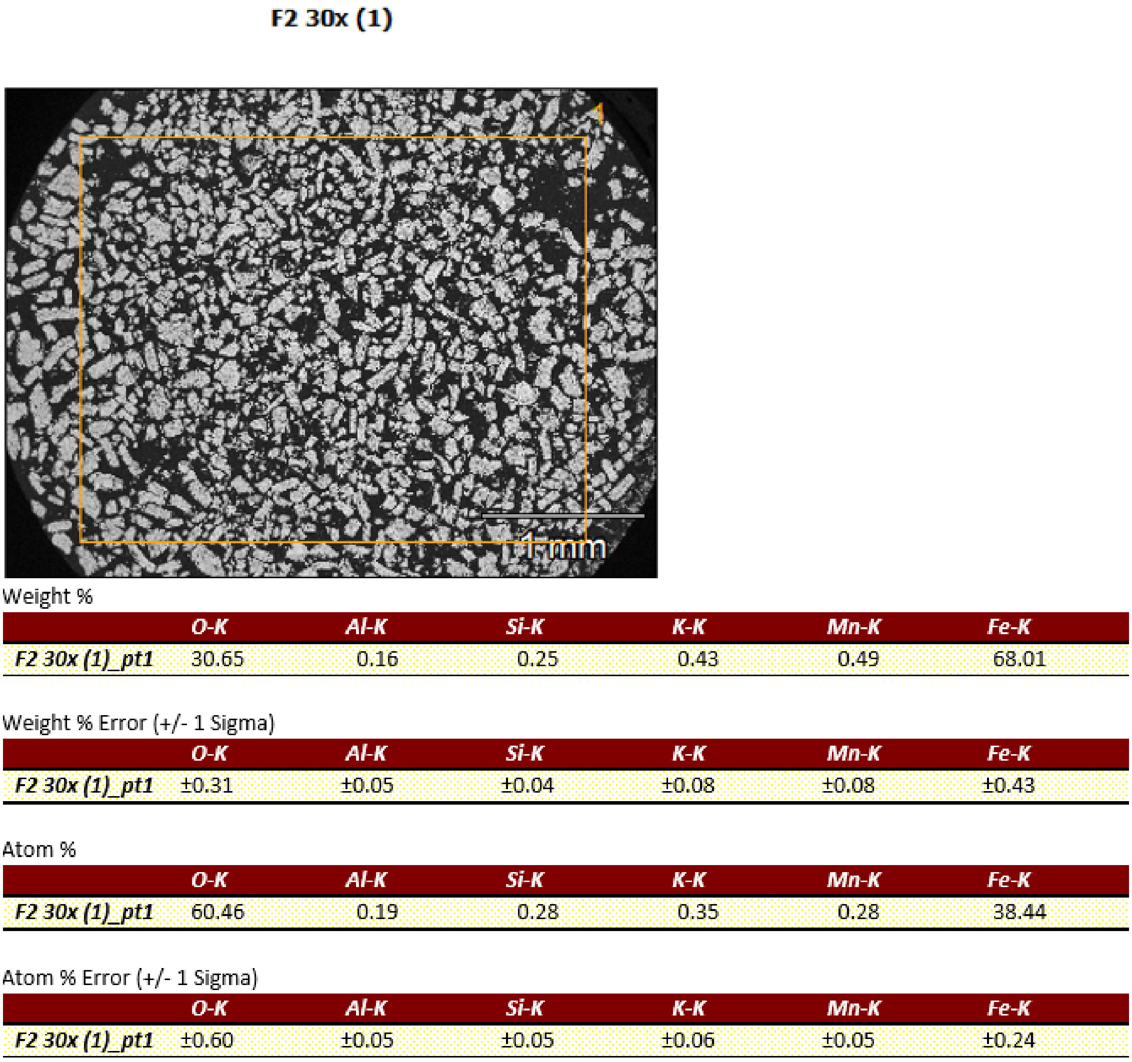

F2 30x (1)

Weight %

	O-K	Al-K	Si-K	K-K	Mn-K	Fe-K
F2 30x (1)_pt1	30.65	0.16	0.25	0.43	0.49	68.01

Weight % Error (+/- 1 Sigma)

	O-K	Al-K	Si-K	K-K	Mn-K	Fe-K
F2 30x (1)_pt1	±0.31	±0.05	±0.04	±0.08	±0.08	±0.43

Atom %

	O-K	Al-K	Si-K	K-K	Mn-K	Fe-K
F2 30x (1)_pt1	60.46	0.19	0.28	0.35	0.28	38.44

Atom % Error (+/- 1 Sigma)

	O-K	Al-K	Si-K	K-K	Mn-K	Fe-K
F2 30x (1)_pt1	±0.60	±0.05	±0.05	±0.06	±0.05	±0.24

Figure A.4: Bulk analysis of Glödskal reduced in the presence of K_2CO_3 , done with SEM-EDS analysis. The oxygen in the epoxy matrix is contributing to the wt% of oxygen in the analysis

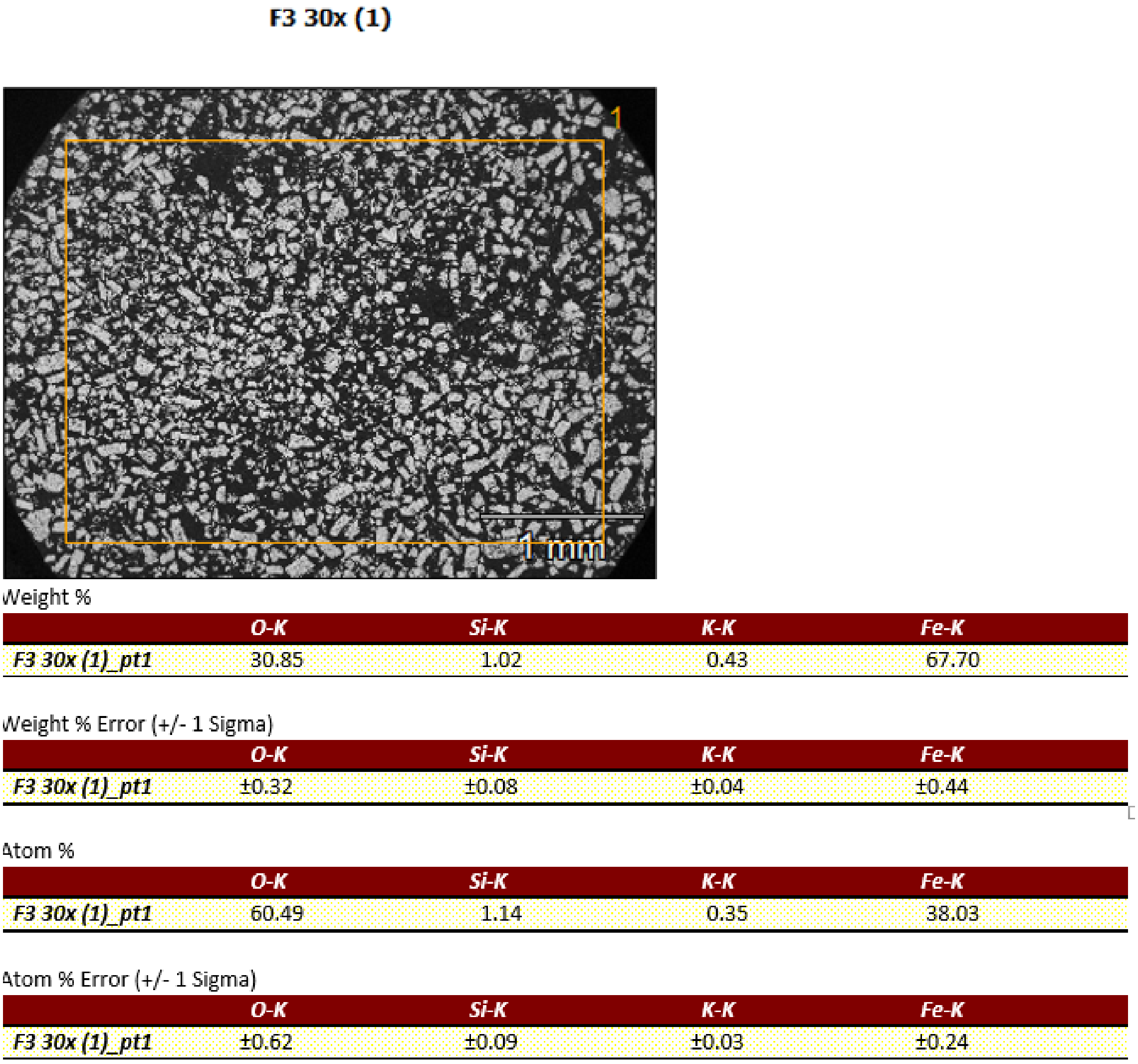

F3 30x (1)

Weight %

	O-K	Si-K	K-K	Fe-K
F3 30x (1)_pt1	30.85	1.02	0.43	67.70

Weight % Error (+/- 1 Sigma)

	O-K	Si-K	K-K	Fe-K
F3 30x (1)_pt1	±0.32	±0.08	±0.04	±0.44

Atom %

	O-K	Si-K	K-K	Fe-K
F3 30x (1)_pt1	60.49	1.14	0.35	38.03

Atom % Error (+/- 1 Sigma)

	O-K	Si-K	K-K	Fe-K
F3 30x (1)_pt1	±0.62	±0.09	±0.03	±0.24

Figure A.5: Bulk analysis of Glödskal reduced in the presence of K_2SO_4 , done with SEM-EDS analysis. The oxygen in the epoxy matrix is contributing to the wt% of oxygen in the analysis

F4 30x (1)

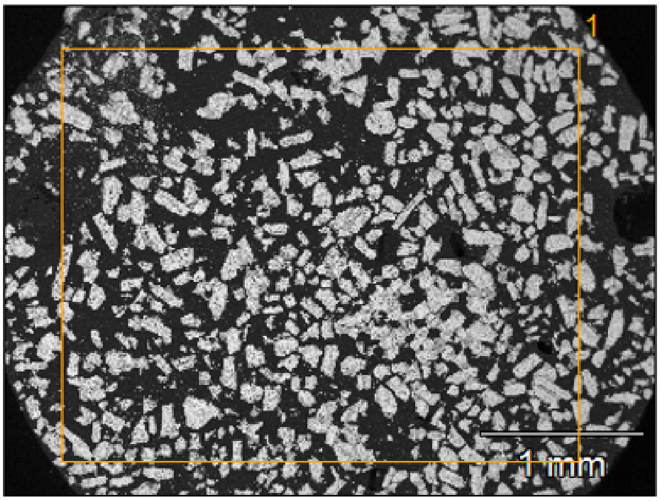

Weight %

	O-K	Si-K	P-K	K-K	Fe-K
F4 30x (1)_pt1	35.80	1.07	4.52	4.39	54.22

Weight % Error (+/- 1 Sigma)

	O-K	Si-K	P-K	K-K	Fe-K
F4 30x (1)_pt1	±0.37	±0.09	±0.11	±0.09	±0.37

Atom %

	O-K	Si-K	P-K	K-K	Fe-K
F4 30x (1)_pt1	63.84	1.08	4.16	3.21	27.70

Atom % Error (+/- 1 Sigma)

	O-K	Si-K	P-K	K-K	Fe-K
F4 30x (1)_pt1	±0.65	±0.09	±0.10	±0.07	±0.19

Figure A.6: Bulk analysis of Glödskal reduced in the presence of KH_2PO_4 , done with SEM-EDS analysis. The oxygen in the epoxy matrix is contributing to the wt% of oxygen in the analysis

LH 30x (1)

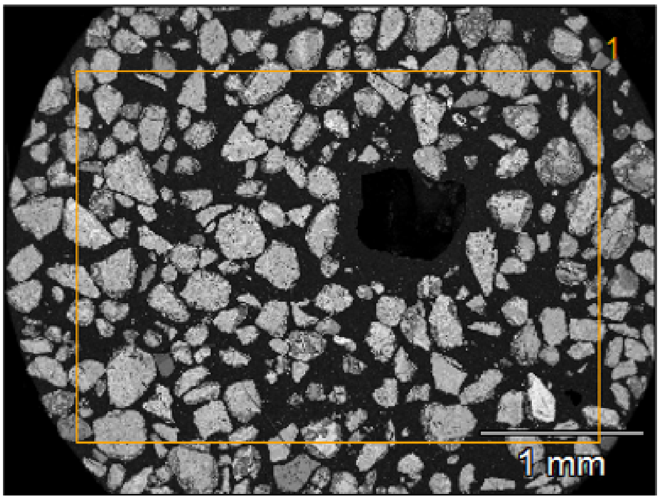

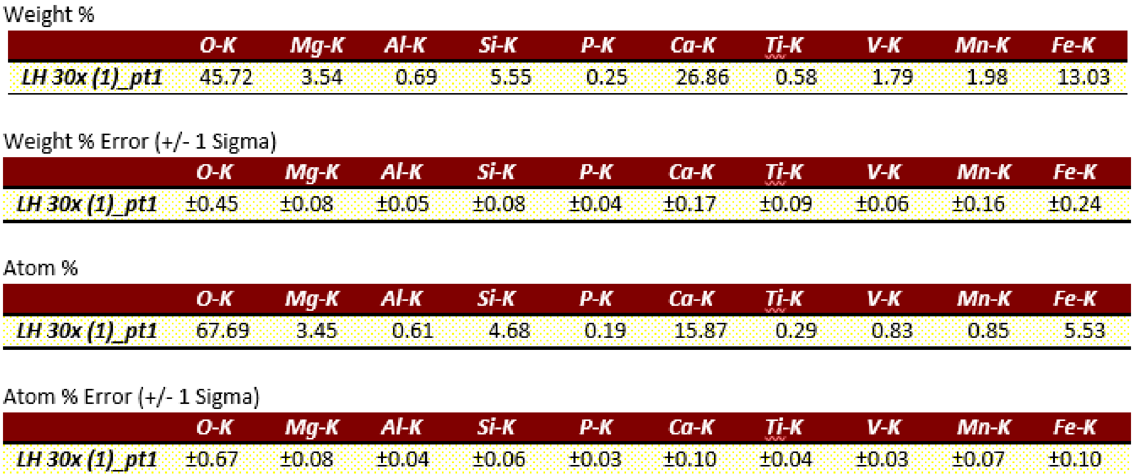

Weight %

	O-K	Mg-K	Al-K	Si-K	P-K	Ca-K	Ti-K	V-K	Mn-K	Fe-K
LH 30x (1)_pt1	45.72	3.54	0.69	5.55	0.25	26.86	0.58	1.79	1.98	13.03

Weight % Error (+/- 1 Sigma)

	O-K	Mg-K	Al-K	Si-K	P-K	Ca-K	Ti-K	V-K	Mn-K	Fe-K
LH 30x (1)_pt1	±0.45	±0.08	±0.05	±0.08	±0.04	±0.17	±0.09	±0.06	±0.16	±0.24

Atom %

	O-K	Mg-K	Al-K	Si-K	P-K	Ca-K	Ti-K	V-K	Mn-K	Fe-K
LH 30x (1)_pt1	67.69	3.45	0.61	4.68	0.19	15.87	0.29	0.83	0.85	5.53

Atom % Error (+/- 1 Sigma)

	O-K	Mg-K	Al-K	Si-K	P-K	Ca-K	Ti-K	V-K	Mn-K	Fe-K
LH 30x (1)_pt1	±0.67	±0.08	±0.04	±0.06	±0.03	±0.10	±0.04	±0.03	±0.07	±0.10

Figure A.7: Bulk analysis of pretreated LD-slag, done with SEM-EDS analysis. The oxygen in the epoxy matrix is contributing to the wt% of oxygen in the analysis

L 30x (1)

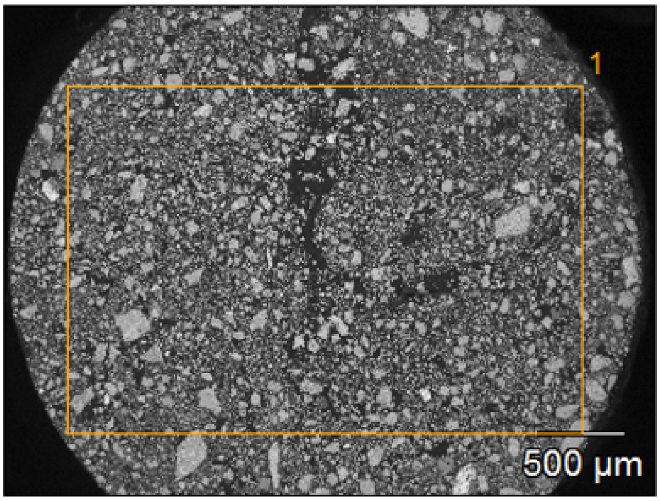

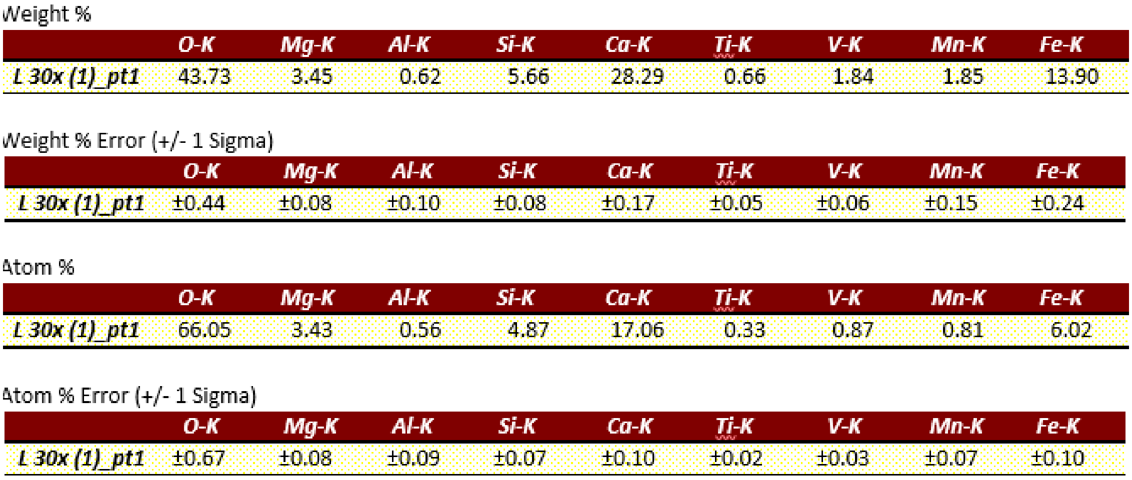

Weight %

	O-K	Mg-K	Al-K	Si-K	Ca-K	Ti-K	V-K	Mn-K	Fe-K
L 30x (1)_pt1	43.73	3.45	0.62	5.66	28.29	0.66	1.84	1.85	13.90

Weight % Error (+/- 1 Sigma)

	O-K	Mg-K	Al-K	Si-K	Ca-K	Ti-K	V-K	Mn-K	Fe-K
L 30x (1)_pt1	±0.44	±0.08	±0.10	±0.08	±0.17	±0.05	±0.06	±0.15	±0.24

Atom %

	O-K	Mg-K	Al-K	Si-K	Ca-K	Ti-K	V-K	Mn-K	Fe-K
L 30x (1)_pt1	66.05	3.43	0.56	4.87	17.06	0.33	0.87	0.81	6.02

Atom % Error (+/- 1 Sigma)

	O-K	Mg-K	Al-K	Si-K	Ca-K	Ti-K	V-K	Mn-K	Fe-K
L 30x (1)_pt1	±0.67	±0.08	±0.09	±0.07	±0.10	±0.02	±0.03	±0.07	±0.10

Figure A.8: Bulk analysis of reduced LD-slag, done with SEM-EDS analysis. The oxygen in the epoxy matrix is contributing to the wt% of oxygen in the analysis

L1 30x (1)

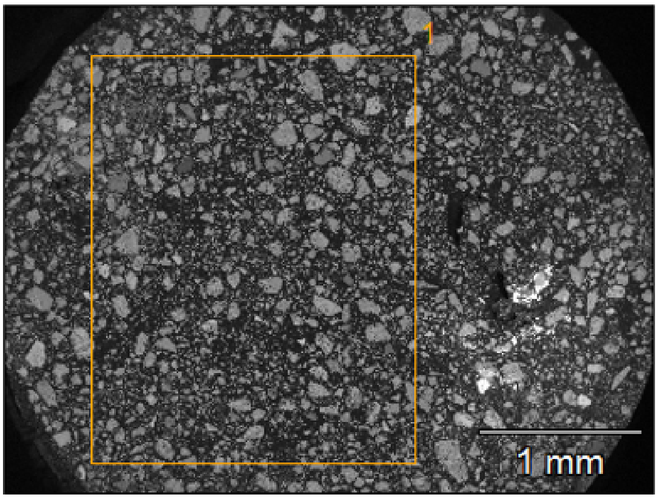

Weight %

	O-K	Mg-K	Al-K	Si-K	P-K	Ca-K	Ti-K	V-K	Mn-K	Fe-K
L1 30x (1)_pt1	45.83	3.43	0.83	6.24	0.18	26.82	0.73	1.77	1.66	12.51

Weight % Error (+/- 1 Sigma)

	O-K	Mg-K	Al-K	Si-K	P-K	Ca-K	Ti-K	V-K	Mn-K	Fe-K
L1 30x (1)_pt1	±0.86	±0.10	±0.05	±0.09	±0.04	±0.20	±0.06	±0.12	±0.18	±0.27

Atom %

	O-K	Mg-K	Al-K	Si-K	P-K	Ca-K	Ti-K	V-K	Mn-K	Fe-K
L1 30x (1)_pt1	67.59	3.33	0.73	5.24	0.14	15.79	0.36	0.82	0.71	5.28

Atom % Error (+/- 1 Sigma)

	O-K	Mg-K	Al-K	Si-K	P-K	Ca-K	Ti-K	V-K	Mn-K	Fe-K
L1 30x (1)_pt1	±1.26	±0.09	±0.05	±0.08	±0.03	±0.12	±0.03	±0.06	±0.08	±0.11

Figure A.9: Bulk analysis of LD-slag reduced in the presence of KCl, done with SEM-EDS analysis. The oxygen in the epoxy matrix is contributing to the wt% of oxygen in the analysis

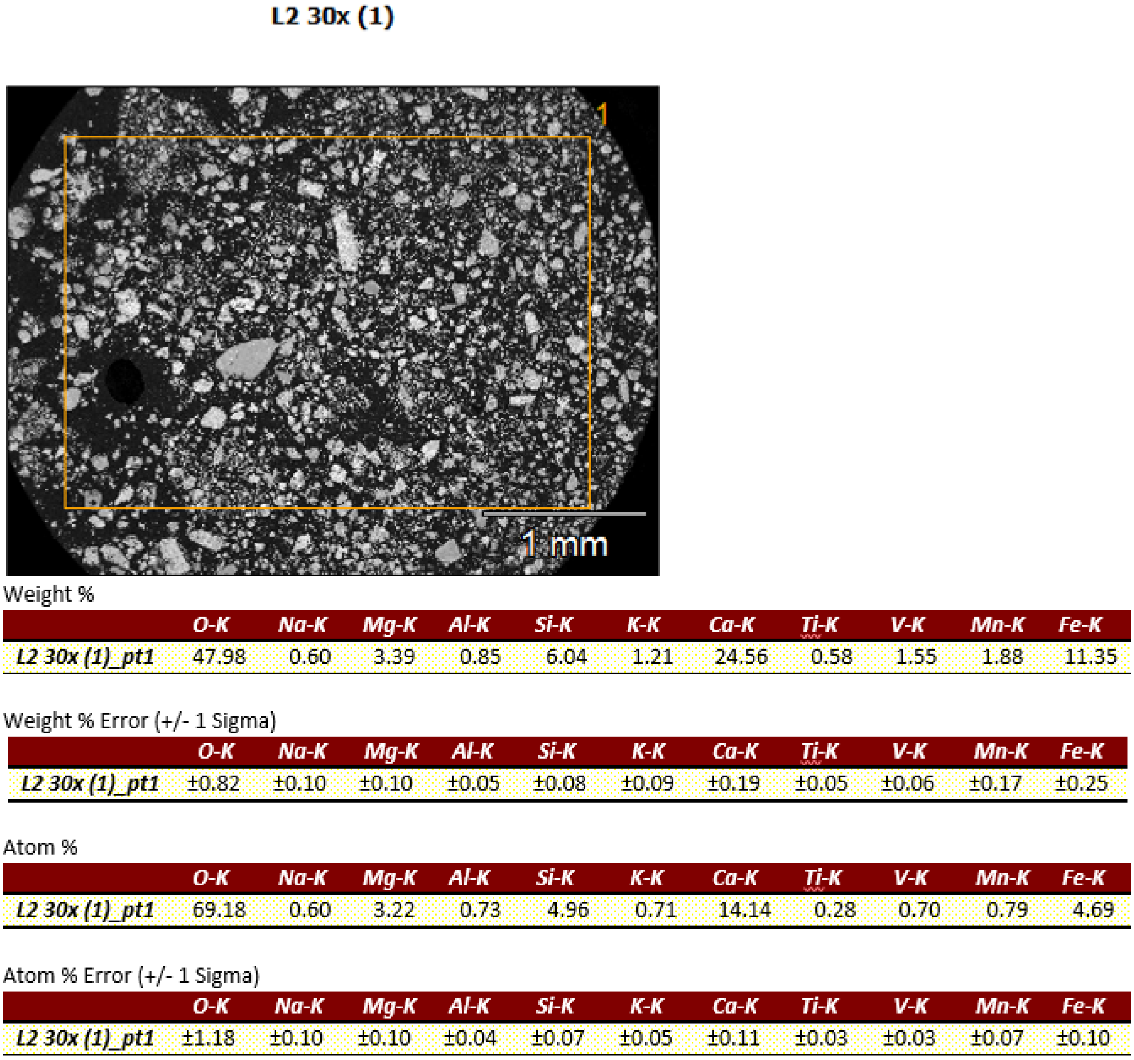

L2 30x (1)

Weight %

	O-K	Na-K	Mg-K	Al-K	Si-K	K-K	Ca-K	Ti-K	V-K	Mn-K	Fe-K
L2 30x (1)_pt1	47.98	0.60	3.39	0.85	6.04	1.21	24.56	0.58	1.55	1.88	11.35

Weight % Error (+/- 1 Sigma)

	O-K	Na-K	Mg-K	Al-K	Si-K	K-K	Ca-K	Ti-K	V-K	Mn-K	Fe-K
L2 30x (1)_pt1	±0.82	±0.10	±0.10	±0.05	±0.08	±0.09	±0.19	±0.05	±0.06	±0.17	±0.25

Atom %

	O-K	Na-K	Mg-K	Al-K	Si-K	K-K	Ca-K	Ti-K	V-K	Mn-K	Fe-K
L2 30x (1)_pt1	69.18	0.60	3.22	0.73	4.96	0.71	14.14	0.28	0.70	0.79	4.69

Atom % Error (+/- 1 Sigma)

	O-K	Na-K	Mg-K	Al-K	Si-K	K-K	Ca-K	Ti-K	V-K	Mn-K	Fe-K
L2 30x (1)_pt1	±1.18	±0.10	±0.10	±0.04	±0.07	±0.05	±0.11	±0.03	±0.03	±0.07	±0.10

Figure A.10: Bulk analysis of LD-slag reduced in the presence of K_2CO_3, done with SEM-EDS analysis. The oxygen in the epoxy matrix is contributing to the wt% of oxygen in the analysis

L3 30x (1)

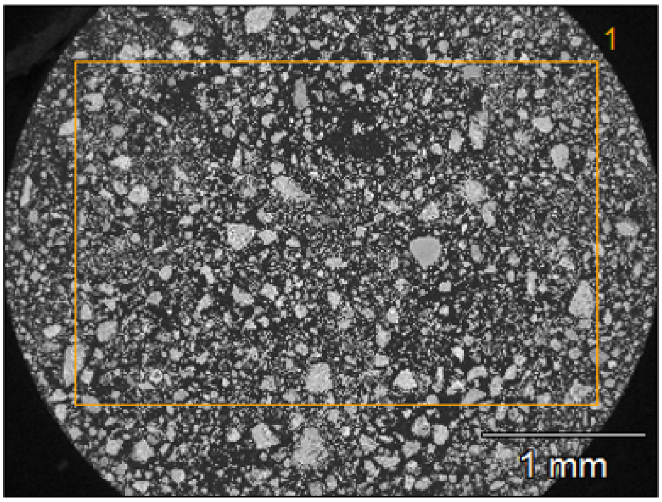

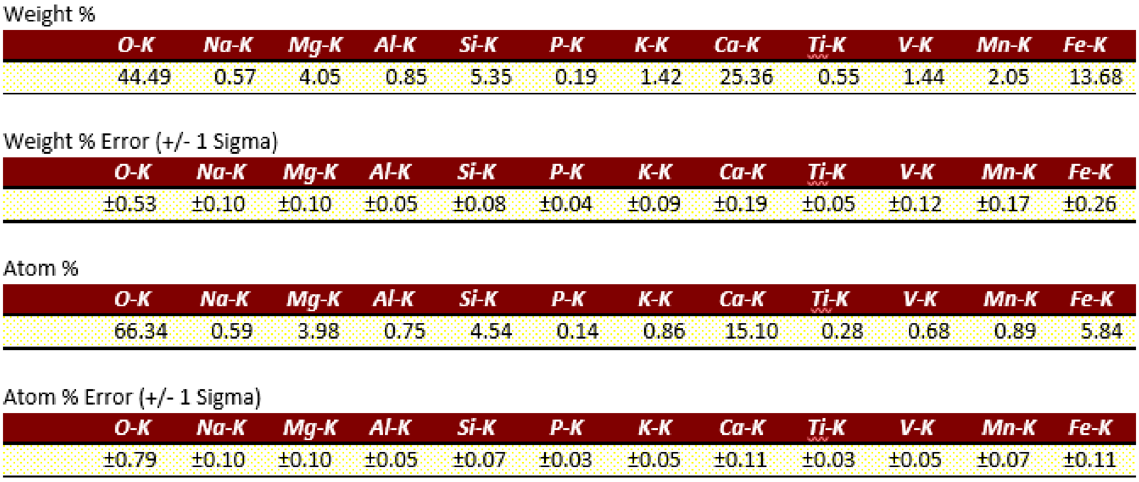

Weight %

O-K	Na-K	Mg-K	Al-K	Si-K	P-K	K-K	Ca-K	Ti-K	V-K	Mn-K	Fe-K
44.49	0.57	4.05	0.85	5.35	0.19	1.42	25.36	0.55	1.44	2.05	13.68

Weight % Error (+/- 1 Sigma)

O-K	Na-K	Mg-K	Al-K	Si-K	P-K	K-K	Ca-K	Ti-K	V-K	Mn-K	Fe-K
±0.53	±0.10	±0.10	±0.05	±0.08	±0.04	±0.09	±0.19	±0.05	±0.12	±0.17	±0.26

Atom %

O-K	Na-K	Mg-K	Al-K	Si-K	P-K	K-K	Ca-K	Ti-K	V-K	Mn-K	Fe-K
66.34	0.59	3.98	0.75	4.54	0.14	0.86	15.10	0.28	0.68	0.89	5.84

Atom % Error (+/- 1 Sigma)

O-K	Na-K	Mg-K	Al-K	Si-K	P-K	K-K	Ca-K	Ti-K	V-K	Mn-K	Fe-K
±0.79	±0.10	±0.10	±0.05	±0.07	±0.03	±0.05	±0.11	±0.03	±0.05	±0.07	±0.11

Figure A.11: Bulk analysis of LD-slag reduced in the presence of K_2SO_4, done with SEM-EDS analysis. The oxygen in the epoxy matrix is contributing to the wt% of oxygen in the analysis

L4 30x (1)

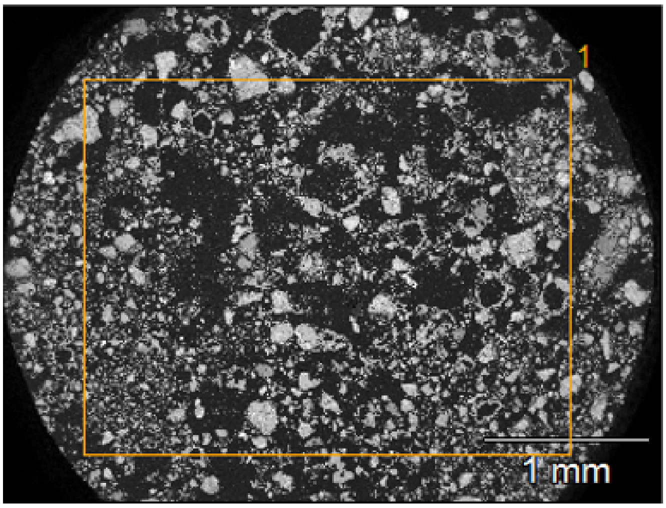

Weight %

	O-K	Mg-K	Al-K	Si-K	P-K	K-K	Ca-K	Ti-K	V-K	Mn-K	Fe-K
L4 30x (1)_pt1	51.65	2.55	0.61	4.94	3.75	2.85	21.59	0.66	1.30	1.44	8.64

Weight % Error (+/- 1 Sigma)

	O-K	Mg-K	Al-K	Si-K	P-K	K-K	Ca-K	Ti-K	V-K	Mn-K	Fe-K
L4 30x (1)_pt1	±0.53	±0.10	±0.06	±0.11	±0.12	±0.11	±0.20	±0.11	±0.07	±0.18	±0.26

Atom %

	O-K	Mg-K	Al-K	Si-K	P-K	K-K	Ca-K	Ti-K	V-K	Mn-K	Fe-K
L4 30x (1)_pt1	71.98	2.34	0.51	3.92	2.70	1.63	12.01	0.31	0.57	0.59	3.45

Atom % Error (+/- 1 Sigma)

	O-K	Mg-K	Al-K	Si-K	P-K	K-K	Ca-K	Ti-K	V-K	Mn-K	Fe-K
L4 30x (1)_pt1	±0.74	±0.09	±0.05	±0.09	±0.09	±0.06	±0.11	±0.05	±0.03	±0.07	±0.10

Figure A.12: Bulk analysis of LD-slag reduced in the presence of KH_2PO_4, done with SEM-EDS analysis. The oxygen in the epoxy matrix is contributing to the wt% of oxygen in the analysis

2. Appendix: SEM-images

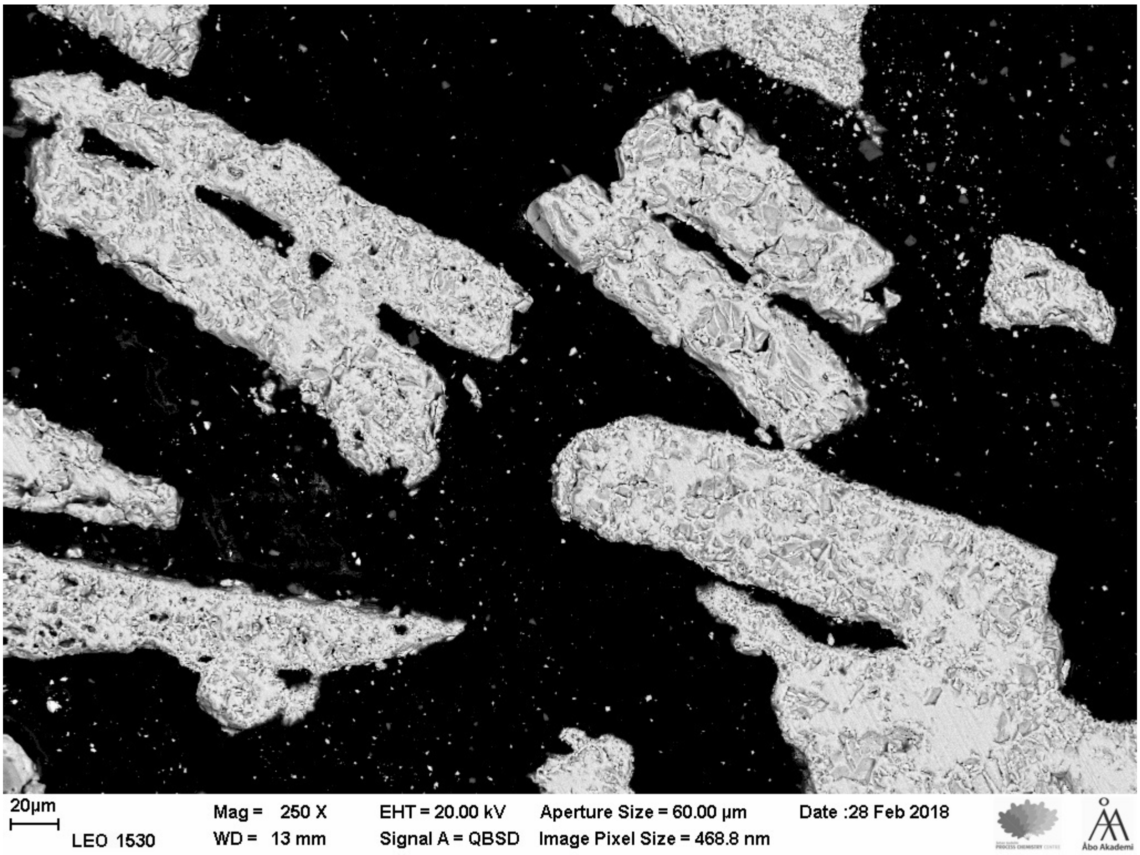

Figure B.1: SEM-image of cross-section of particles in pretreated, ungrinded sample of Glödskal, showing sintering.

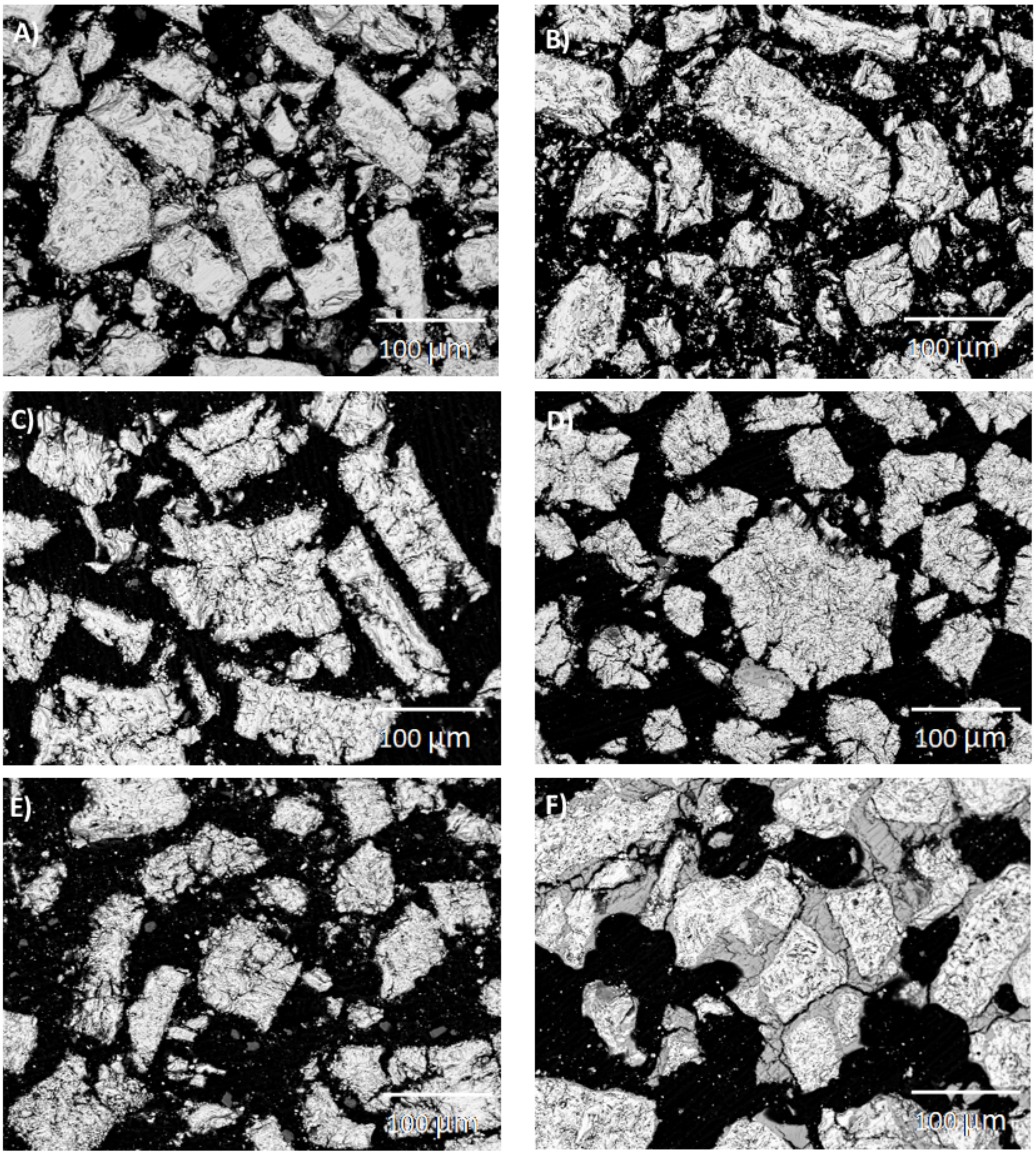

Figure B.2: SEM-images of cross-section of Glödskal taken at 250x magnification. A) Pretreated, grinded Glödskal and reduced samples of B) Glödskal C) Glödskal + KCl D) Glödskal + K_2CO_3 E) Glödskal + K_2SO_4 F) Glödskal + KH_2PO_4.

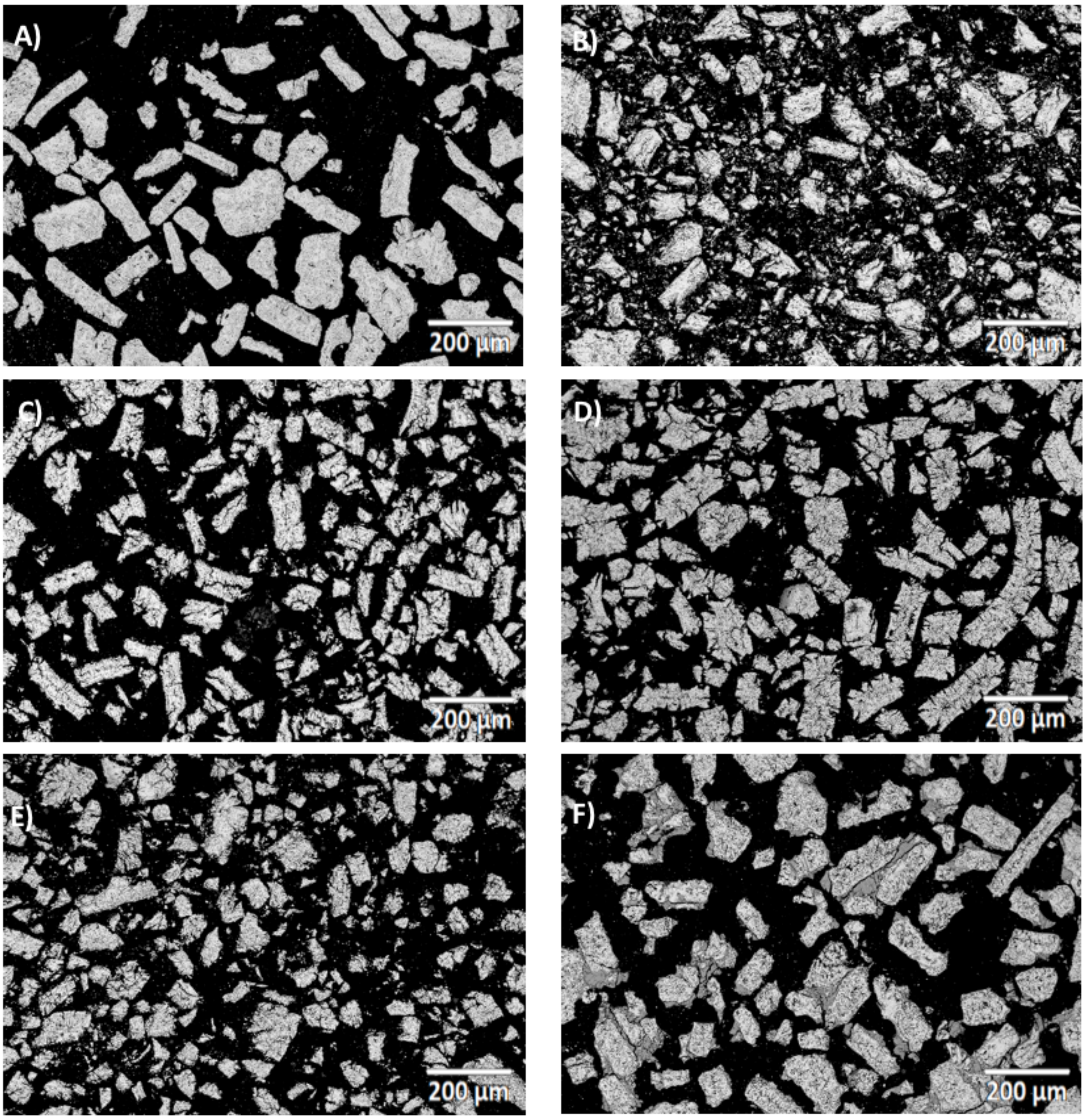

Figure B.3: SEM-images of cross-section of Glödskal taken at 100x magnification. A) Pretreated, grinded Glödskal and reduced samples of B) Glödskal C) Glödskal + KCl D) Glödskal + K_2CO_3 E) Glödskal + K_2SO_4 F) Glödskal + KH_2PO_4.

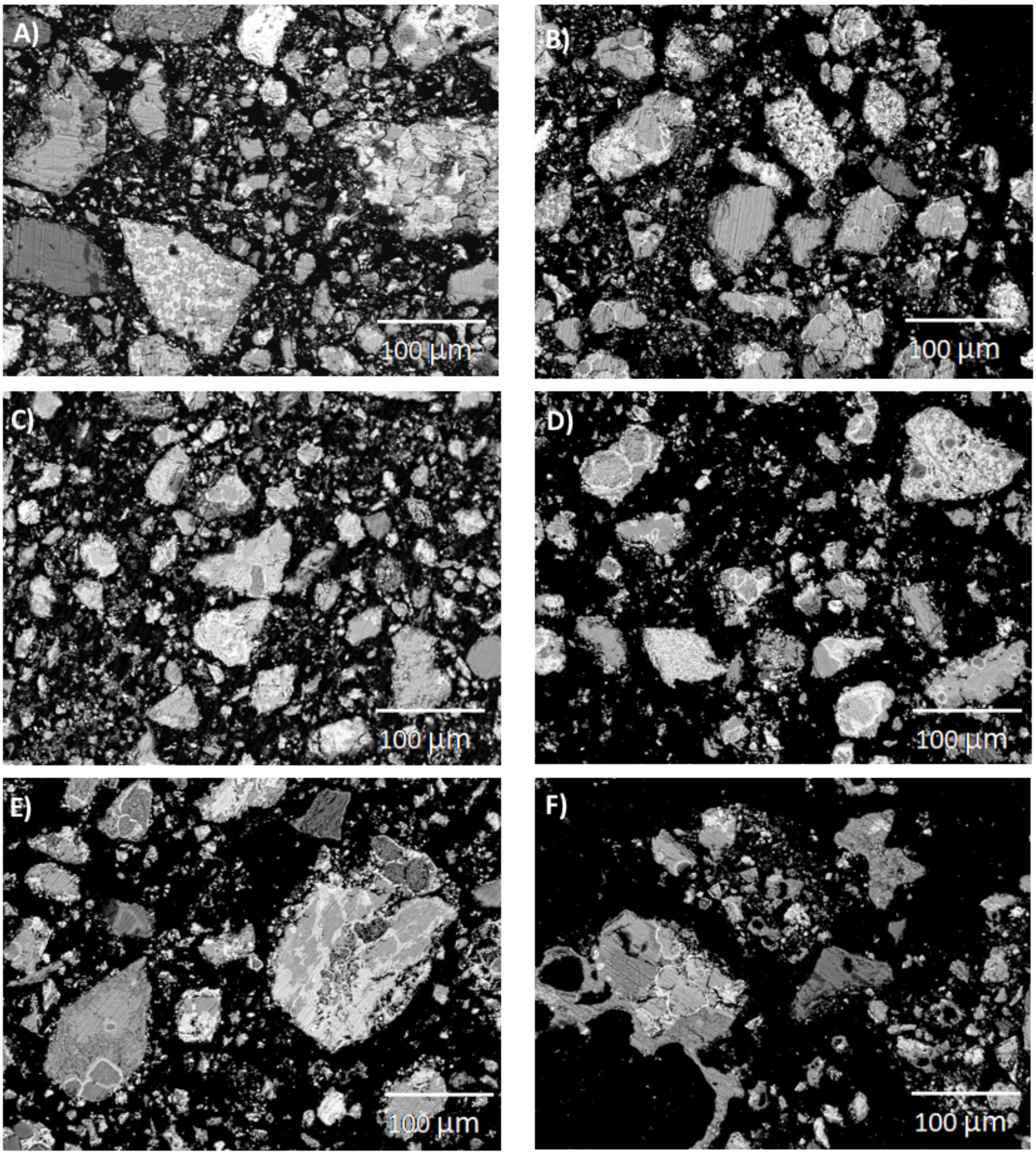

Figure B.4: SEM-images of cross-section of LD-slag taken at 250x magnification. A) Pretreated, grinded LD-slag and reduced samples of B) LD-slag C) LD-slag + KCl D) LD-slag + K_2CO_3 E) LD-slag + K_2SO_4 F) LD-slag + KH_2PO_4.

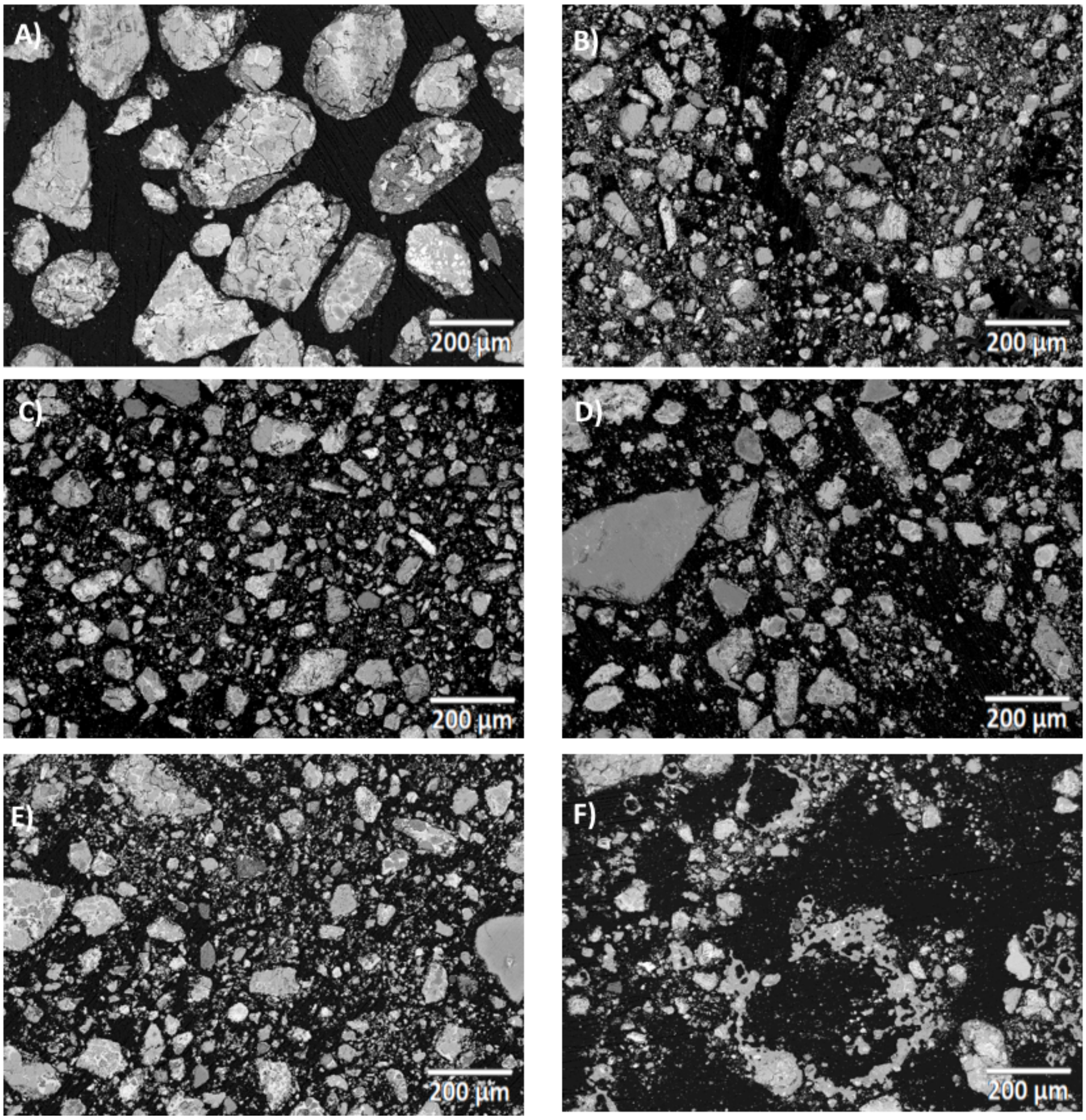

Figure B.5: SEM-images of cross-section of LD-slag taken at 100x magnification. A) Pretreated LD-slag (not grinded) and reduced samples of B) LD-slag C) LD-slag + KCl D) LD-slag + K_2CO_3 E) LD-slag + K_2SO_4 F) LD-slag + KH_2PO_4.

3. Appendix: Elemental maps

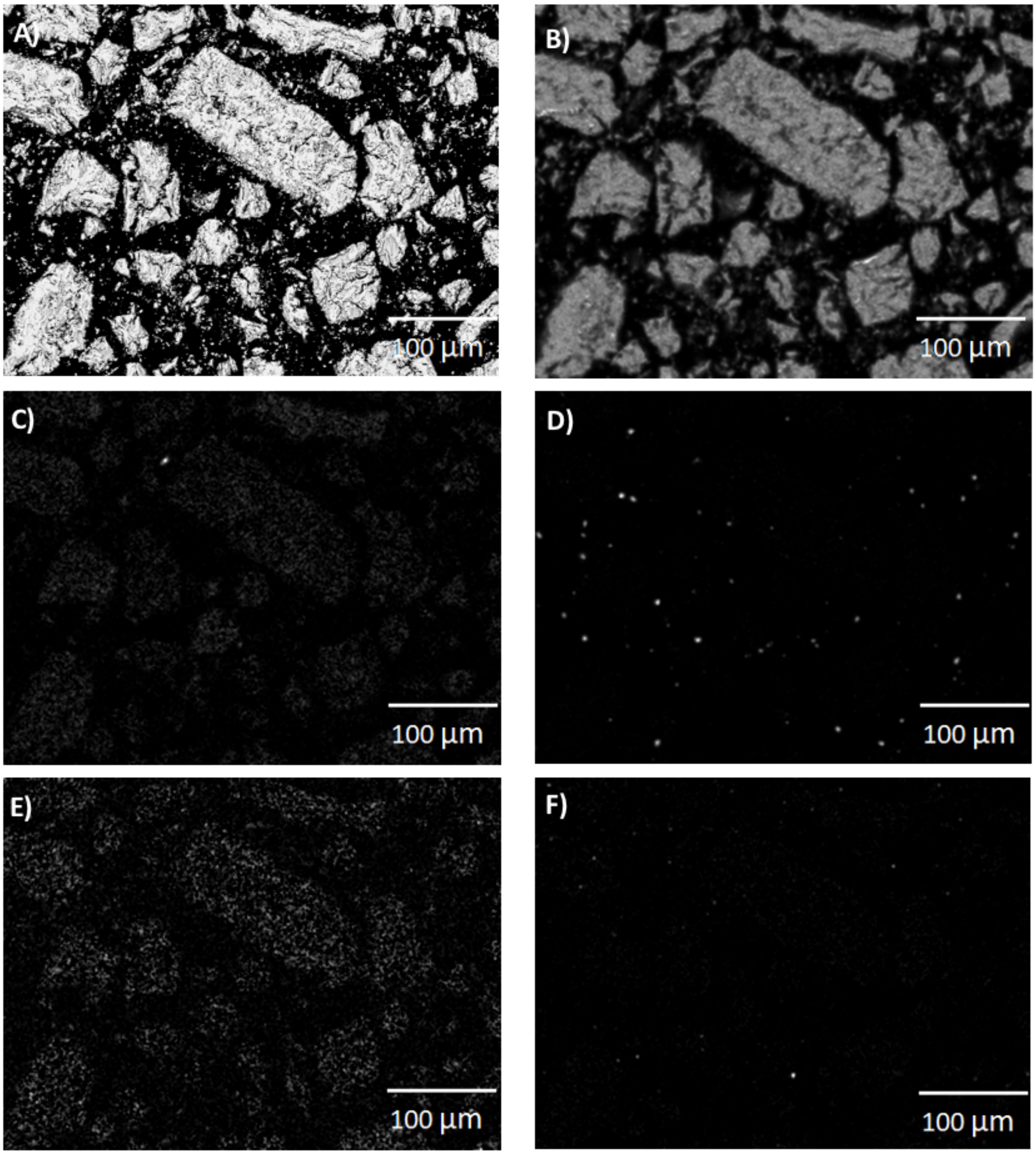

Figure C.1: SEM-EDS elemental maps of the cross-section of Glödskal reduced with no salt present A) SEM-image and elemental maps of B) Fe C) Mn D) Si E) Al F) Ca

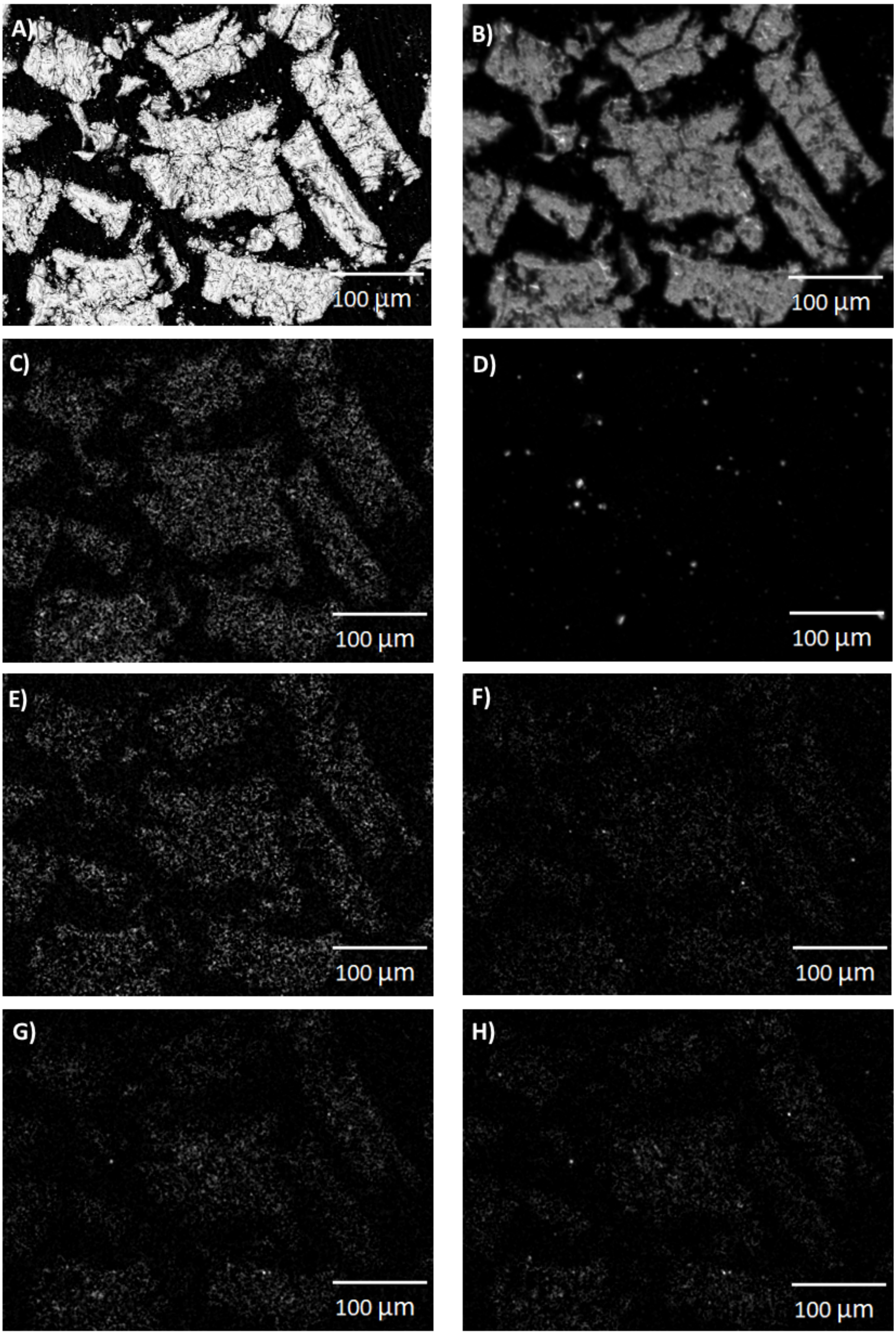

Figure C.2: SEM-EDS elemental maps of the cross-section of Glödskal reduced in the presence of KCl A) SEM-image and elemental maps of B) Fe C) Mn D) Si E) Al F) Ca G) K H) Cl

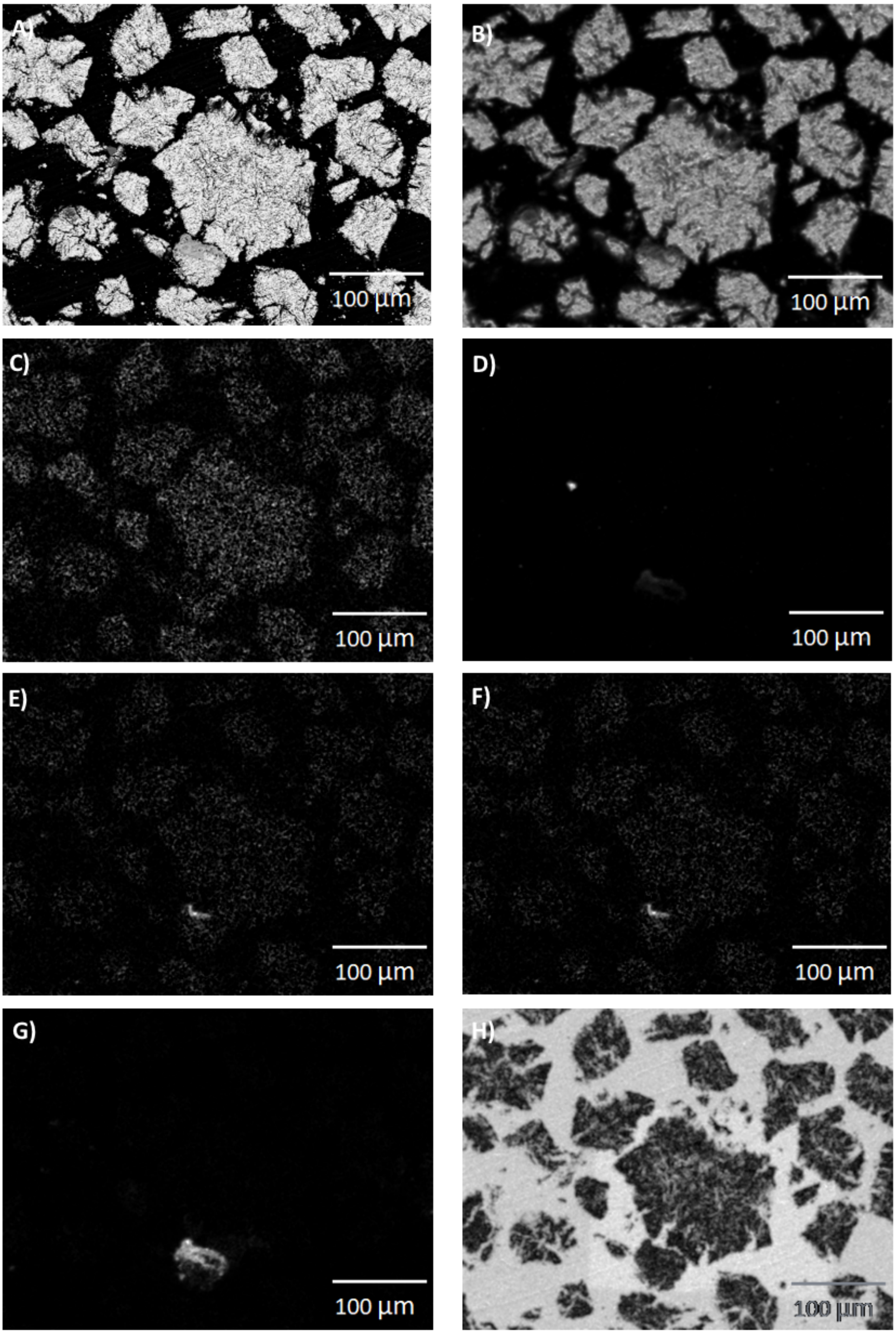

Figure C.3: SEM-EDS elemental maps of the cross-section of Glödskal reduced in the presence of K_2CO_3 A) SEM-image and elemental maps of B) Fe C) Mn D) Si E) Al F) Ca G) K H) C

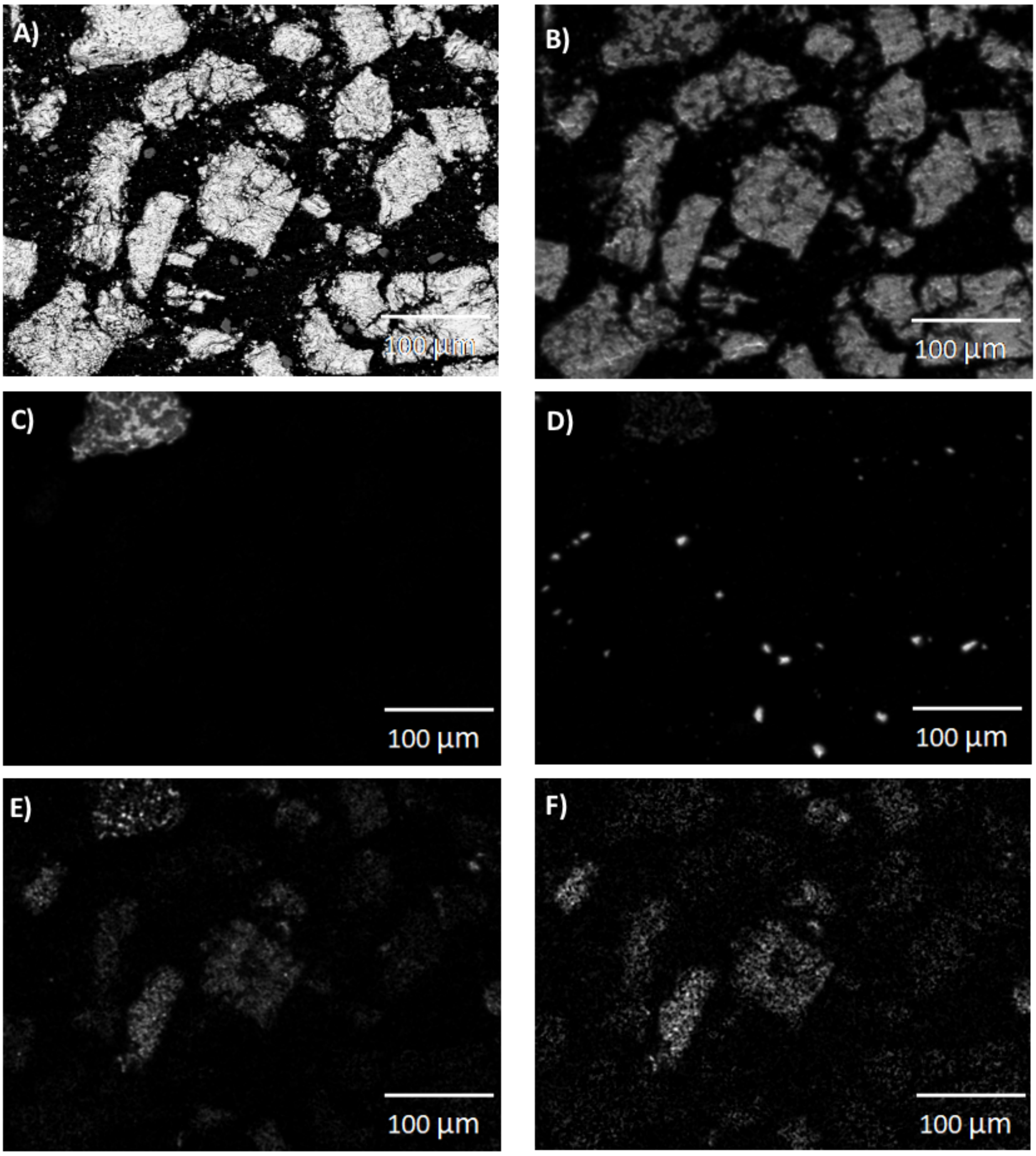

Figure C.4: SEM-EDS elemental maps of the cross-section of Glödskal reduced in the presence of K_2SO_4 A) SEM-image and elemental maps of B) Fe C) Mn D) Si E) Al F) Ca G) K H) S

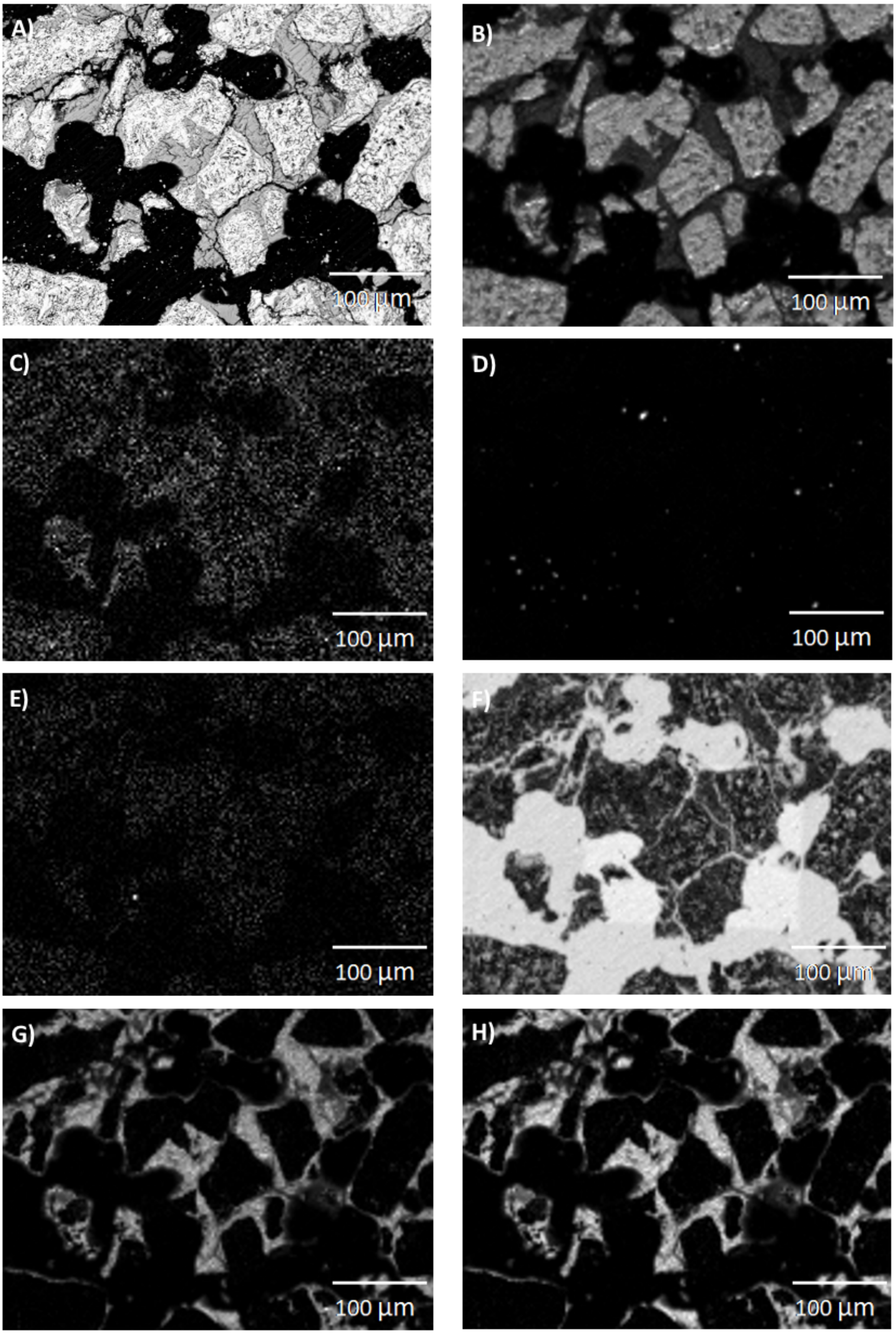

Figure C.5: SEM-EDS elemental maps of the cross-section of Glödskal reduced in the presence of KH_2PO_4 A) SEM-image and elemental maps of B) Fe C) Mn D) Si E) Al F) C G) K H) P

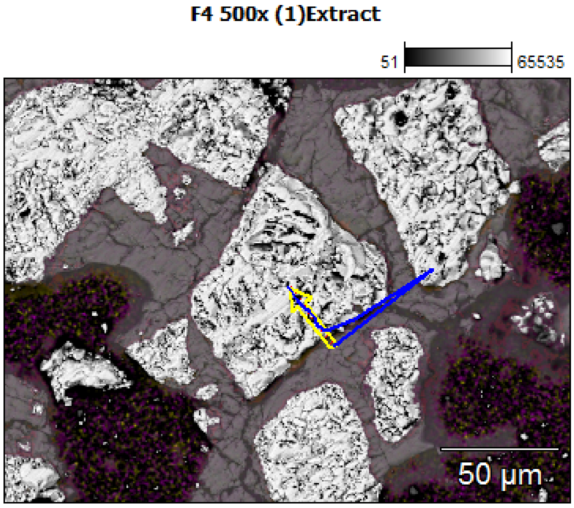

Figure C.6: Linescan on a particle of Glödskal reduced in the presence of KH_2PO_4 showing the concentration gradient of K in the blue curve.

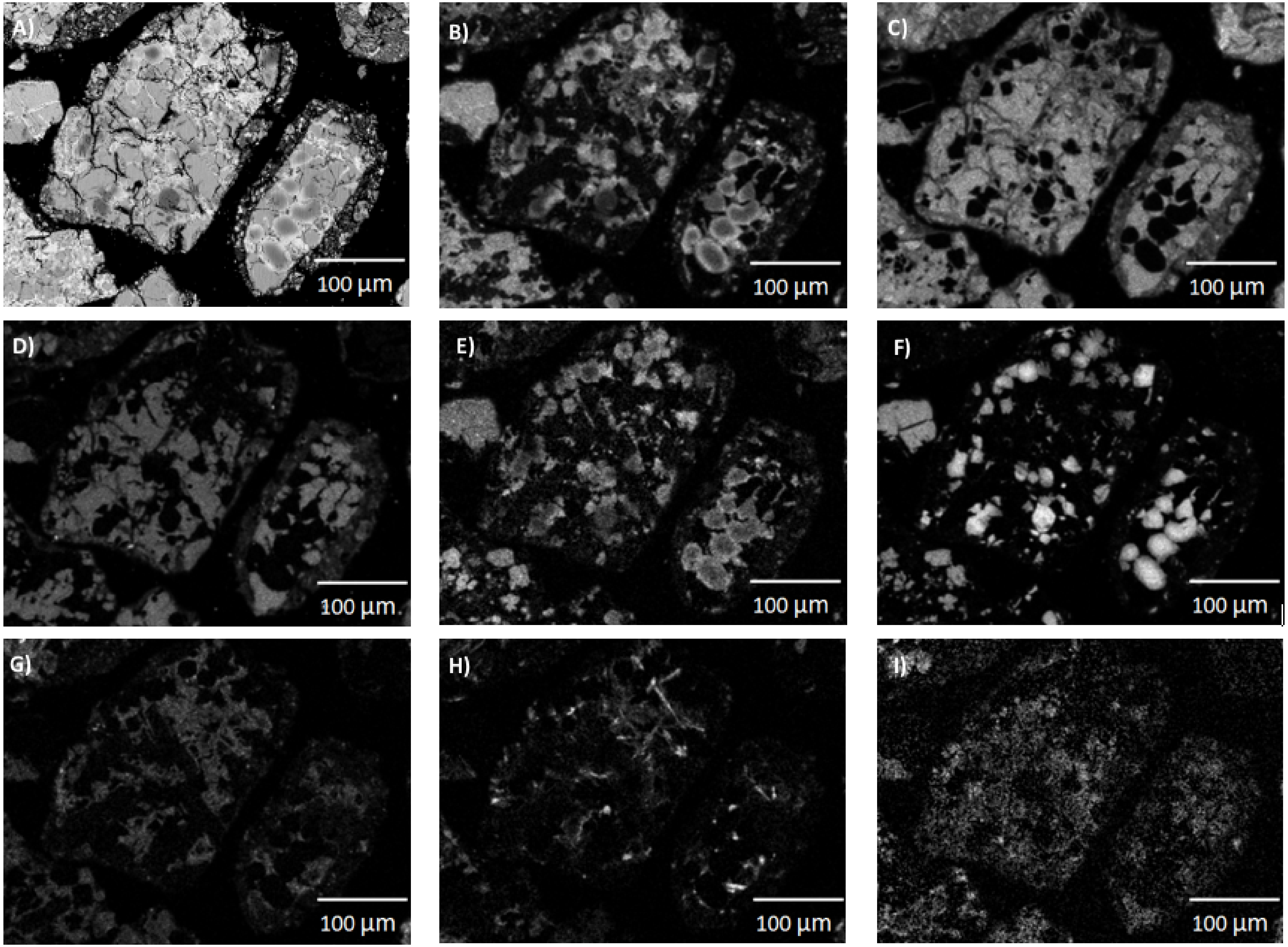

Figure C.7: SEM-EDS elemental maps of the cross-section of pretreated, ungrinded LD-slag A) SEM-image and elemental maps of B) Fe C) Ca D) Si E) Mn F) Mg G) V H) Ti I) P.

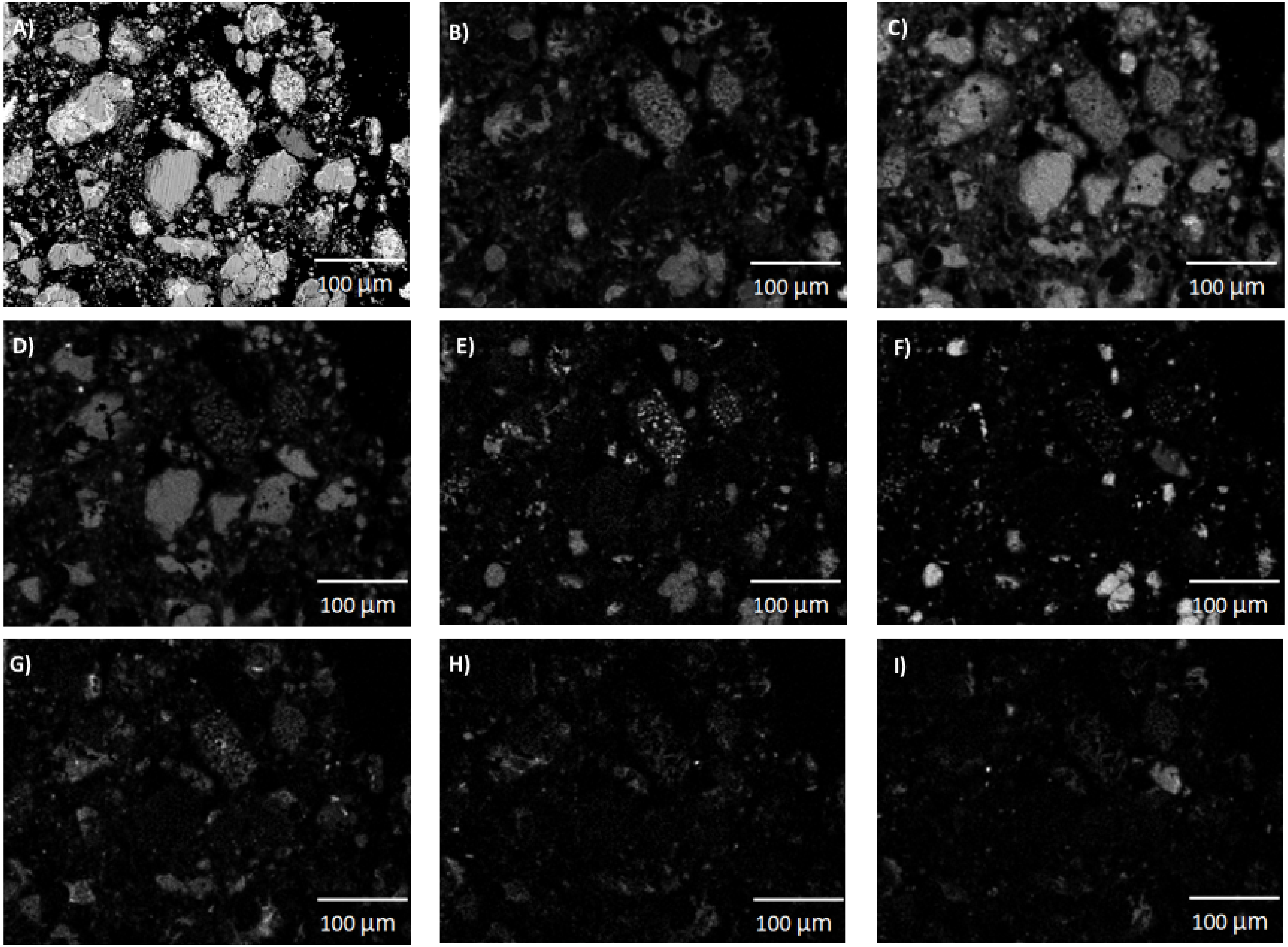

Figure C.8: SEM-EDS elemental maps of the cross-section of LD-slag reduced without salt A) SEM-image and elemental maps of B) Fe C) Ca D) Si E) Mn F) Mg G) V H) Ti and I) Al.

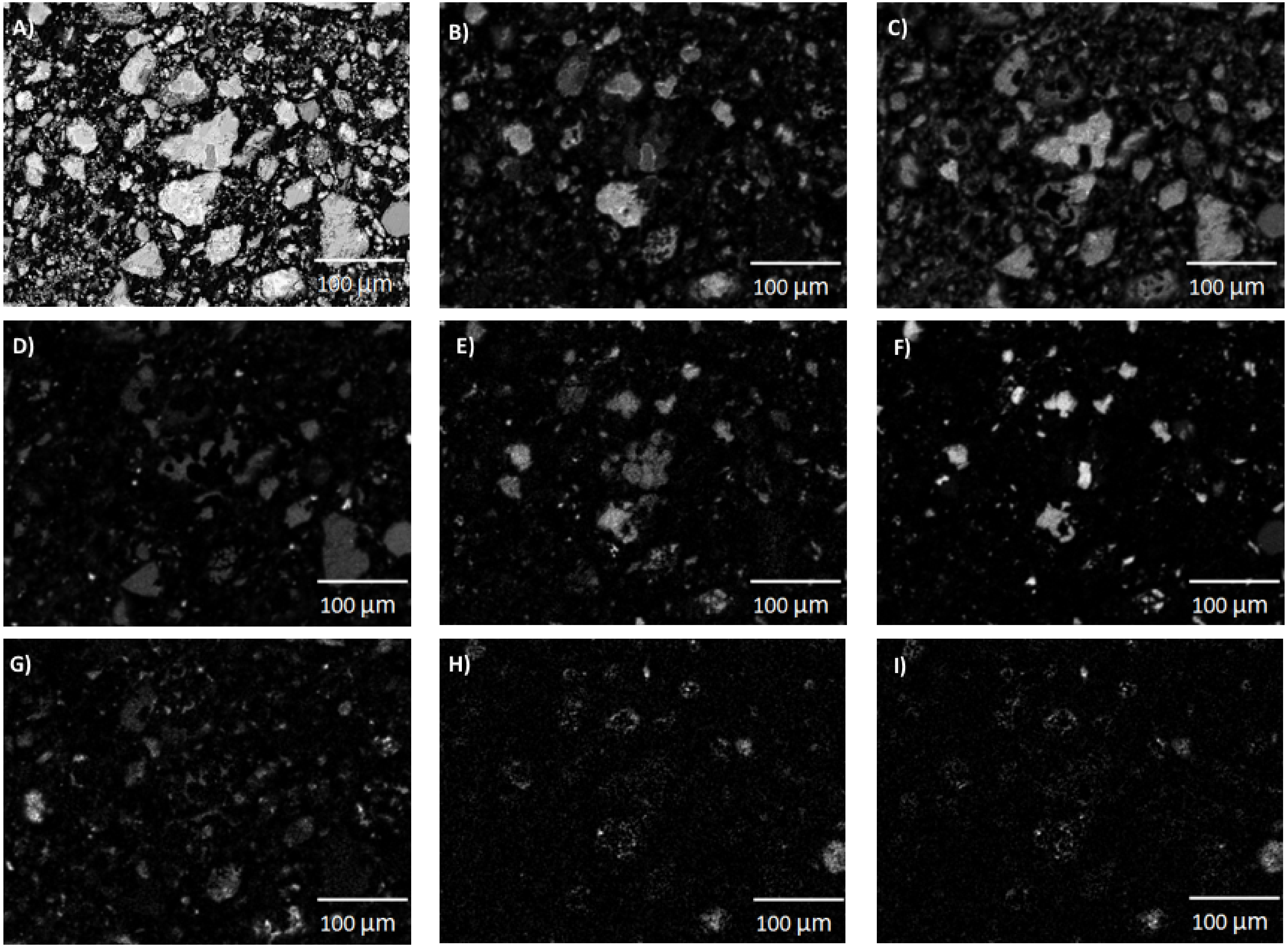

Figure C.9: SEM-EDS elemental maps of the cross-section of LD-slag reduced in the presence of KCl A) SEM-image and elemental maps of B) Fe C) Ca D) Si E) Mn F) Mg G) V H) K and I) Cl.

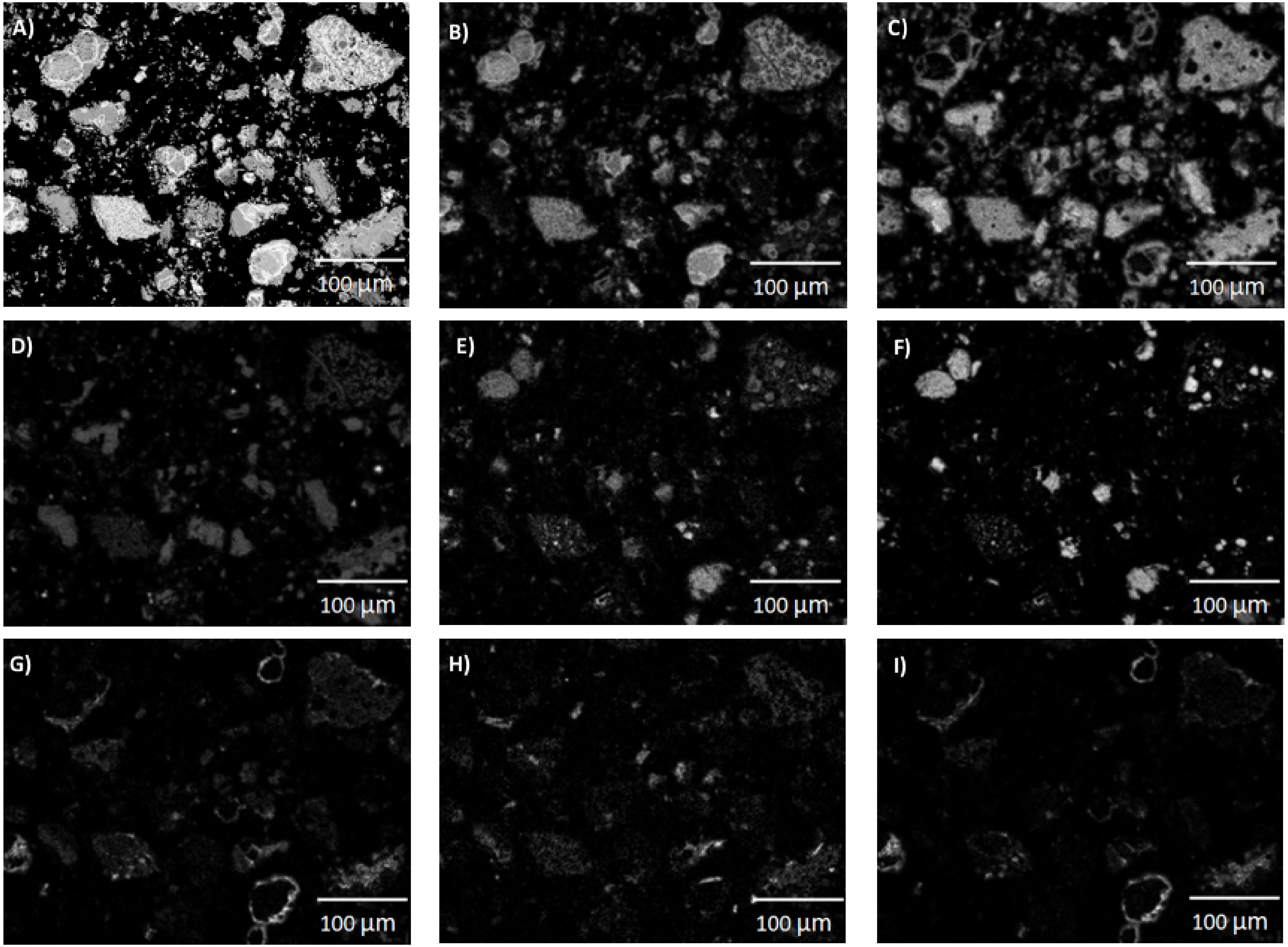

Figure C.10: SEM-EDS elemental maps of the cross-section of LD-slag reduced in the presence of K_2CO_3 A) SEM-image and elemental maps of B) Fe C) Ca D) Si E) Mn F) Mg G) V H) Ti and I) K.

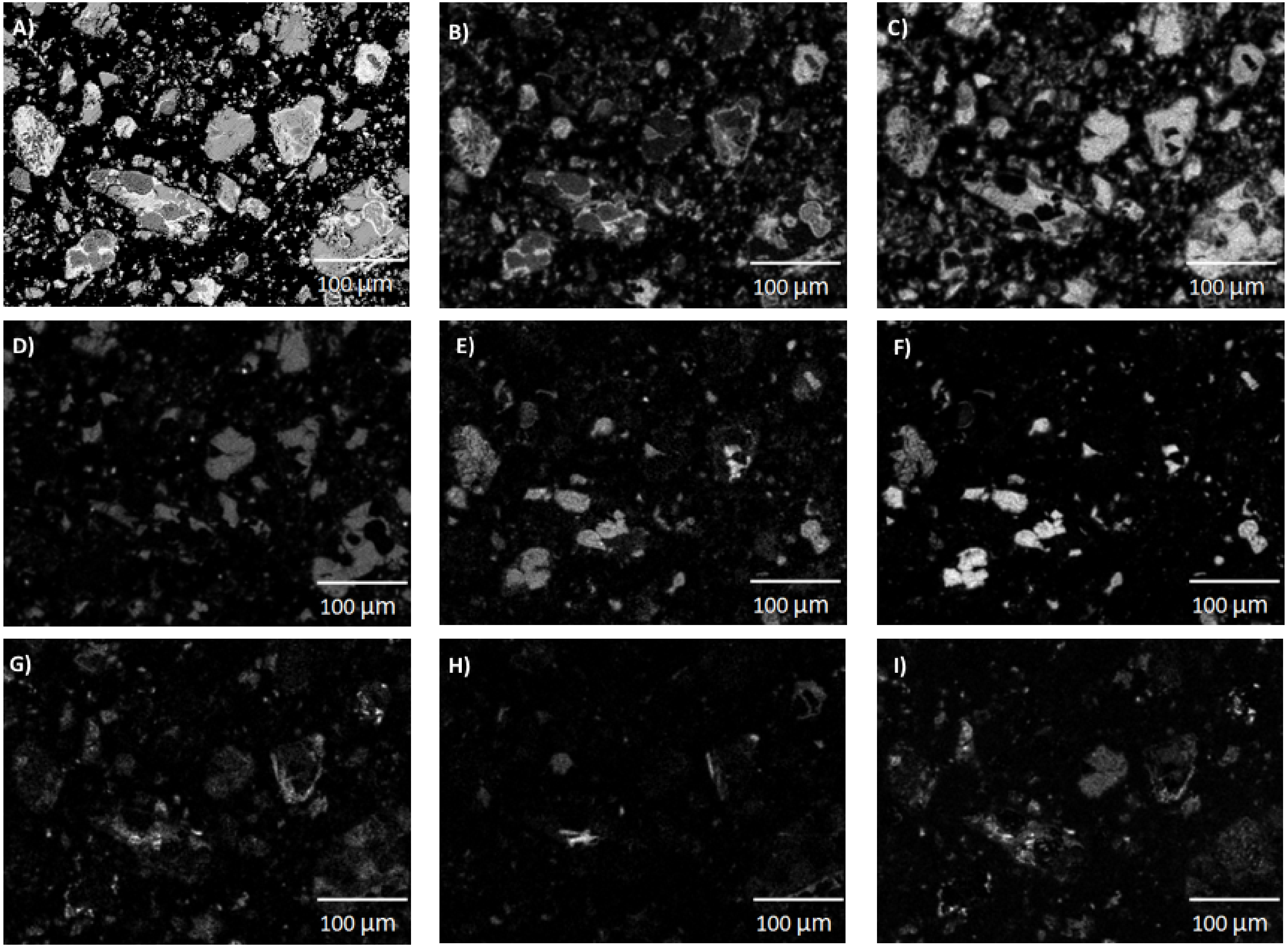

Figure C.11: SEM-EDS elemental maps of the cross-section of LD-slag reduced in the presence of K_2SO_4 A) SEM-image and elemental maps of B) Fe C) Ca D) Si E) Mn F) Mg G) V H) Ti and I) K.

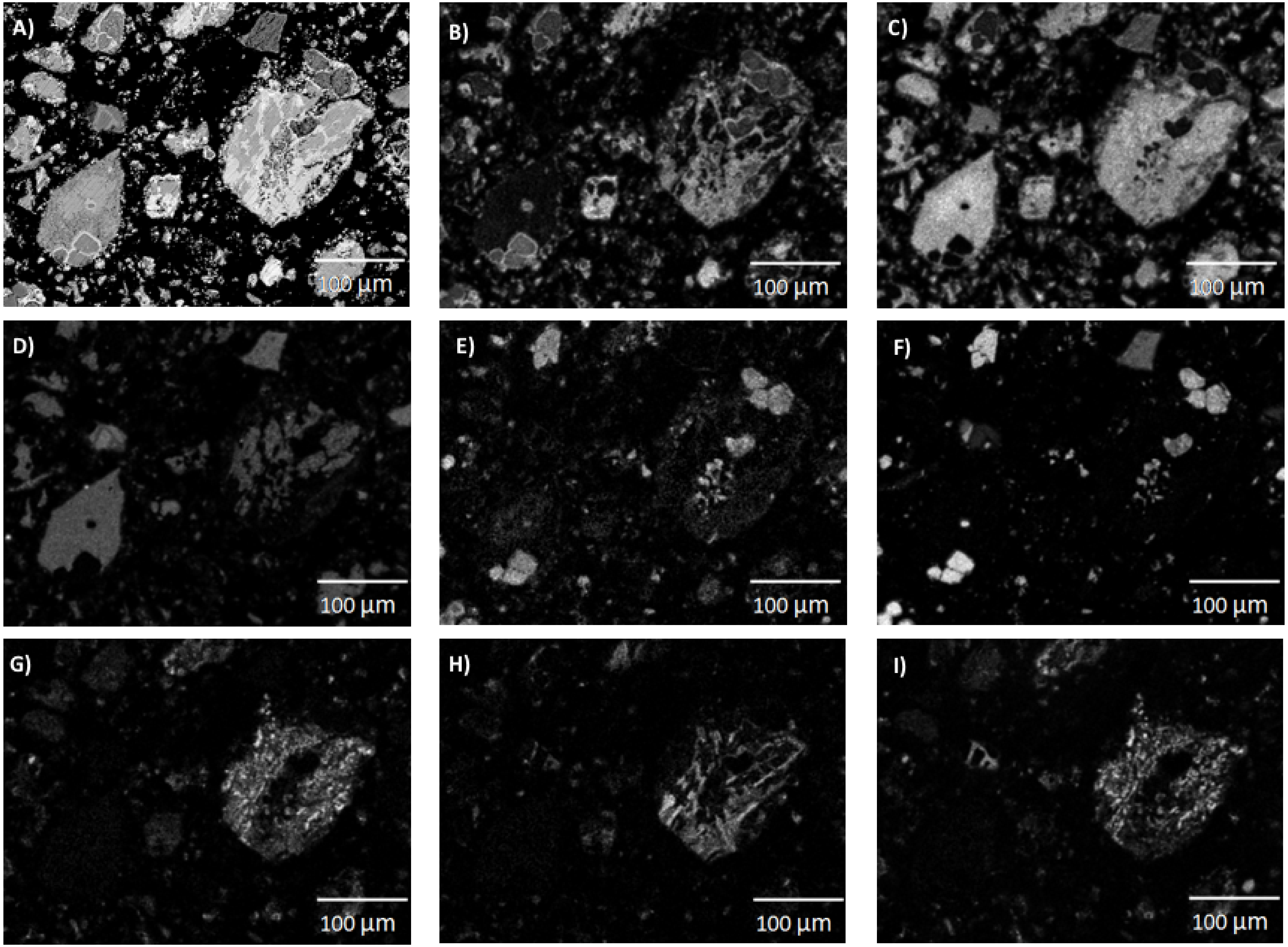

Figure C.12: SEM-EDS elemental maps of the cross-section of LD-slag reduced in the presence of K_2SO_4 A) SEM-image and elemental maps of B) Fe C) Ca D) Si E) Mn F) Mg G) V H) Ti and I) K.

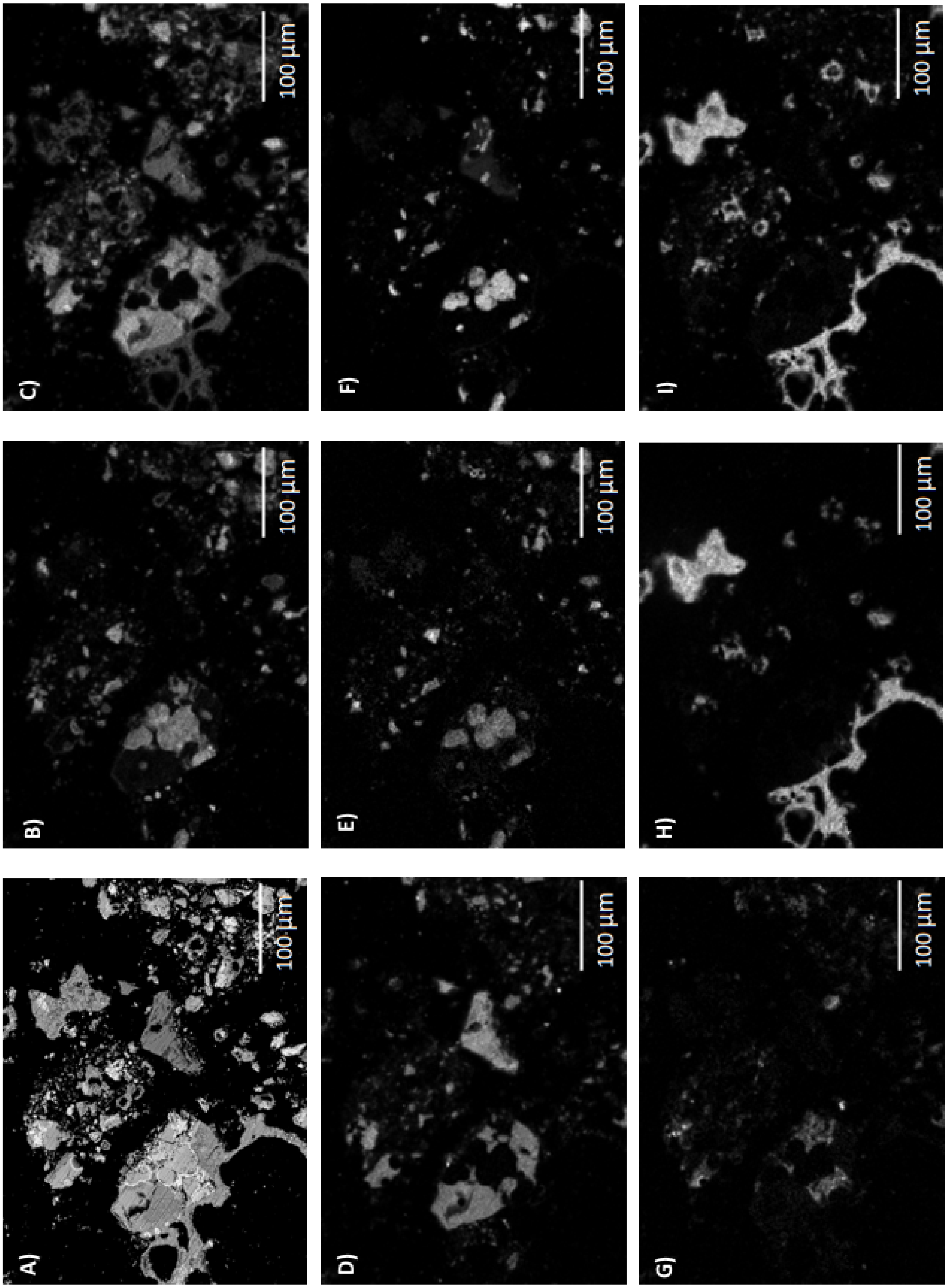

Figure C.13: SEM-EDS elemental maps of the cross-section of LD-slag reduced in the presence of KH_2PO_4 A) SEM-image and elemental maps of B) Fe C) Ca D) Si E) Mn F) Mg G) V H) K and I) P.

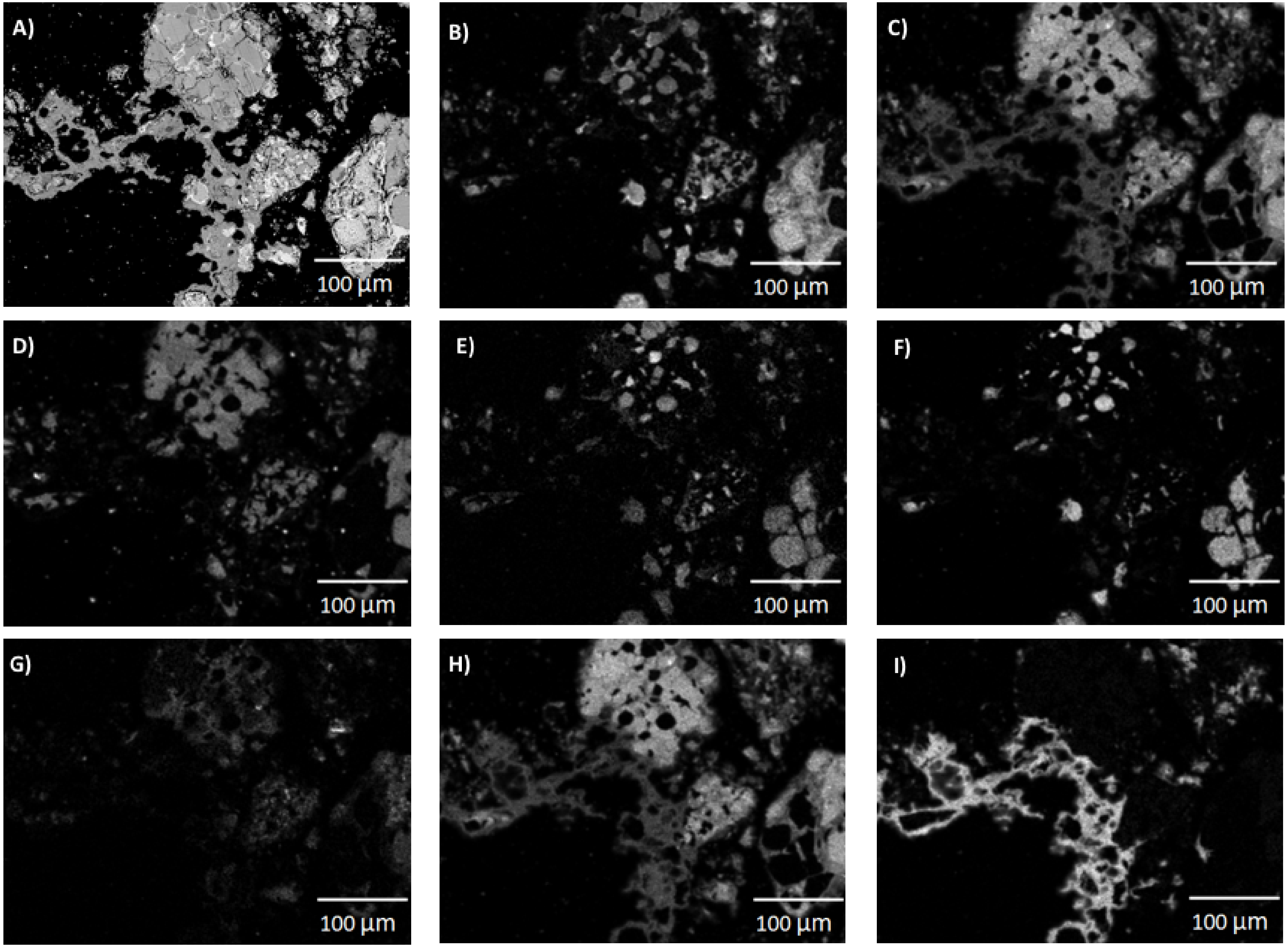

Figure C.14: SEM-EDS elemental maps of the cross-section of LD-slag reduced in the presence of KH_2PO_4 A) SEM-image and elemental maps of B) Fe C) Ca D) Si E) Mn F) Mg G) V H) K and I) P.

4. Appendix: TGA results

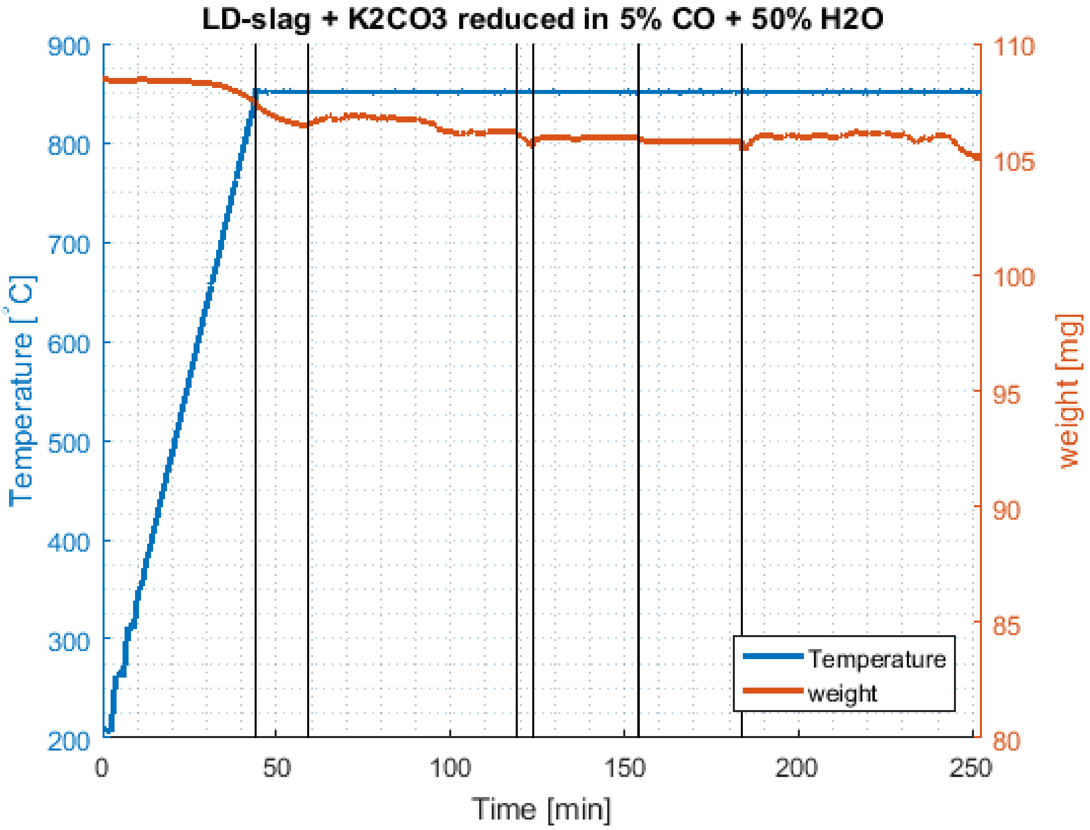

Figure D.1: TGA results for the first run done using LD-slag+K_2CO_3.